Stony Brook University

Development of a Multi-Modal Neuroimaging Fusion Approach to Study Rehabilitation of Aphasia Stroke Patients.

A Dissertation Presented

by

Mayuresh Sudhakar Korgaonkar

to

The Graduate School

in Partial Fulfillment of the

Requirements

for the Degree of

Doctor of Philosophy

in

Biomedical Engineering

Stony Brook University

December 2008

Stony Brook University

The Graduate School

Mayuresh Sudhakar Korgaonkar

We, the dissertation committee for the above candidate for the

Doctor of Philosophy degree, hereby recommend

acceptance of this dissertation.

Mark E. Wagshul, Ph.D. – Dissertation Advisor
Associate Professor, Department of Radiology, Stony Brook University

Terry Button, Ph.D. – Chairperson of Defense
Associate Professor, Department of Radiology, Stony Brook University

Lilianne R. Mujica-Parodi, Ph.D.
Assistant Professor, Department of Biomedical Engineering, Stony Brook University

Nancy Squires, Ph.D.
Professor and Chair, Department of Psychology, Stony Brook University

Candice Perkins, M.D.
Assistant Clinical Professor, Department of Neurology, Stony Brook University

This dissertation is accepted by the Graduate School

Lawrence Martin
Dean of the Graduate School

Abstract of the Dissertation

Development of a Multi-Modal Neuroimaging Fusion Approach to Study Rehabilitation of Aphasia Stroke Patients.

by

Mayuresh Sudhakar Korgaonkar

Doctor of Philosophy

in

Biomedical Engineering

Stony Brook University

2008

Language is a complex higher order cognitive function and has been one of the most popular areas of research over the past two centuries. Impairment of the ability to produce and/or comprehend language, also called aphasia, is a common functional disability seen in many stroke patients. Cerebral function reorganization immediately post-stroke and over a period of therapy can predict extent of damage and final outcome of recovery in these patients. A thorough understanding of how the brain rewires post-stroke can help clinicians to make informative decisions about rehabilitation strategies most appropriate for an individual patient. The goal of this dissertation was to use currently existing neuroimaging techniques – functional MRI (fMRI), diffusion tensor imaging (DTI), electroencephalography (EEG) and resting state BOLD MRI - to develop a multi-modality neuroimaging tool to study brain plasticity in aphasia patients. Using fMRI as a focal point for integration of all modalities, we have developed and

investigated methods to combine information from these modalities and identify potential markers of cerebral reorganization. We hypothesize that individual task difficulty maybe a critical confound in interpreting changes in brain function in stroke patients. Using our developed battery of language production and comprehension tasks, we have shown that task difficulty effects in language function can be highlighted in healthy subjects and are also found to change with age. This developed tool will be useful for future studies of aphasia stroke patients in evaluating effects of clinical drugs and different rehabilitation strategies in successful recovery of these patients.

Table of Contents

List of Figures

List of Tables

Acknowledgements

I am deeply indebted to my advisor, Dr. Mark Wagshul, for his constant support and mentoring throughout my graduate school years. It has been a wonderful experience right from the first semester when I joined his lab. I thank him for his guidance, unconditional encouragement and for teaching me how to approach and solve any given problem. His dedication and integrity towards his work will always be an inspiration for me throughout my future career and life.

I want to express my sincere gratitude to Dr. Nancy Squires and Dr. Candice Perkins, co-PIs on my thesis project. It has been such a wonderful learning experience working with them. I have been very fortunate to have Dr. Squire's vast experience in the field of neuropsychology and Dr Perkin's clinical expertise throughout this project. I am very grateful to Dr. Squires for allowing me to use her lab space and equipment for running all the EEG studies.

I would also like to thank my committee members, Dr. Lillianne Mujica-Parodi and Dr. Terry Button. Thanks to Dr. Mujica-Parodi for giving me the opportunity to work in her lab and gain research experience in my initial years at Stony brook. Thanks to Dr. Button for instructing me though several courses as part of the medical physics track. These courses have been very informative and imparted me with knowledge and appreciation for the field of medical imaging.

Thank you to all my friends and fellow colleagues at Stony Brook. Faith and Tony Cardone, Sachin Jambawalikar, Anne Katz, Prakhar Verma and Unnati Shah, all of

you have made my stay at Stony Brook a memorable one. Thanks for all your help and friendship.

Last, but not the least, I would like to thank my family and my loved ones. To Preeti, the special person in my life, you have been a constant moral support and motivation over the past five years. You have truly filled my life with so much joy, love and happiness. Thanks to Yoganand, for always being supportive and a great brother. To my parents, who have unconditionally supported me and been there for me throughout. They have always strived for the best education and opportunities for both me and my brother. Their blessings, encouragement and love have always helped me overcome the most difficult challenges. I dedicate this thesis to them.

Chapter 1

Introduction

Stroke, also called brain attack or cerebrovascular accident, is the third leading cause of death and the leading cause of disability in the United States. Stroke affects nearly four out of five Americans – either themselves or someone they know. On an average, a stroke occurs every 45 seconds, someone dies every 3 minutes and those who survive are left with significant physical and emotional after effects.

The brain is an extremely complex organ that controls various body functions. In the event of a stroke, blood supply to a part of the brain is interrupted which results in the sudden loss of neuronal function. One of the effects of stroke is aphasia, or the loss or impairment of the ability to produce and/or comprehend language. It is estimated that approximately 1,000,000 individuals in the United States have aphasia and approximately 80,000 individuals acquire aphasia every year. Anyone can acquire aphasia, but prominent are individuals from the middle and later age groups and constitute an equal number of men and women.

Aphasia results from damage to the language centers of the brain. The area and extent of damage may result in the ability to speak but not write, or vice versa, or display a wide variety of other deficiencies in reading, writing, and comprehension. Based on the area of damage or nature of disability, aphasia can be classified into various types (See Table 1.1).

Aphasia recovery generally depends on the type of brain insult. In case of transient ischemic attack (TIA) i.e. temporary obstruction of blood flow to the brain due

to stroke, aphasia recovery takes place without treatment and takes about a few hours to a few days. For most aphasic cases, language recovery is neither quick nor complete and demands some form of speech-language therapy. This therapy is targeted at improving the patient's ability to communicate by helping the person to use remaining abilities, to restore language abilities as much as possible, or to learn other methods of communication. The effect of therapy depends on the cause, extent and nature of stroke insult, and the age and health of the patient.

Current research in aphasia is targeted at exploring new ways in evaluation and treatment to further understand brain function. Medical imaging techniques like Positron Emission Tomography (PET), Computed Tomography (CT), Magnetic Resonance Imaging (MRI) and functional Magnetic Resonance Imaging (fMRI) are being used to define brain functions, determine the severity of brain damage and predict the severity of aphasia. Using these techniques a thorough understanding of language disabilities in various types of aphasia can be acquired, which may help to design various treatment strategies and to evaluate them.

The goal of this dissertation is to develop a neuroimaging tool using a multimodality fusion approach to better understand brain functions, dynamics and architecture in aphasics and healthy subjects. Such a tool could be used to study brain plasticity and evaluation of effectiveness of different aphasia treatment strategies.

(Statistical and general information from www.asha.org and the National Institute on Deafness and other Communication Disorders October 1997 - NIH Pub. No. 97-4257)

Type of Aphasia	Repetition	Naming	Auditory-Comprehension	Fluency
Broca's	Moderate-severe	Moderate-severe	Mild difficulty	Non-fluent, effortful, slow
Wernicke's	Mild-moderate	Mild-severe	Defective	Fluent paraphasic
Conduction	Poor	Poor	Relatively good	Fluent
Mixed Transcortical	Moderate	Poor	Poor	Non-fluent
Transcortical Motor	Good	Mild-severe	Mild	Non-fluent
Transcortical Sensory	Good	Moderate-severe	Poor	Fluent
Global	Poor	Poor	Poor	Non-fluent
Mixed	Non-fluent	Moderate	Moderate	Mild (worse than Broca's nonfluent)
Anomic	Mild	Moderate-severe	Mild	Fluent

Table 1.1: A brief summary of different types of aphasia and their effects.

Chapter 2

Background: Language - A Higher Order Cognitive Function

Language has been one of the most popular areas of research over the past two centuries. Language is a highly complex higher order cognitive function with even the most basic task of generating a single word requiring different levels of cognitive processing. The complexity of language can be realized from this neuroscientific description by Cathy Price [1]:

"Language is the mental faculty that we use to communicate. It involves the association of sounds and symbols with meaningful concepts and enables us to describe our external environment and abstract thoughts. The effective use of language requires the interaction of memory with sensory input and motor output systems. The principal types of memory required for language are phonological (the sounds of words), orthographic (the spellings of words) and semantic (our knowledge of the word). Sensory input to these memories can be via auditory processing (for spoken words, environmental sounds and music), visual processing (for written words, objects, faces and sign), or tactile processing (Braille). Motor output enables the expression of concepts via articulation, writing, signing or drawing; it can either be self generated (in response to internally generated thought) or stimulus driven (e.g. in response to written or heard words)."

The past two centuries has witnessed a number of theories related to language processing. Popular and earliest among them are: the *neurological models* of language developed in the 19th century by Broca, Wernicke and Lichtheim; and the *cognitive*

models suggested by the 20th century psychologists [1]. Based on lesion and postmortem studies, the 19th century models identified the role of brain regions recruited at different stages of language processing. The neurological model for repetition of heard speech and read visual words is shown in Figure 2.1. Cognitive models, on the other hand, were primarily focused on the complexity of language functions rather than their neurological underpinnings. Using behavioral studies, they sought to better understand interactions of various subcomponents involved at different levels of language processing. They also proposed existence of more than a single route depending upon specifics of language processing (e.g. semantic vs. non-semantic involvement). One such cognitive model proposed by Patterson and Shewell with complex sub component interactions and multiple routes for word processing is shown in Figure 2.2.

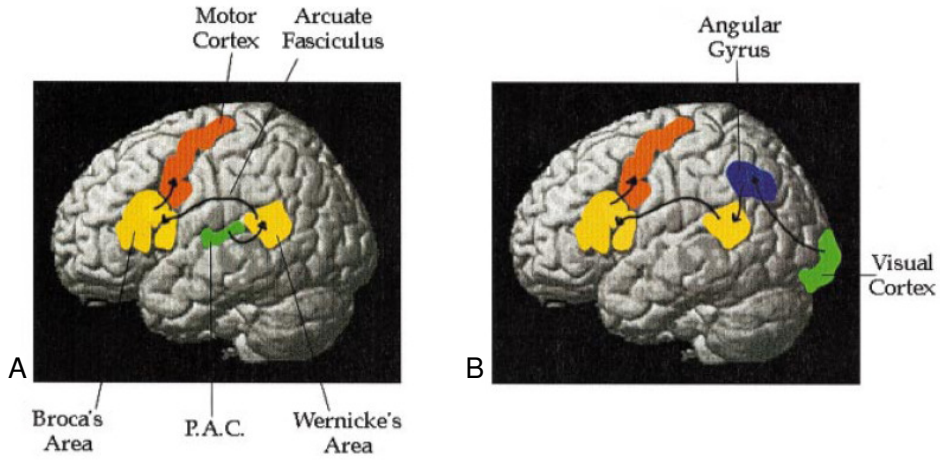

<u>Figure 2.1</u>: The 19th Century Neurological Model for Language (Figure taken from [1]):
Arrows indicate sequence of language processing.

- **A. Repetition of Heard Speech:** Primary auditory cortex (P.A.C.) – area which processes auditory speech input; Wernicke's area – comprehension of auditory word; Broca's area – generation of motor representation of the heard word; Arcuate Fasciculus – pathway connecting Wernicke's to Broca's area; Motor Cortex – Output speech production.
- B. **Reading Components:** Visual Cortex – Visual word processing; Angular Gyrus – access to representation of visual word; same path followed from thereon to final word production i.e. Wernicke's area, Arcuate Fasciculus, Broca's area and Motor cortex

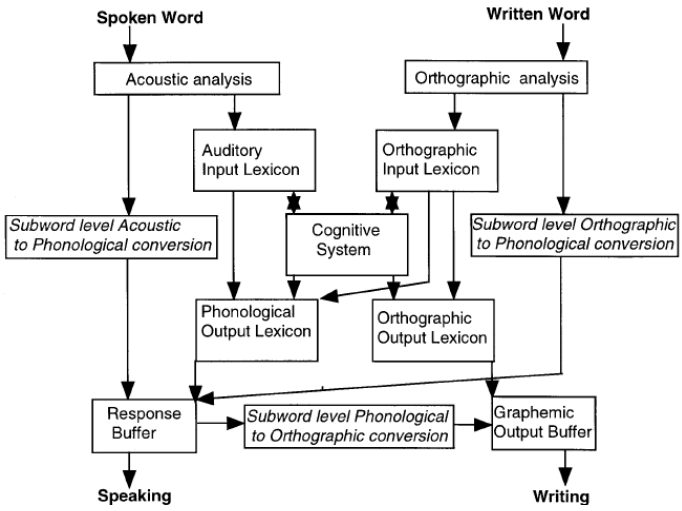

Figure 2.2: The 20th Century Cognitive Model for word processing by Patterson & Shewell in 1987 (Figure taken from [1]). Left side of the model describes processing associated with heard or spoken speech and right side with reading and writing. The model shows four key components involving four lexicons: 1. auditory input lexicon corresponds to the auditory images of speech; 2. orthographic input lexicon corresponds to visual images of words; 3. auditory output lexicon corresponds to motor images of speech; and 4. orthographic output lexicon, not specified in the neurological model but specifies the motor images for writing. Cognitive system includes the concept of words. The model incorporates more than one route for reading and speaking, for example, words can either be read via orthographic analysis, the orthographic input lexicon and the phonological output lexicon or, directly by converting parts of words to respective phonemes and integrating those phonemes in the response buffer. An important difference compared to the neurological model is the lack of neurological information with associated components.

The contribution of neuroimaging over the past decade has revolutionized the understanding of language and tested the validity of these proposed models. New models have been proposed which help us better understand the complexities of language. Based on neuroimaging evidence, Price has proposed one such advanced model which combines previous neurological and cognitive models (Figure 2.3) [1]. This model revalidates the existence of a semantic and non-semantic route with the role of additional areas (depending on nature of semantic information) for word reading.

The next few sections aim at reviewing the word production mechanism, subcomponents involved and their functional organization in tasks used in our research, namely, picture naming and verb generation. A language comprehension task to tap the

semantic processing in language is also discussed. Finally, a review of the application of language function to study brain reorganization in aphasia is provided.

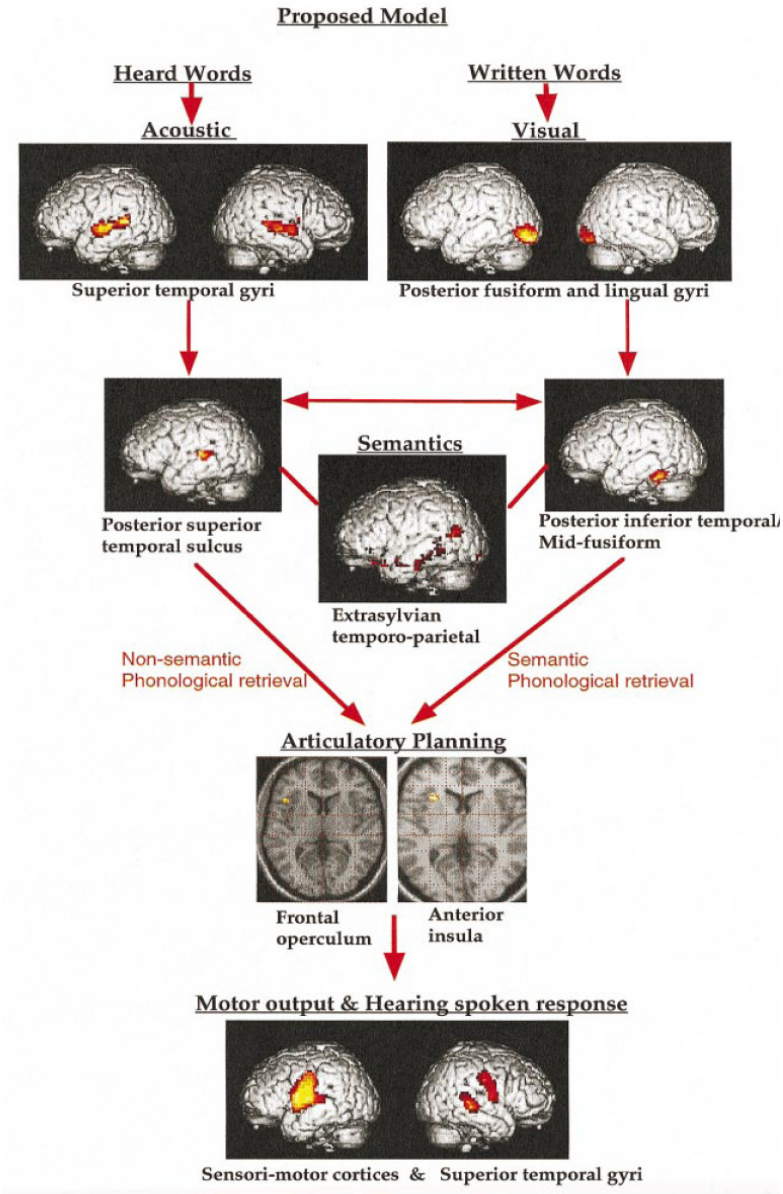

Figure 2.3: Price's Proposed Model for Word Processing based on NeuroImaging Data (Figure taken from [1]): Top row: Acoustic processing of heard words and Visual Processing of written words. Second row left: Phonological processing of speech sounds relative to environmental sounds. Second row middle: Semantic decisions relative to phonological decisions on the same words. Second row right: Retrieving the name (lexical semantics) relative to seeing visual controls and saying "okay" or "yes". Third row: Transverse slices showing the anterior insula and frontal operculum activations during phonological output. Fourth row: Motor areas for articulation and auditory processing of spoken response for reading aloud relative to silent reading.

2.1 Word Production (Picture Naming and Verb Generation):

Word production is a demanding, cognitive process. A number of stages and sub-stages are parsed before a single word is produced. This cognitive complexity is even more enhanced when sentences are generated. The neuroscience field has a long way to go before all complexities in higher level language production are sorted out. A wide range of neuro-psych, electrophysiology and neuroimaging research has provided us an understanding of single word production at subcomponent level. Using a meta-analysis approach with these studies, Indefrey and Levelt have provided a framework of the processing components involved in speech production and cerebral regions associated with them [2, 3]. Different tasks used in word production studies like picture naming, verb generation, noun generation, word reading, word repetition, generating words starting with a particular letter etc., differ in the type of lead-in processes and also in terms of the level of entry in the core processes. Both picture naming and verb generation contain all processing levels in word production. The components involved with different word production tasks are shown in Figure 2.4. Details of these components and their associated cerebral regions proposed by Indefrey and Levelt are given below. Figure 2.5 shows a schematic representation of the cerebral regions and temporal windows for the components involved in picture naming.

Tasks	(silent) Picture naming	(silent) Verb or Noun generation	(silent) Reading	(silent) Pesudoword reading	(silent) Generation from initial letters	(delayed) Word repetition
Lead-in Processes	visual object recognition	visual or auditory word recognition, visual imagery, word association	visual word recognition	visual grapheme, conversion of graphemic to phonological code	retrieving and reading orthographic word patterns, some semantic processing	auditory word perception or audio-phonological parsing, articulatory loop rehersal
Core Processes						
conceptual preparation	✓	✓	?		?	
lexical concept						
lexical selection	✓	✓	?		✓	(✓)
lemma						
phonological code retrieval	✓	✓	✓		✓	(✓)
phonological code						
phonological encoding	✓	✓	✓	✓	✓	✓
phonological word						
phonetic encoding	(✓)	(✓)	(✓)	(✓)	(✓)	✓
gestural score						
articulation	(✓)	(✓)	(✓)	(✓)	(✓)	✓
spoken word						

Figure 2.4: Different word production tasks and their sub components (Figure taken from [2, 4]. Check mark indicates involvement of the component process in the task. Check mark in parentheses indicates that the component's involvement depends on the details of the task. Phonetic encoding and articulation, for instance, are involved in overt, but not in silent word production tasks.

1. Lead-in Processes:

The lead-in process in picture naming is visual object recognition i.e. visual complexity, color, object category etc. For verb generation, a visual or auditory word

recognition process is triggered. For a concrete noun, a visual image of the noun will be generated and that image activates one or more associated actions in the long term memory. When the noun is abstract, long term memory maybe accessed without visual imagery. The cerebral regions recruited for the lead-in processing stage are:

Picture Naming: Ten regions are activated mainly during picture naming: left anterior insula, left posterior inferior temporal and fusiform gyri, bilateral medial occipital lobe, right caudate nucleus, left midbrain, and the medial and right lateral cerebellum. Five of these regions – left anterior insula, left posterior fusiform gyrus, left and right medial occipital lobe and right medial cerebellum – are also found activated during word reading, suggesting an involvement in visual processing, the principal lead-in component common to both picture naming and reading.

Verb generation: Left anterior superior frontal gyrus, right anterior insula, right mid superior and middle temporal gyri, left caudate nucleus, and right thalamus are the regions associated with word generation. The left anterior frontal and middle temporal gyri, right anterior insula, and left caudate are specifically related to the lead-in processes of word generation, whereas right mid superior temporal gyrus and left thalamus are found in word reading as well.

The posterior fusiform gyrus and the insula were suggested to be involved in the later stages of visual processing because of their absence during pseudo word reading. The medial occipital activations were also associated with the processing of nonlinguistic visual features (like string length etc) because of their presence during both word and pseudo word reading tasks.

2. *Conceptual preparation, lexical and lemma selection:*

Conceptual preparation involves assimilating properties of a viewed picture or word and generating lexical concepts semantically associated with them. Syntactic representations for each lexical concept, also called lemma, are retrieved from the mental lexicon. Next depending upon the communicative situation and the experimental task, the appropriate lexical concept and corresponding lemma is selected for expression. For example, if a picture of a labrador is shown, lexical concepts like ANIMAL, DOG, LABRADOR etc. could be activated. If the task is to name the animal in the picture, the lexical concept DOG will be selected for expression.

The mid segment of the left middle temporal gyrus was found associated with the conceptual and/or lexical selection processes in word production. Apart from the conceptual preparation for lexical selection, a number of other conceptual processes are involved in word generation - like the semantically guided search processes in word generation (served by the anterior frontal regions), as well as from the prelinguistic conceptual processes involved in object recognition and categorization (served by the ventral temporal lobe). These are however suggested to be a part of the lead-in processes.

3. *Phonological code retrieval:*

Phonological code retrieval is the first major step in generation of the articulatory shape of a word. Only the selected lemma will activate retrieval of phonological codes of each of its morphemes. Morphemes represent segments or division of phonemes of the whole word. This phonological code retrieval activates the left posterior superior and middle temporal gyri i.e. the Wernicke's area and the left thalamus. The posterior

superior temporal lobe has been also found to be activated during word comprehension indicating that a common store of lexical word form representations is accessed in both word production and comprehension.

4. Phonological encoding:

During this stage the spelled out segments of the phonological code are incrementally clustered in syllabic patterns. For example, to syllabify the word '*persist'*, the first two segments /p/ and /e^{r}/ will be clustered to form the first syllable /pe^{r}/; next the remaining four segments will be clustered to form the second syllable /sIst/. Each syllable is also called a phonological score.

The left posterior inferior frontal gyrus (Broca's area) and left mid superior temporal gyrus are two areas which are found to be associated with phonological encoding. Only the Broca's area has been observed to be active for processing of pseudo words indicating a functional difference between the Broca's area and the left mid superior temporal gyrus within non-lexical phonological processing. Broca's area is also found to be activated in tasks involving phonological processing of language comprehension.

5. Phonetic encoding and articulation:

As soon as a syllable is programmed, its gestural score is retrieved from the mental syllabary. The syllabary is the repository of abstract motor representations for each syllable. From the syllable scores, a gestural pattern also called an articulatory score or gestural score for the word is generated. This is called phonetic encoding. Articulation

involves generating least-effort solutions for execution of these gestural scores. These solutions provide motor instructions for the respiratory, laryngeal and the supralaryngeal systems involved in fluent articulation.

The primary motor and sensory areas, i.e. the right and left ventral (and to some extent dorsal) precentral gyri and the right and left ventral postcentral gyri are the areas activated for production of abstract articulatory gestures and their articulation. These sensorimotor activations were also observed in control conditions for which the same word was said for every stimulus, confirming their recruitment for articulation. Other regions found activated only for overt tasks are: left anterior superior temporal gyrus – associated with overt pronunciation, right SMA – related to complex motor planning and imagination of articulation, and the left and medial cerebellum – associated with motor activity.

6. Self perception:

This component of word processing involves self monitoring of generated speech and enters the same processing pathway that is used for normal speech comprehension. Bilateral superior temporal activations are associated with self monitoring.

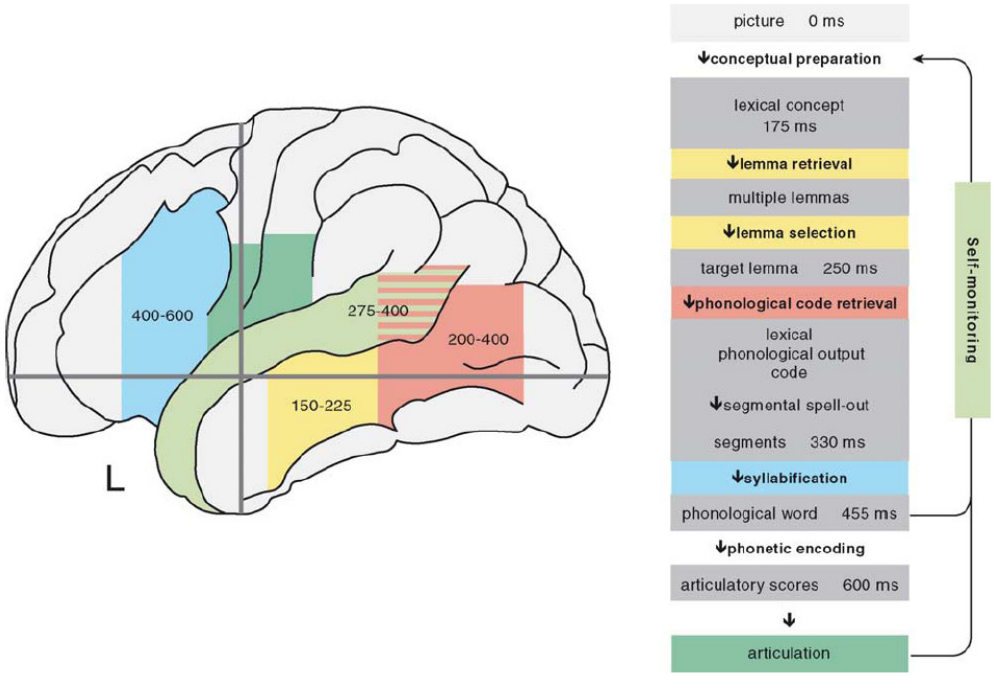

Figure 2.5: (Left) Schematic representation of the cerebral regions and temporal components for word production in picture naming (Figure taken from [5]). Identical colors indicate relation between regions and processing subcomponents (Right). The numbers indicate the time-windows in milliseconds during which the regions are activated during picture naming from the onset of the picture stimuli. Further regions activated with phonetic encoding and articulation (not shown) are the right sensorimotor cortex, the right SMA, left and medial right cerebellum, left and right thalamus, and right midbrain. The region involved with self monitoring is the right mid superior temporal gyrus.

2.2 Language Comprehension:

Language processing mainly involves two components: *syntactic* i.e. processing of syntax and *semantic* i.e. processing of meaning or context of language. While a number of studies have concentrated on studying these two processes separately, it is suggested that there is both temporal separation (early vs. late) as well as overlap between these processes [6]. In summary it has been suggested that language comprehension consists of the following three phases: Phase 1 (100-300ms) represents the initial syntactic structure formation, Phase 2 (300-500ms) during which the lexical

semantic and morphosyntactic processes take place with the goal of thematic role assignment (or N400 effect), and Phase 3 (500-1000ms) during which the different types of information are integrated. From electrophysiology studies, syntactic processing is correlated with two components: a left anterior negativity (LAN), which occurs during an early time window (100-500ms) and a late centro-parietal positivity termed P600, which occurs between 600 and 1000ms. Semantic processing is correlated with both the N400 and also the P600 component (which is associated with the integration of the semantic and syntactic information) [7]. Functional neuroanatomy studies of sentence processing have identified separable temporo-frontal networks. The semantic processes are mainly subserved by the left temporal regions (medial and superior temporal gyrus) and involve recruitment of the frontal cortex (BA 45/47) when strategic or memory aspects come into play; while the syntactic processes involve the left anterior superior temporal gyrus, BA44 and the adjacent fontal operculum. The next section will cover a review of N400 and semantic processing.

Semantic Processing & N400:

As discussed above, electrophysiology studies, also called event related potentials (ERP), related to semantic processing in language comprehension have shown that semantic priming or semantic deviation affects the amplitude of an ERP component called N400 [8, 9]. N400 is the negative deflection of the ERP signal between 300 and 500ms and peaking approximately around 400ms post-stimulus onset. In addition to reflecting neural activity associated with processes related to semantic or lexical access of

word representations, N400 has alternatively shown to be related to processes integrating word representations with current context [10]. For example, consider the sentences *"the boy ate the book"* and *"the boy ate the ice-cream"*. The latter sentence semantically makes sense whereas the former sentence is semantically incorrect and would elicit higher N400 amplitude (more negative). If a target word e.g. *"dog"* is preceded by a semantically related prime - *"animal"* or a semantically unrelated prime – *"box"*; N400 effect would be reduced in the case of semantically primed word as compared to when the target word is preceded by the semantically unrelated word (N400 priming effect) [10].

Both functional imaging [11, 12] and electrophysiology [13, 14] studies separately as well as in conjunction [15, 16] have been used to map the neural generators associated with N400. As mentioned before, the left superior temporal cortex has been found to correlate with the N400 effect and inferior frontal cortex playing the main role in stimulus selection or retrieval.

The clinical significance of using ERP components to access language function has been established using patient case studies as well as patient group populations [17, 18]. Using a revised version of the Peabody Picture Vocabulary Test, which uses a picture followed by a congruent or incongruent spoken word and requiring no response from the patient, D'Acry *et al.* have shown existence of correlation between the N400 responses with the language comprehension ability (measured by standardized neuropsychological testing) of patients affected by a left hemisphere stroke [19]. This kind of assessment is advantageous in comparison to standard neuropsychological

methods requiring task performance for motor and language assessment in stroke patients.

2.3 Aphasia, Brain Reorganization and Language function:

Brain plasticity or neuroplasticity is the capacity of the brain to modify organization of its neuron networks and location of specific information processing functions as a result of experiences during development. The human brain is not *"hard wired"* with fixed and immutable neuronal circuits. Gray matter can actually shrink or thicken; neural connections can be forged and refined or conversely weakened and severed. Changes in our abilities manifest changes in our physical brain. With age, certain brain machinery tends to decline. However the plastic nature of the brain allows for the possibility of reinvigorating these brain machineries. This is clearly evident from studies which have shown evidence of the development of a compensatory brain memory network in older adults to counteract age related neurocognitive decline as compared to young adults [20]. The same mechanism is responsible for functional recovery in response to a cortical injury or cerebral damage.

The understanding of the bases for brain plasticity comes from studies of neural connections which have indicated that afferent cells after damage can produce new connections based upon a process called synaptic reorganization. Three forms of synaptic reorganization have been observed: 1. sprouting of new axons increasing the number of terminals in the normal dendrite area, 2. development of terminals in the new target area; and 3. extension or termination of afferents on cells that are not the normal target areas

(hemisphere contralateral to the injury). These changes in excitability in adjacent and contralateral homotopic regions of a cortical lesion is the consequence of reduced collateral (i.e. in ipsilateral perilesional regions) and transcallosal (i.e. in contralateral homotopic regions) inhibition. Netz *et al.* have shown that this inhibition of neurons in neighboring areas and parts of the bilateral network, not participating in the performance of a particular function, is necessary for the lateralization or specialization of certain brain areas for that function [21].

Recovery from aphasia (due to stroke or due to tumors developed over time) implies functional reorganization of the language system in the brain. Many neuroimaging studies have suggested the importance of areas surrounding the infarction in recovery [22-24], whereas others have suggested an essential role of the contralateral undamaged hemisphere [25-28]. Some have also suggested the role of both hemispheric areas in recruitment for recovery [29]. Most informative have been the studies which have followed language recovery over the course of rehabilitation of aphasic patients [25, 30-34]. While most of these studies have observed language rehabilitation from subacute phases (12days to 3months post stroke) to chronic phases (more than 5 months post stroke), Saur and colleagues have monitored language reorganization from the acute (1.8 days post stroke) to the chronic phase (321 days post stroke) [30]. They suggest that the course of language recovery begins with a moderate amount of early activation of non-infarcted ipsilateral language structures, followed by an upregulation with recruitment of the homologue language structures and finally a re-shift into the ipsilateral hemisphere.

In terms of quality of restored language function, improvement depends upon the undamaged portions of the language network in the left hemisphere (i.e. the dominant

half of the brain) and to a lesser extent on the homologous right hemisphere areas [35]. This is also evident from a recent study by Winhuisen and colleagues [36, 37] which used repetitive transcranial magnetic stimulation of inferior frontal gyral (IFG) language sites identified using PET. They found that the contralateral IFG is essential for residual language function for patients who do not recover complete left IFG function at 10 days post stroke [36]. This compensatory potential was however less effective than in patients who recovered left IFG function. The follow-up study [37] of the same patients 8 weeks after stroke indicated that patients with right IFG role in language at 10 days post stroke, showed language improvement at 8 weeks post stroke only if they had regained left IFG activity. Also, there was a shift of language function to the left IFG with no new right IFG activations observed at 8 weeks. These results indicated a restoration of transcallosal inhibition after recovery of the left hemispheric areas reducing the role of the right IFG in language function. Belin *et al.* have also linked increased right hemispheric activity in chronic aphasic patients with failed or faulty recovery attempts in the sense of maladaptive plasticity or the breakdown of interhemispheric control within the distributed neural network [38]. In contrast, the activation of neighboring regions in the ipsilateral hemisphere and efficient function recovery is probably due to intact collateral inhibition. Another factor affecting functional recovery related to cerebral reorganization is the speed of development of brain lesions. In the case of aphasia developed over a period of time on account of a slow progressive damage (e.g. due to a tumor) , the shift in language function to the right hemisphere indicates better recovery [39].

These numerous studies of language functional reorganization have been summarized to deduce a hierarchical organization of aphasia recovery [40]. However, this proposed model is not valid in all types of aphasia for all language functions:

- Almost complete recovery of function is only possible by restoration of the original activation pattern within the network of the dominant hemisphere.
- If the primary centers are damaged, reduction of collateral inhibition leads to the recruitment of the perilesional areas. An incomplete but satisfactory improvement of language function is possible following this intrahemispheric compensation.
- If the ipsilateral network components are severely damaged, reduction of transcallosal inhibition causes activation of contralateral hemispheric areas. This interhemispheric compensation involving homotopic contralesional areas contributes to an improvement in function which is dependent on the extent of the functional shift between hemispheres, but not as efficient as the intrahemispheric compensation. However, in the case of patients with slowly developing brain damage (as in tumors), language performance can be preserved or completely restored despite the interhemispheric shift in function.

To summarize, evaluation of language function using neuroimaging methods can provide insight on aphasia recovery. This dissertation proposes the use of a picture naming and verb generation task to evaluate language production. Using these two word production tasks, we expect to map the different cerebral areas associated with language processing discussed above. In addition, a language comprehension task, different from standard forms of semantic processing tasks used earlier is also proposed. This task taps the contextual aspect of semantic processing. The next two chapters give a brief overview

of the different neuroimaging methods used to probe the brain function involved in these tasks.

Chapter 3

Background: Magnetic Resonance Imaging (MRI)

MRI is an imaging method based principally on the sensitivity to the presence and magnetic properties of water (protons). Water constitutes 70-90% of most tissues and the properties and amount of water is different between tissues and also changes with disease or injury. This makes MRI a very sensitive diagnostic tool for imaging different types of tissues. Unlike other imaging techniques which image using ionizing radiation (like x-rays, CT), there are no known damaging effects associated with MRI. This chapter introduces the basic concepts of MRI and gives a brief overview of the specific MR imaging techniques used in this dissertation.

3.1 Principles of Magnetic Resonance Imaging

Hydrogen nuclei are by far the most abundant in human body and the most commonly imaged nuclei in MRI. A hydrogen nucleus consists of a single proton. The proton has a property called nuclear spin and its behavior is similar to that of a spinning charged particle. This nuclear spin creates a nuclear magnetic moment and when the proton is place in a magnetic field, it experiences a turning force, known as a torque. In addition, the proton has an odd numbered atomic mass (i.e. 1) because of which its spin results in an angular momentum (J). The magnetic moment and the angular momentum are in the same direction and scale by a factor γ ($\mu = \gamma J$), called the gyromagnetic ratio. This value is 42.58 MHz/T for hydrogen.

Within a given volume there are many hydrogen nuclei with their spins oriented randomly, making the net magnetization infinitesimally small. Therefore, a strong magnetic field (conventionally applied in the z direction), B_0, needs to be applied to increase the net magnetization value. Because of the applied field, a torque is induced on the spins, causing the protons to precess about the axis of the magnetic field. This change in angular momentum over time is given by:

$$\frac{dJ}{dt} = \mu \times B_o$$

From this equation, it is clear that the proton spin will only precess about the magnetic field axis when it is oriented at an angle to the field, and the frequency of this precession, called the Larmor frequency, is given by: $\omega_o = \gamma B$

There are two states for the protons: one when the protons are aligned along the magnetic field (low energy state) and the other when they are anti-aligned with the field (high energy state). The low energy, parallel state is slightly more stable with more protons in this state. The relative populations of the two states depend upon temperature and strength of the applied field (B_0). The sum of all magnetic moments from spins within a volume, the net magnetization, provides the basis for the MRI signal. However, this net magnetization cannot be measured directly under equilibrium conditions. Hence an indirect approach to perturb the spin system away from equilibrium and then measure the response of the system is performed. This is usually done by applying a secondary external field (B_1). The energy deposited by this field must match the electromagnetic radiation required to change from low energy state to the high energy state. This energy is applied for an extended period of time at the same Larmor frequency of the spins. These

main steps in MRI signal generation are divided into: spin excitation, spin relaxation and signal detection, and image reconstruction. A detailed overview of these steps can be found in [41].

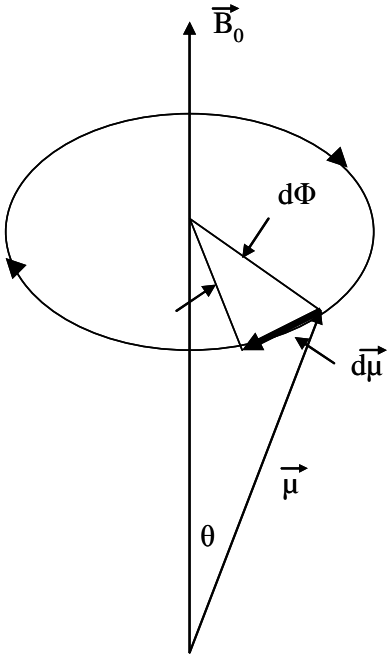

Figure 3.1: Geometric representation of the precession of a proton's spin about a magnetic field Bo. Arrows indicate direction of precession. Figure adapted from [41].

The previous section provided an understanding of how a spin behaves in an applied magnetic field. BOLD fMRI and diffusion tensor imaging (DTI) require an understanding of the concept of 'phase' and how it changes in the presence of a gradient magnetic field, field inhomogeneities and spin motion. This is covered in the next two sections.

Spins in a linear gradient magnetic field:

Consider a uniform distribution of water producing a net MR signal due to the applied static field B_o. Now if a gradient G, i.e. a spatially linear magnetic field in addition to the static field, is applied over space, the net magnetic field experienced by a

proton depends on its position. As the Larmor frequency is dependent on the experienced magnetic field, protons precess at different frequencies depending on their position in space. The spins which are precessing faster appear to move apart with respect to those which are precessing slower. The combined effect is a fanning out of spins due to dephasing. The speed at which this happens depends on the gradient amplitude or strength. The total angle of dephasing depends upon the product of the gradient strength and its duration, also known as gradient moment. For a proton at position x with a gradient G applied for time t, the phase Φ of the proton is given as:

$$\phi(x,t) = \gamma \cdot xG \cdot t$$

When the gradient is turned off, all protons will experience the same static magnetic field and will return to the same precession rate. However, the final phase of the proton will be remembered. Figure 3.2 shows the change in phase due to a linear magnetic gradient.

If another gradient with a reversed polarity (i.e. negative amplitude) is applied, it will have an exactly opposite effect i.e. spins which precessed faster before will now start to precess slower and the ones which had a slower rotation earlier will now speed up. When the gradient moment of the second applied gradient is equal to that of the first, all spins will be pointing in the same original direction. At this point in time, we get a measurable MR signal, known as gradient echo. Figure 3.3 shows dephasing and rephasing of spins by bipolar gradients to form a gradient echo.

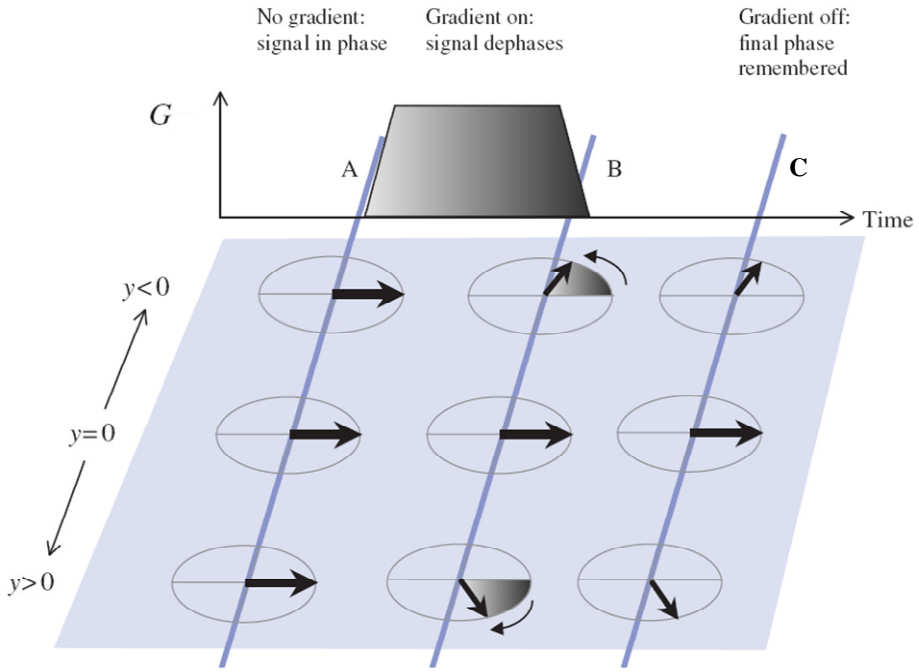

Figure 3.2: Phase due to the application of a linear gradient field (G). Figure taken from [42].y represents the position of proton spins. Phase of a spin (shown by bold arrow) at any time is dependent on the applied gradient field and on the position of the spin. A – phase of the spins before application of gradient; B – phase of the spins at the end of the applied gradient; and C – phase after gradient is turned off.

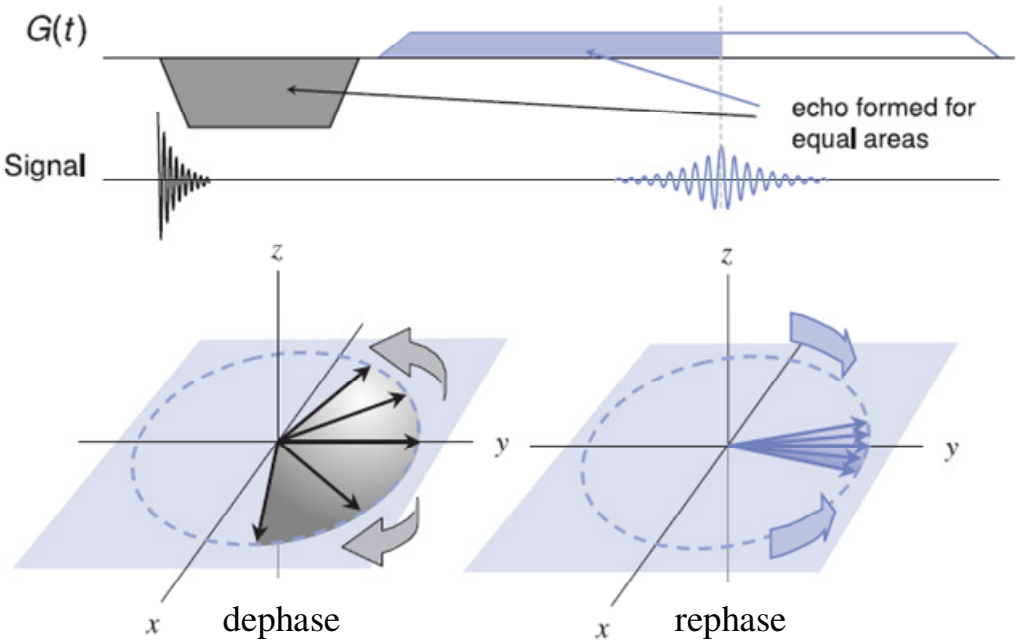

Figure 3.3: Generation of gradient echo. The first gradient causes the spins to dephase and the second opposite gradient rephases them. Complete rephasing results in gradient echo. Phase of spins represented by arrows. Figure taken from [42].

Effect of spin motion on phase:

We have seen that a linear magnetic gradient has the capability of encoding phase dependent on the position of the spins. A negative applied gradient causes these dephased spins to rephase with the amount of rephasing experienced again dependent on position of the spins. If the spins were to move during the time between the application of the dephase and rephase gradients, these displaced spins will not experience complete rephasing resulting in a loss of coherence and loss of MR signal. DTI uses this change in phase to map motion and is explained in more detail later.

Effect of field inhomogeneities and spin interactions on phase:

The discussion so far assumed an ideal MR experiment, where the field is completely homogeneous and the spins are stationary throughout. However, in reality this is never true. Under the influence of the applied excitation pulse, all the spins are tipped into the transverse plane. Initially, all the spins are precessing around the main field at their respective Larmor frequencies, but have the same phase i.e. initially all spins are coherent in phase. Over time, neighboring spins tend to interact with each other causing some spins to precess faster and some slower i.e. the spins become out of phase resulting in a loss of coherence. At any point of time, the MR signal is proportional to the net magnetic moments of all the spins and the loss of coherence causes the MR signal to decay over time. This decay mechanism is known as T_2 decay.

In addition to this spin-spin interaction, if the external field is also inhomogeneous, variation in the magnetic field from location to location causes spins at different spatial locations to precess at different frequencies, also leading to the loss of

coherence. Combined effects of both spin interaction and field inhomogeneity leads to signal loss known as T_2* decay. This concept of T_2* decay is responsible for the BOLD fMRI signal and is explained in the later sections.

3.2 Being BOLD with MRI – Imaging Brain Function using Magnetic Resonance

Grey matter is the primary tissue associated with functional activation. Long before fMRI, specific regions of grey matter were associated with different simple cognitive processes. The advent of fMRI has led to the understanding of complex cognitive processes and the different brain structures related to them.

3.2.1 What does fMRI tell us about neuronal activity?

Neurons are the basic information processing unit of the central nervous system. Any kind of sensory, motor or cognitive process is realized mainly through the following two neuronal activities: 1. integrative activity, i.e. a coalition of inputs of numerous associated neurons and 2. signaling activity, resulting primarily from the activity of axons which transmit the outcome of the integrative processes to one or more other neurons. These neuronal activities are demanding in terms of energy requirements in the form of adenosine triphosphate (ATP). Because the brain does not store energy, it must create ATP energy through the oxidation of glucose. The increased blood flow, in response to this need, supplies cells with glucose and oxygen. Thus cortical areas associated with a particular function will have a local increase in blood flow as compared to other areas not

associated with the same function. Measuring the response to this metabolic demand and characterizing the cortical areas associated with this demand is the main principle used by fMRI. fMRI is thus an indirect measure of the neuronal activity.

3.2.2 Imaging this metabolic demand using MR

Hemoglobin is the carrier of oxygen in blood. The hemoglobin molecule has magnetic properties that differ depending upon whether or not it is bound to oxygen. Oxygenated hemoglobin (Hb) is diamagnetic i.e. it has no unpaired electron and zero magnetic moment. In contrast, deoxygenated hemoglobin (dHb) is paramagnetic i.e. it has an unpaired electron and a significant magnetic moment. Completely deoxygenated blood has a magnetic susceptibility (i.e. an effective shift of the main magnetic field due to the magnetic moment of dHb) about 20% greater than fully oxygenated blood.

As discussed in the previous section, in the presence of a magnetic field, hydrogen atoms (which are abundant in water molecules in the brain) absorb energy that is applied at the precession frequency. After this step of applying radio-frequency excitation, the hydrogen atoms emit energy at the same radio frequency until they gradually return to their equilibrium state. The MRI scanner measures the sum total of the emitted radiofrequency energy. The measured radio-frequency signal decays over time owing to various factors, including the presence of inhomogeneities in the magnetic field. Because of the paramagnetic nature of deoxyhemoglobin, there is an increase in inhomogeneity of the magnetic field. Greater inhomogeneity results in different hydrogen

atoms experiencing different magnetic strengths. This results in loss of phase coherence due to the T2* effect and thus decreased image intensity.

By using a MR pulse sequence which is sensitive to this T2* effect (gradient echo with long TR and medium TE) [43], changes in magnetic field inhomogeneity of the magnetic field within each small volume of tissue resulting from changes in blood oxygenation can be measured. The images from this sequence will have a higher MR signal where the blood is highly oxygenated and a lower MR signal where the blood is highly deoxygenated. Utilizing this simple change in signal, regions of the brain that demonstrate a hemodynamic response due to activation can be located.

Imaging these changes in blood flow with changes in brain function requires these images to be acquired very rapidly, atleast at the same rate as the physiological changes of interest. Simple gradient echo sequences are limited in the number of slices and how frequently these slices can be collected. These sequences acquire images by filling up the k-space in a line by line fashion, which necessitates a large number of separate excitations for a moderate image resolution. For functional imaging with a reasonable spatial resolution, a relatively large k-space needs to be sampled following a single excitation pulse. Echo planar imaging sequences which rely on filling the entire k-space using rapid gradient switching following a single excitation have shown application in collecting these functional images and are commonly used for fMRI [44, 45].

Developed functional language tasks with fMRI will help us to map the functional language architecture in healthy subjects. fMRI will serve as an important marker to evaluate severity of stroke insult and study how brain reorganizes with post-stroke rehabilitation.

3.3 Diffusion Tensor Imaging

3.3.1 Theory of Diffusion

In 1827, the English botanist Robert Brown noticed that pollen grains when suspended in water followed a zigzag random path. This random translational motion (Brownian motion) of molecules, resulting from the thermal energy carried by these molecules, is called diffusion. When the motion of these molecules is unrestricted, the scope of movement of each of these molecules is a sphere around the molecule, resulting in *isotropic diffusion*. However, when this motion is restricted in some way in one particular direction, the scope of movement is an ellipsoid with the direction of the main axis of the ellipsoid representing the preferred direction of motion. This type of diffusion is called *anisotropic diffusion*. This is the main principle behind the underlying success of diffusion MRI where the random, diffusion driven displacements of molecules probe tissue structure [46].

During typical diffusion times of about 50msec, water molecules in the brain move approximately 10μm, bouncing, crossing, or interacting with many tissue components such as cell membranes, fibers, or macromolecules. The overall effect observed in a diffusion MRI voxel of several mm^3 reflects, on a statistical basis, the diffusion of the water molecules present within that voxel. This diffusion distribution may provide clues to the structure and geometric organization of the tissue and axonal structures. Namely, water molecules should move easily along axonal bundles rather than perpendicular to them because of fewer obstacles for movement along the fibers and

hence give useful information about fiber integrity which may be useful in assessing a number of neurological disorders.

3.3.2 Diffusion weighted MR

MR pulse sequences can be made diffusion sensitive by adding a pair of pulsed magnetic field gradients (diffusion gradients) into the sequence. The most common type of diffusion gradient design is the Stejskal-Tanner Scheme [47] where the first diffusion gradient is applied between the excitation pulse and the refocusing 180° pulse, and the second gradient is applied between the 180° pulse and the echo (Figure 3.4).

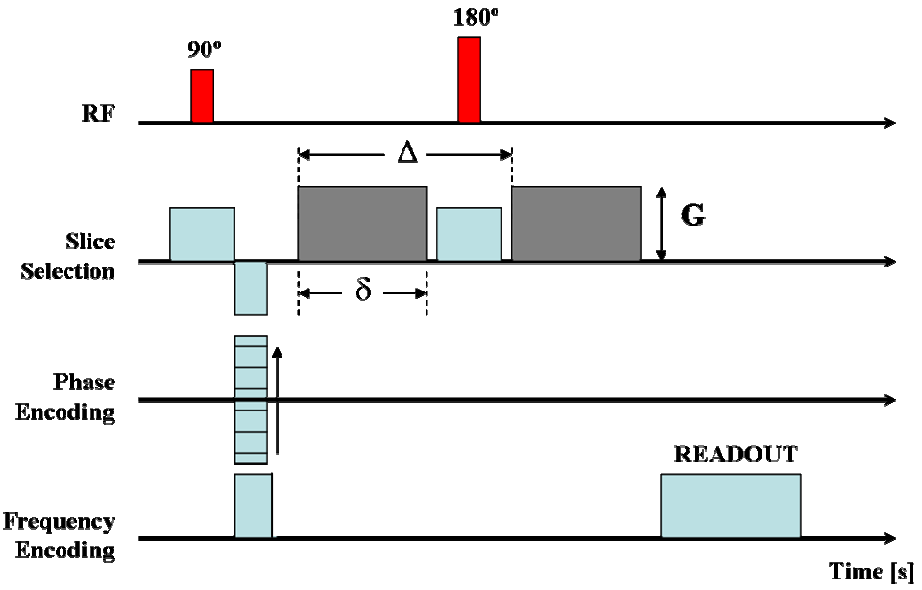

Figure 3.4: Spin Echo MR Sequence with Diffusion Gradients (Grey). Gradients can be applied on any of the three imaging axes or a combination thereof. RF – Radiofrequency pulses applied - 90° excitation pulse followed by 180° refocusing pulse; G – gradient strength; Δ – separation between gradients; δ – diffusion gradient duration. G, Δ & δ determine the amount of diffusion weighting.

As explained earlier, the effect of the diffusion gradients is to introduce a spatially dependent phase accumulation. Gradients can be applied in any direction i.e. x, y or z or a

linear combination of these. However the diffusion effect will be measured only in the direction of the applied gradients. Hence, for a stationary spin, the phase accumulation due to the first gradient is matched in amplitude but reversed in sign to the phase accumulation due to the second gradient. The result is that for stationary spins the net phase change is zero. For spins that move during the experiment (i.e., diffusing water molecules), the phase accumulations due to the first and second gradients are not matched in amplitude, thus resulting in a net phase change. As diffusion is a random walk, the motion of spins is incoherent within the voxel and will have different phases. This results in a loss of phase coherence and signal attenuation. The amount of diffusion weighting will depend on the strength of the encoding gradients (i.e., how strongly the phase accumulation depends on spatial location), and on the duration of the experiment (i.e., for how long diffusion and phase dispersion is allowed to occur). These parameters are summarized into a single number called '*b*-factor'. For a simple pair of pulsed gradients, the b-factor is given by the Stejskal-Tanner expression:

$$b = \gamma^2 \cdot G^2 \cdot \delta^2 \cdot \left(\Delta - \frac{\delta}{3} \right)$$

where γ is the gyromagnetic ratio, G is the gradient amplitude, and δ and Δ are the temporal duration and separation of the diffusion-encoding gradients, respectively.

The signal value from a spin echo MR experiment can then be represented as

$$S \propto PD \cdot \left(1 - e^{-TR/T_1}\right) \cdot e^{-TE/T_2} \cdot e^{-bD}$$

where S is the spin echo signal value, PD is the proton density, T_1 and T_2 are relaxation times, D is the diffusion coefficient and represents the motion of the water molecules, and

TR & *TE* are the related to the timing of excitation (called repetition time) and the preparation time (called echo time) of the MR signal respectively. In order to obtain the diffusion coefficient (*D*), signal value of the same voxel at two different measurements in time is required. By changing only the b value (say b_0) and keeping all other parameters the same, signal intensity (S_o) value can be obtained. The diffusion coefficient value can be obtained from these two signal intensity values at two different *b* values.

$$S_o \propto PD \cdot \left(1 - e^{-TR/T_1}\right) \cdot e^{-TE/T_2} \cdot e^{-b_o D}$$

$$D = -\ln\left(\frac{S}{S_o}\right) \Big/ \left(b - b_o\right)$$

By solving this equation for every pixel, an apparent diffusion coefficient (ADC) map can be obtained. The diffusion value obtained is related to the actual diffusion value and contains contributions from other movement sources like micro-circulation in pseudo-random capillary systems, bulk flow and motion effects etc. Hence the intensity of each pixel is often referred to as an apparent value of diffusion and is proportional to the extent of diffusion. In an ADC image, bright regions (high ADC, e.g. CSF) will have water molecules which diffuse faster than those in dark regions (low ADC, e.g. grey matter). However, this ADC map is a representation of diffusion only in the direction of the applied gradient.

3.3.3 Diffusion Tensor

The information obtained from the above calculation is sufficient to represent isotropic diffusion. However for anisotropic diffusion, the direction of diffusion

(represented by the direction with maximum ADC value) is more informative in terms of determining fiber/axonal orientation. Three independent measurements along the x, y and z axes are not enough because fiber orientation is not always along one of these axes. To accurately find the orientation with the largest ADC, the concept of diffusion tensor is used [48].

According to this concept, measurements along different axes are fitted to a 3D ellipsoid (the ellipsoid representing average diffusion distance in each direction, not ADC). The properties of the 3D ellipsoid, namely, the length of the longest and two orthogonal axes (called eigenvalues, λ_1, λ_2, and λ_3) and their orientations (called eigenvectors, ν_1, ν_2, and ν_3) can be defined by six parameters. Therefore, ADC measurements along at least six axes are enough to calculate the ellipsoid (more measurements along other directions will improve the determination of the diffusion ellipsoid). To convert the measurement results (more than six ADC) to these six parameters, a 3 x 3 symmetric matrix called a tensor is used: (where each element of the matrix represents the component of diffusion in the direction given by its subscript)

$$D = \begin{bmatrix} D_{xx} & D_{xy} & D_{xz} \\ D_{yx} & D_{yy} & D_{yz} \\ D_{zx} & D_{zy} & D_{zz} \end{bmatrix}$$

Once the diffusion ellipsoid is determined, the information can be reduced to the vector of the longest axis (ν_1), which indicates the fiber orientation. To visualize these 3D vectors, a color coded orientation map is generated [49].

3.3.4 Parameters derived from DT-MRI

Trace or Mean Diffusivity:

Trace is sum of the three diagonal elements of the diffusion tensor (i.e. $D_{xx} + D_{yy} + D_{zz}$). Mean diffusivity is given by Trace/3.

Diffusion Anisotropy:

Diffusion anisotropy is a scalar measure which has been calculated in a number of ways. However, the common principle of these anisotropy indices is that they represent how much the diffusion ellipsoid deviates from a sphere.

Anisotropy Ratio (A_{ratio}):

The simplest anisotropic index is the ratio between the largest and smallest eigenvalue. If the diffusion tensor is isotropic, the anisotropy ratio will be 1.

$$A_{ratio} = \frac{\lambda_1}{\lambda_3}$$

Fractional Anisotropy (FA):

Fractional Anisotropy is a measure of fraction of the tensor that can be assigned to anisotropic diffusion. The numerator represents the variance of the three eigenvalues about their mean and the denominator represents the magnitude of the tensor. Thus fractional anisotropy is a normalized measure which takes values from zero (when diffusion is isotropic) to one (when diffusion is constrained along one axis only).

$$FA = \sqrt{\frac{3}{2}} \frac{\sqrt{(\lambda_1 - \langle\lambda\rangle)^2 + (\lambda_2 - \langle\lambda\rangle)^2 + (\lambda_3 - \langle\lambda\rangle)^2}}{\sqrt{\lambda_1^2 + \lambda_2^2 + \lambda_3^2}}$$

$$\langle\lambda\rangle = \frac{\lambda_1 + \lambda_2 + \lambda_3}{3}$$

In addition to these measures, other measures like relative anisotropy, volume ratio and skewness parameters obtained from diffusion data have been used previously [46].

3.3.5 Tractography

For many applications, the use of color labeling is useful for identifying specific WM tracts and visualizing their rough trajectories. An alternative strategy is white matter tractography (WMT), which uses the diffusion directional information given by the direction of the principle eigenvector (v_1) in every voxel. By viewing fiber orientation in one voxel and following a path of smooth transition in orientation from one voxel to the next, one can gain an impression of the trajectory of the major white matter pathways. WMT increases the specificity of WM pathway estimates and enables the 3D visualization of these trajectories, which may be challenging using cross-sectional color maps. Most WMT algorithms estimate trajectories from a set of "seed" points. Two classes of algorithms are available for WMT:

Deterministic Tractography Algorithms:

Deterministic or streamline WMT algorithms use the major eigenvector field to define the local trajectory directions at each step. The integration of deterministic

pathways may be performed using simple step-wise algorithms including FACT [50] and Euler integration. Continuous integration methods such as 2nd or 4th order Runge-Kutta [51], which enable more accurate estimates of curved tracts, are also commonly used.

Probabilistic Tractography Algorithms:

Probabilistic WMT algorithms are based upon some sort of iterative Monte Carlo approach where multiple trajectories are generated from the seed points with random perturbations to the trajectory directions [52, 53]. These algorithms create a distribution of tracts, which can be used to estimate the probability of connectivity for every voxel. The connection probabilities may be used as a surrogate measure of WMT confidence.

Irrespective of the type of algorithm used, basic thresholds must be applied while computing fiber tracts. One threshold is the FA parameter discussed above. For example if a voxel is entered with a low FA value, then the tracking process has probably led to an area of grey matter or CSF and should stop. Another threshold parameter is the angle between the primary eigenvector within that voxel and the equivalent vector in the neighboring voxels (i.e. once this angle exceeds a certain threshold, the likelihood that the neighboring voxel is connected by an actual WM tract is low).

3.3.6 DTI Applications

The main advantage of DTI is its ability to provide rich anatomical information about white matter – fiber integrity and fiber orientation. Although the white matter looks

homogeneous on a conventional MRI, it has a very complex structure and DTI is sensitive to this complexity. Before the invention of DTI, white matter anatomy studies were mainly based on post-mortem dissection or invasive tracing in animals. The ability to trace white matter pathways of the whole human brain has helped visualize how these pathways change with pathology including brain tumors [54], multiple sclerotic lesions [55] and vascular malformations [56]. Ultimately, this may be useful for surgical planning and provide useful information on locations of critical structures to avoid [57]. In addition to identifying pathology, WMT may provide useful insight about brain compensatory mechanism by visualizing reorganization following a disease, surgery or rehabilitation [58].

With respect to studies of aphasia and language function, tractography of the language anatomy can prove useful in understanding patterns of aphasia deficits. Using DTI with specific hypotheses concerning the connectivity of language networks, Catani and colleagues identified white matter tracts that extend not only between Broca's area and Wernicke's area (arcuate fasciculus) but also between Wernicke's area and the inferior parietal lobule and between the inferior parietal lobule and Broca's area [59]. This may suggest the existence of a parallel processing pathway via the inferior parietal lobule in addition to the arcuate fasciculus. Makris *et al.* have segmented the superior longitudinal fascicle (SLF) into four sub-components (the arcuate fascicle being one of them) and have suggested that investigating these different SLF components may increase specificity in investigations of structural-functional and anatomical-clinical characteristics [60]. Parker *et al.* have investigated the existence of two pathways from the primary auditory cortex (Wernicke's area) to the prefrontal areas (Broca's area) – a

dorsal pathway including the arcuate fascicle and a ventral pathway running anterior along the superior temporal gyrus – using DTI [61]. They have also showed stronger connections for both these pathways in the dominant hemisphere. In addition to isolating WM pathways connecting the classical language regions, special interest has also been in studying associations of white matter asymmetry with language lateralization [62-65] and individual cognitive abilities [66].

Quantitative measures obtained from DTI have served as useful markers in a number of patient studies. WM structures have also shown to serve as useful predictors of brain development. Using DTI, our goal is to track the underlying white matter structure and establish relationship with functional measures. Future studies can then evaluate whether or not these relationships or individual DTI measures can be used to predict brain reorganization in aphasia patients.

3.4 Resting State BOLD fMRI

A typical fMRI experiment consists of an experimental condition, which results in a neuronal response causing increased oxygen consumption, along with a baseline or "rest" condition. The MR image intensities of the experimental condition are then contrasted with recordings obtained during the rest condition to obtain a statistical measure which indicates how well the MR signal time-series explains the experimental task time-course. This seems to indicate that the quantification of the fMRI signal to a great extent depends on the appropriate definition of the baseline or the "rest" condition. This has led to increased interest of the neuroimaging community in characterizing

neuronal processes underlying the "rest" condition i.e. the state of the brain when the subject is doing nothing . But is the brain really doing nothing when we are in the "resting state"? If the brain is doing something, what is provoking this brain activity? Can we get any useful information from this resting state brain activity? These are some of the questions underlying the development of the low frequency resting state BOLD technique. The following discussion aims at answering these questions and reviews the resting state BOLD technique currently used.

The first evidence of brain activity during the rest condition was demonstrated by Ogawa *et al.* when they observed 2% fluctuations in the BOLD signal image intensities during the resting condition in between the experimental conditions [67]. Weisskoff *et al.* supported this finding by showing that the resting state BOLD fMRI signal frequency spectrum had signal characteristics in addition to the cardiac and respiratory related signals [68]. Finally, Biswal *et al.* were the first to show that in the absence of external stimuli, the bilateral primary motor cortices had synchronous low frequency BOLD signal oscillations and were functionally connected [69]. The BOLD signal oscillations during resting state were shown to take place in the frequency range of 0.012Hz to 0.1Hz. A number of studies have investigated the cause for origin of these low frequency BOLD fluctuations. While initially these fluctuations were thought to be associated with physiological noise , vascular modulation, cardio-respiratory motion or MR artifacts [70], a number of careful studies have ruled out these possibilities and shown these fluctuations to be of neuronal origin [71-74]. Subsequent studies were able to show functional connections using these low frequency BOLD oscillations for other sensory modalities as well [75, 76].

The theory of "default mode" of brain function was first proposed by Raichle *et al.* from observations from a PET study [77]. They suggested the existence of a network of brain regions during the rest condition which show signal attenuation during goal-directed tasks. Another study by the same group have attributed the main components of this network to self-referential mental activity [78]. Fransson readdressed this "default mode" hypothesis using the low frequency BOLD fMRI oscillations [79]. Fransson's study not only supports the existence of this *introspectively oriented* "default mode" network, but also suggests an existence of a second *extrospectively oriented* attention network which interrupts the default mode network on a routine basis. Most of the above studies have been limited because of the use of a region of interest cross correlation approaches which are driven by certain hypotheses. Using data driven independent component analysis (ICA), a variety of different coherent resting state networks have been shown to be simultaneously extracted [80-82]. Using a probabilistic ICA approach, Damoiseaux *et al*. have identified up to 10 functionally relevant patterns, associated with cognitive and sensory processing in addition to the "default mode" network, and which are consistent across subjects and sessions [81].

The primary advantage of resting state fMRI is its ability to map functional connectivity over the entire brain without the need of an experimental task. As highlighted by Xiong *et al*. [83], functional connectivity analyses in studies relying on an experimental task, to a great extent are dependent on: 1. the brain regions engaged in performing the task; 2. the degree of detection of this engagement which depends on the difference between the task and control states in the experiment; and 3. variability of degree of engagement of different brain regions. This means that task induced functional

connectivity analyses may be an underestimate of the size and number of areas involved in task performance and may not reflect true anatomical connectivity. Resting state functional connectivity analyses, on the other hand are more likely to detect all neural network components related to a particular brain region. The absence of a consistent task performance over all subjects however may introduce an unidentified, uncontrolled task bias when interpreting single subject data due to a wide range of unfocussed chaotic cognitive and sensory processes taking place in the brain during rest. This effect however would average out when interpreting results from a group of subjects. In addition, careful subject instructions before data collection could also help minimize these unfocussed processes. Although resting state fMRI surpass the task fMRI in terms of correlations between spatially remote neurophysiologic events i.e. *functional connectivity*, they do not imply how these correlations are mediated i.e. *effective connectivity* [84]. Effective connectivity maps between brain activations is commonly obtained in task fMRI data sets using methods like Dynamic Casual Modeling (DCM) and Structural Equation Modeling (SEM) [85].

Resting state fMRI to date has shown to have application in investigating the effect of disease and/or medication on the brain. There have only been a few attempts to use resting state fMRI to study functional connectivity in stroke and aphasic patients [86]. It would be interesting to evaluate the full potential of this technique in studying functional reorganization of patients with therapy. Not having to perform a task may serve as a significant benefit in studying aphasic patients who are limited in performing treatment evaluation tasks. One of the goals of this dissertation research is to evaluate the potential of resting state fMRI in studying functional reorganization.

Chapter 4

Background: Electroencephalography and Brain Function

Electroencephalography (EEG) is a procedure that measures electrical brain activity through the skull and scalp. It is the difference in voltage between two different recording locations plotted over time. EEG reflects thousands of simultaneously ongoing brain processes and the brain response to a certain stimulus or event of interest is not visible by simply analyzing a continuous EEG. However, time-locking EEG epochs to the onset of stimulus and averaging these epochs over trials, have shown to improve the sensitivity of EEG to particular cognitive effects in response to the stimuli. These time-locked signal averages are called event related potentials (ERP). An ERP waveform is thus a time-series of scalp voltages (usually in the range of microvolts) over time (in range of milliseconds), where fluctuations in voltage (N400, P600 etc) provide information regarding the brain function of the subject. Contemporary ERP studies typically record EEG from multiple scalp electrode sites, thereby giving ERP data a spatial parameter (topographic mapping) which complements the temporal or frequency information intrinsic to time-series data. By quantifying the ERP data in this spatio-temporal domain, questions of interest concerning how cognitive and electrophysiological states change over time can be answered.

Interpretation of these recorded ERP waveforms require an understanding of what sources generate these potentials and how these potentials are mediated from inside the brain to electrode sites on the scalp. ERPs are essentially inhibitory and excitatory postsynaptic potentials of the pyramidal cells generated in the cortex of the brain. This

signal which arises from thousands of synchronized pyramidal cell postsynaptic potentials is greatly modified by the time it reaches the recording electrode on the scalp. The major factors modifying the original signal are:

- The electrical conductivity properties of tissues which lie between the electrical source and the recording electrodes (e.g. brain parenchyma, CSF, skull, scalp).
- The electric field generated by the source and it's orientation with respect to the recording electrode (i.e. to what extent the generator is aimed towards the electrode).
- The conductive properties of both the recording electrodes and the scalp-electrode interface (size of electrodes, electrical properties of the electrodes etc.).

Understanding how current flows from the source to the electrode (also called volume conduction) is required for estimating the location of these sources. For any scalp recorded EEG signal, there are an infinite number of possible source distributions within the brain volume which can explain or 'fit' the scalp recorded signal i.e. one or more generators in different locations in the brain can produce the same EEG finding. This means that it is theoretically impossible to know the location of the EEG generators in the brain with only scalp recorded EEG information (also known as the *inverse problem*). By adding constraints based on anatomical and physiological information, and assumptions about the nature of sources (like small focal sources or temporally uncorrelated sources) the solution space for these sources can be dramatically reduced. Estimating anatomical information of neuronal activity using electrophysiological data and above listed

assumptions is called source analysis. Details about source analysis are given in the next section.

4.1. Source Analysis

The analysis of neural sources relies on the solution of two fundamental problems. The *forward problem* concerns calculation of scalp potentials given the neuronal currents in the brain, whereas the *inverse problem* involves estimating neuronal currents from EEG data. The basic question posed by both these problems is how to model any neuronal activation so that the source of the electric field can be mapped from the observed EEG signal.

The forward problem is solved by specifying a set of conditions – compartments, surfaces, conductivities for the head model, also referred to as forward model or volume conductor. The forward model essentially allows projecting a source or source network through modeled compartments and tissue interfaces to reach the electrode surface and provide an estimate of electric signals at the electrodes. Often multiple spherical shells modeling the brain surfaces or more complex four layered realistic models with compartments such as brain, cerebrospinal fluid, skull and scalp surfaces segmented from the patient's MRI scan are used to model the forward problem. For a specific electrical source, the forward model will enable the computation of a specific potential field at its surface, thus resulting in a unique solution. For example, the *i*-th source can be modeled with a simple equivalent current dipole $\mathbf{q_i}$, uniquely defined by: location represented by vector r_i, strength q_i, and orientation coefficients θ_i. For K such simultaneously active

sources at time *t*, the observed EEG signal at the electrode x_j positioned at p_j can be modeled as:

$$x_j(r_i, q_i, t) = \sum_{i}^{K} G(r_i(t), p_j) \cdot q_i(t) + \varepsilon$$

where *G* is a function which relates each dipole and its contribution to the potential observed at the *j*-th electrode; and ε represents the electrode noise. The function G is calculated using the parameters of the forward model and electrode location.

In contrast to the forward problem, the inverse problem has no unique solution. As described above, an infinite number of source permutations can be found to explain a specific potential field recorded at the surface. To make this problem solvable, a number of mathematical constraints are incorporated into inverse modeling algorithms. Two main inverse modeling approaches used are dipolar and distributed modeling methods.

Dipolar methods assume the existence of one to three dipoles and attempt to determine the dipole parameters which best fit the measured data. Clearly, the dipolar method is over determined, in the sense that there are far more data sampling points (electrodes) than there are dipole parameters in determining the solution. Two commonly used dipolar inverse algorithms are moving and rotating dipoles. For a particular instant in time, the moving algorithm allows a dipole source freedom in space to assume location, orientation and strength to best explain the measured EEG data at that instant. The rotating algorithm on the other hand constraints the dipole to a location in space with freedom of orientation and strength to explain the variance in the measured data across any time interval.

In contrast to the dipolar methods, the distributed models make no assumption on the number of dipoles to solve the inverse problem. Instead they assume that there are simultaneously active multiple sources across multiple locations at a given instant of time. The predefined solution space (whole brain or even just the cortical volume) is split into multiple points, each representing a mini dipole, fixed in space but free to assume any orientation and strength. Using this mini dipole network the best source configuration to explain the measured data is determined. Theoretically many solutions are possible for any measured EEG signal and unique solutions are often achieved using post processing constraints. Current density methods like minimum norm least squares (MNLS) and low resolution electromagnetic tomography (LORETA) are commonly used distributed inverse algorithms with different constraints. Inverse problem for current density methods can be represented as:

$$\Delta^2 = D(j) + \lambda M(j)$$

$$D(j) = \| Gq - m \|^2$$

Here the product term *Gq* gives the forward calculated data vector, while *m* is the real measured data. The data term *D(j)* is essentially a measure of the goodness of fit between the predicted and measured data. *M(j)* is model term which provides constraints to obtain a unique solution. λ is regularization parameter which links the model term to data term *D(j)* and serves to achieve equilibrium between goodness of fit and closeness to the model. If λ is very large, the model term dominates and large reconstruction errors may occur, whereas if λ is very small, chaotic source distributions are reconstructed which mainly explain the noise in the data. The optimal value of λ is calculated using the χ^2

criterion which relies on the assumption that a reasonable Δ^2 is in the order of the amount of noise in the data (other methods like L-curve criterion have also been used for estimating λ [87]). The ultimate goal of the algorithm is to determine a reliable estimate of the regularization parameter and the model term by minimizing the variance Δ^2. Different current density methods depend on how the model term is defined. In case of MNLS, the model term used is estimated to be proportional to the square of the strength of the reconstructed currents i.e. the energy (integral of the squared current density) of all source currents is minimized. In the LORETA method, the modeling constraint is on the smoothness of the intensity profile of the reconstructed current density distribution i.e. it makes an assumption that neighboring sources are more likely to undergo synchronous depolarization during an evoked response.

4.2. Applications of ERP in studying language function

The earliest ERP studies in language production have focused on locating and verifying association of various components generated during simple word production [88, 89]. Using a simple picture naming task and a non-semantic picture rotation task, Stuss *et al.* [88] were able to show that the negative peak between 300 and 500ms (also called N400) for naming pictures as compared to viewing controls is associated with semantic processing in picture naming. The more recent ERP studies have mainly concentrated on estimating the time course and chronological order of various stages involved in language production. Most of the tasks used in these studies have been *go-nogo tasks* which make use of the concept of generation of a lateralized readiness

potential (LRP) [90] which is associated with response preparation and the N200 component which is associated with response inhibition as markers for different stages. The onset/presence of LRP indicates that the information required in deciding whether a response needs to be given or not is being processed; while the N200 effect is considered as a marker that this information has been already analyzed. For example, Van Turennout *et al.* used three versions of the go-nogo tasks and LRP to study temporal properties of semantic and phonological encoding in speech production [91]. By interchanging the roles of semantic and phonological information in making the go-nogo decisions, they found that semantic information is encoded about 120ms before phonological information. In another LRP study, the same group found that syntactic processing takes place about 40ms before phonological encoding [92]. Using N200, Rodriguez-Fornells *et al.* studied the relative time courses of semantic and phonological processing during both language production and comprehension and concluded that although the two language tasks showed the expected differences in order of semantic and phonological processing, they differed in terms of temporal distance between the engagement of the two processes [93]. In case of verb generation, Rowan and colleagues used both ERP and fMRI to show that semantic retrieval related recruitment of the temporal and frontal areas are spaced in time. They found that the recruitment of temporal areas preceded the frontal regions [94]. Language ERP studies of semantic processing have been mainly based on studying N400 effects by semantic priming or semantic violation in sentences. A review of these studies can be found under the language comprehension section in Chapter 2.

A number of studies have shown temporal features from EEG related to language function. Some of these features have been used as markers of intactness of semantic

processing. It would be interesting to evaluate if these features change with brain reorganization following stroke. Along with functional MRI, these markers could help improve our understanding of language function in healthy and aphasic subjects.

Chapter 5

Scope of Research

Over the past two decades, a number of neuroimaging modalities have shown useful potential in studying brain dynamics. In particular in aphasia, a thorough understanding of how the brain compensates with disease and attempts to reorganize itself can help neurologists strategize and evaluate rehabilitation therapies to improve outcomes of these patients. This dissertation contributes to developing and evaluating a multi-modality neuroimaging tool with potential application in studying and understanding brain function deficits and brain functional reorganization in aphasics.

The principal hypothesis for this dissertation is that a multimodality neuroimaging approach will allow for a better understanding of neural dynamics of reorganization. Each neuroimaging modality by itself is limited by the nature and extent of information it can provide. A single neuroimaging modality that can help us understand and study all brain dynamics in a noninvasive manner is yet to be developed. This has resulted in using of more than one modality and multimodality fusion approaches gaining popularity among researchers and clinicians. This dissertation uses Functional MRI (fMRI), Event Related Potentials (ERP), Diffusion Tensor Magnetic Resonance Imaging (DT-MRI) and Resting State MRI techniques in a multimodal fusion approach to complement each other in understanding neural dynamics. The development and evaluation of this multimodal approach is done using a series of sub-hypotheses formulated within the following five specific aims. Each of these specific aims will be addressed in a separate subsequent chapter.

Specific Aim 1: Development of language task protocol for fMRI and ERP testing.

In order to identify brain regions recruited for language function and study how the brain adapts to functional loss, language tasks need to be developed. Task difficulty modulations in functional tasks including language have shown to better highlight language functional regions. In this section, two language production tasks and one semantic decision-making comprehension task, to be used with fMRI and ERP and with inherent task difficulty modulation, will be developed. Stimuli for these tasks will also be evaluated.

Rationale: A battery of language tasks including picture naming, verb generation and comprehension will help to study different functional architectures related to different types of language processing. Modulation of task difficulty can be identified from task response times.

Specific Aim 2: Evaluation of task difficulty in picture naming and verb generation.

The effect of task difficulty, investigated in a number of cognitive tasks, has shown increases in functional recruitment with increase in difficulty. Most of these studies have defined task difficulty in an objective sense. In this work, a subject-specific definition of task difficulty will be evaluated as compared to a commonly used objective definition of difficulty. Individual subject variability in task difficulty will also be quantified and changes in functional organization in language task difficulty with age will also be evaluated.

Rationale: A subjective definition of task difficulty will be more suitable in studying language function in aphasic stroke patients, where one would expect a large degree of variability in task difficulty from subject-to-subject and with age.

Specific Aim 3: Integration of fMRI and ERP to study language function and task difficulty.

Hemodynamic-based imaging modalities like fMRI, PET or near infrared optical imaging are known to provide good spatial resolution for mapping functional activity. With the most efficient designs, a maximum temporal resolution of 1s can be achieved with these modalities. Electro-magnetic based modalities like ERP or MEG on the other hand provide excellent temporal resolution on the order of 0.001s but are limited in terms of their spatial localization. This specific aim will serve to combine spatial information of fMRI with temporal information from ERP by modeling the conductive current source distribution in the head and using a source constraint approach.

Rationale: fMRI and ERP together can provide better understanding of brain dynamics in functional activation and reorganization

Specific Aim 4: Study White Matter (WM) Connectivity and Structure-Function Associations.

Over the past few years DT-MRI has evolved as a potential diagnostic tool. WM changes have been correlated with disease progression or reduction and also with cortical functional activations. The purpose of this aim is to optimize DT-MRI to study WM

connectivity, develop an automated algorithm to map WM fiber tracts associated with GM activations and establish DTI quantitative markers of functional reorganization.

Rationale: Both qualitative and quantitative structure-function relationships could be useful markers to study functional reorganization and responsiveness to aphasia therapy.

Specific Aim 5: Study and evaluation of functional connectivity and low frequency fluctuations in resting state brain activity with BOLD fMRI.

Low frequency fluctuation BOLD fMRI signal changes (0.012-0.1Hz) in the resting brain has shown potential to study functional connectivity without the use of a functional task in both healthy and patient populations. This specific aim will serve to establish language resting state functional connectivity between various brain regions. Functional seeded correlation approach and data driven independent component analysis (ICA) approaches for connectivity markers will be investigated.

Rationale: Resting state BOLD fMRI could obviate performance of functional task to establish functional connectivity which would have particular implications in functionally challenged aphasic patients. Resting state connectivity could be used as a marker for evaluation of responsiveness to aphasia therapy or to study functional reorganization.

Chapter 6

Development of Language Task Protocol for fMRI and ERP testing

6.1 Introduction

Different language tasks highlight different functional architectural organizations in the brain depending on the nature of the language processing initiated. Picture naming and verb generation, two widely used language tasks with healthy and patient populations, recruit the word generation functional architecture of the brain [2]. On the contrary, language comprehension tasks with semantic/non-semantic choices will recruit the brain regions involving language semantic decision making. This distinction highlights the need for using more than a single task to study different functional aspects of language processing. A battery of language tasks including picture naming, verb generation and language comprehension will help investigators study different functional architectures related to different components of language processing.

Our hypothesis is that task difficulty in both the objective and subjective sense maybe an important factor in studying functional organization as compared to the traditional task and baseline subtraction methods. The ambiguous nature of brain activity in response to different baseline conditions may be the main reason for discrepancies of results of functional organization previously seen in the literature [95]. We propose that the difficulty in performing a simple task like picture naming or verb generation can be estimated from the total time required to perform the task. Stimulus evaluation for selection of the most appropriate stimuli which can effectively define task difficulty is

required. This would help standardize the task over a population of subjects and patients. Also, one of the specific aims of this thesis is to combine fMRI and ERP modalities for a better understanding of brain dynamics involved in language processing. The most important underlying assumption in fMRI-ERP fusion studies is that the response collected using either modality is from the same neural generators. This accentuates the need for a common design for the two modalities. The goal of this chapter was to develop neuroimaging tasks appropriate for both fMRI and EEG neuroimaging modalities, with stimuli chosen to vary over a range of difficulty appropriate for both healthy and patient populations.

6.2 Methods

6.2.1 Stimuli

Picture Naming Task:

The picture stimuli for the task consisted of line drawings taken from the Peabody Picture Vocabulary Test [96], a common test used with aphasia patients. A total of 200 pictures were collected. The control stimuli for the task were generated by scrambling some of the picture stimuli to match the majority of stimuli for size and shape. Scrambling was done to the extent of minimizing the possibility of any mental unscrambling.

Verb Generation Task:

The stimuli for the verb generation task consisted of common nouns for which an associated verb can be generated. A total of 150 noun stimuli were obtained from a word frequency database [97]. The control stimuli for the task consisted of unpronounceable non-words consisting of vowels only and matched for length with the nouns.

Language Comprehension Task:

The language comprehension task was divided into 4 categories: a. animal and non-animal; b. edible and non-edible; c. professions requiring college education and those which do not; and d. recreational and non-recreational activities. A list of stimuli for each category and subcategory was generated and was first screened for agreement in categorization by 10 individuals. Only those stimuli with 100% categorization agreement were used for behavioral testing. Unpronounceable non-words generated using vowels and matched for length with the category stimuli were used as control stimuli.

6.2.2 Behavioral Tests

A group of 10 individuals underwent a behavioral study to test the stimuli from the three tasks. All stimuli except for the control stimuli were used for behavioral testing.

Picture Naming Task:

Each individual was subjected to the entire picture stimulus set; one picture presented at a time and instructed to covertly generate a name for the picture on the screen. Subjects were instructed to press a button on a response pad as soon as but only after they had mentally named the picture. The response time for each picture was

measured from the onset of the picture presentation until the time of the button press. For pictures not named, no reaction time was assigned.

Verb Generation Task:

Similar to the picture naming task, each individual was subjected to the entire noun stimuli set, one noun at a time. Individuals were instructed to covertly generate a verb associated with the noun displayed and press a button as soon as they had generated the verb. Response time for each noun was measured as above.

Language Comprehension Task:

Individuals were presented each of the above 4 categories, one category at a time. Each category consisted of a question followed by the list of both the subcategory options in random order, each option displayed one at a time. For example, the category question "Which of the following is an animal?" was followed by the following options: zebra, pencil, cube, cheetah, and so on. For the option displayed, individuals answered the question by thinking either "Yes" or "No" and pressed a corresponding button. Response times were measured from the onset of the option to the time of button press.

6.3 Results

6.3.1 Behavioral Data

The reaction times for each stimulus from the behavioral tests were averaged over all individuals. The plots below summarize the results from this study (Figures 6.1-6.3).

For the picture naming and verb generation task, the absicca represents the reaction time bins and the ordinate represents the total number of stimuli in each bin. Group 1 and Group 2 represent our apriori classification of easy and difficult stimuli. For the picture naming task, stimuli with reaction times between 0.4s and 0.6s were classified as *"easy to name"*, whereas stimuli between 0.6s and 1.1s were regarded as *"difficult to name"* picture stimuli. Stimuli with reaction times less than 0.4s or greater than 1.1s were regarded as too easy or too difficult and were excluded. For the verb generation task, nouns with reaction times between 0.6s and 1.1s were regarded as *"easy to generate verb for"*, and those between 1.3s and 1.8s were regarded as *"difficult to generate verb for"*. Stimuli with reaction times greater than 1.8s were regarded as too difficult and excluded. Stimuli with reaction times between 1.1s and 1.3s were excluded to obtain sufficient separation between the easy and difficult stimuli types.

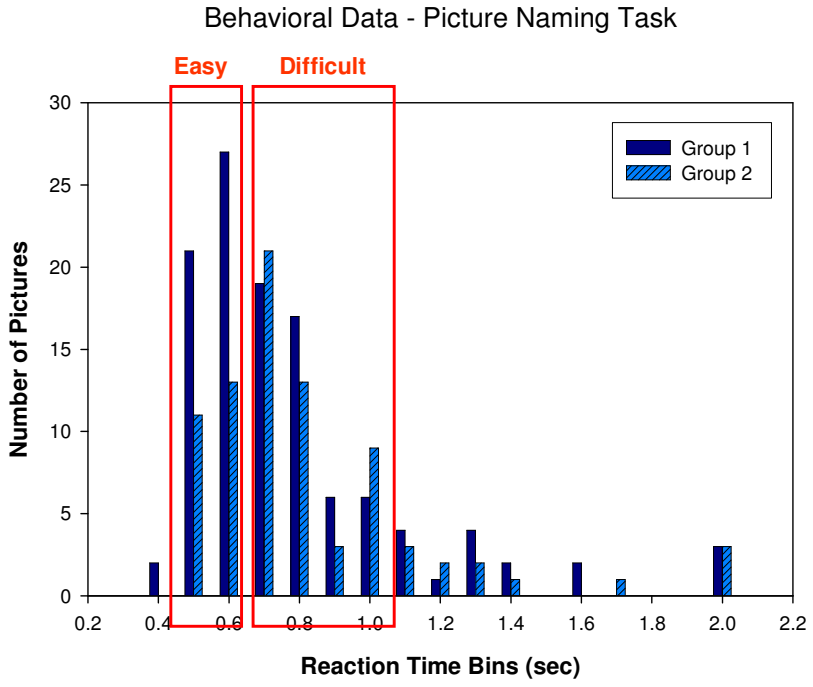

Figure 6.1: Reaction time classification of stimuli for picture naming task. Red boxes indicate the time window of the stimuli selected. Group 1 & 2 represent our apriori classification of easy and difficult stimuli.

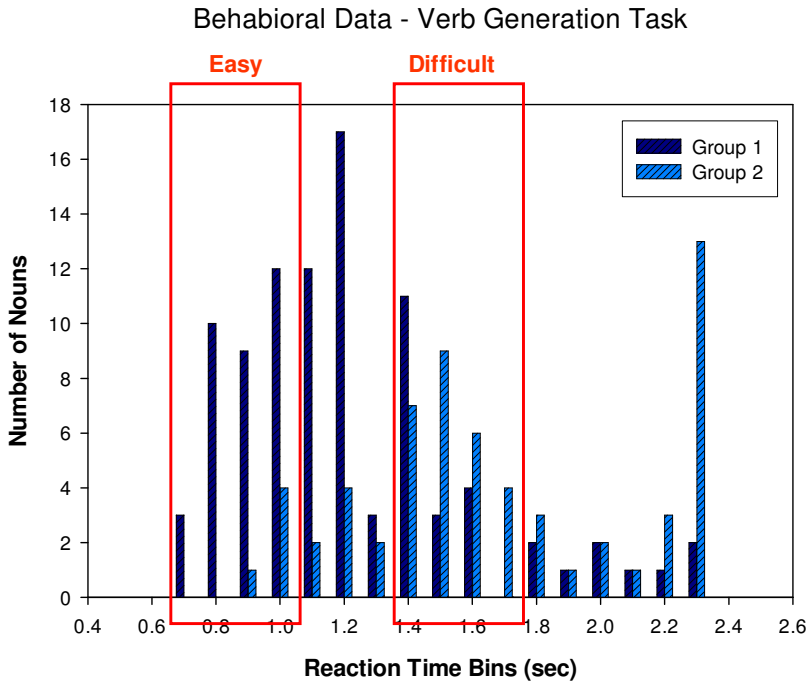

Figure 6.2: Reaction time classification of stimuli for verb generation task. Red boxes indicate the time window of the stimuli selected. Group 1 & 2 represent our apriori classification of easy and difficult stimuli.

For the language comprehension task, the absicca represents stimuli categories and ordinate represents reaction time in seconds (Figure 6.3). This task is different from the above two tasks and individual stimuli were not classified, only the general categories. Based on the reaction times, the "animal/non-animal" and the "edible/non-edible" categories were regarded as *"easy to comprehend"* categories whereas the "professions requiring college education or not" and the "recreational/non-recreational activities" were regarded as the *"difficult to comprehend"* categories.

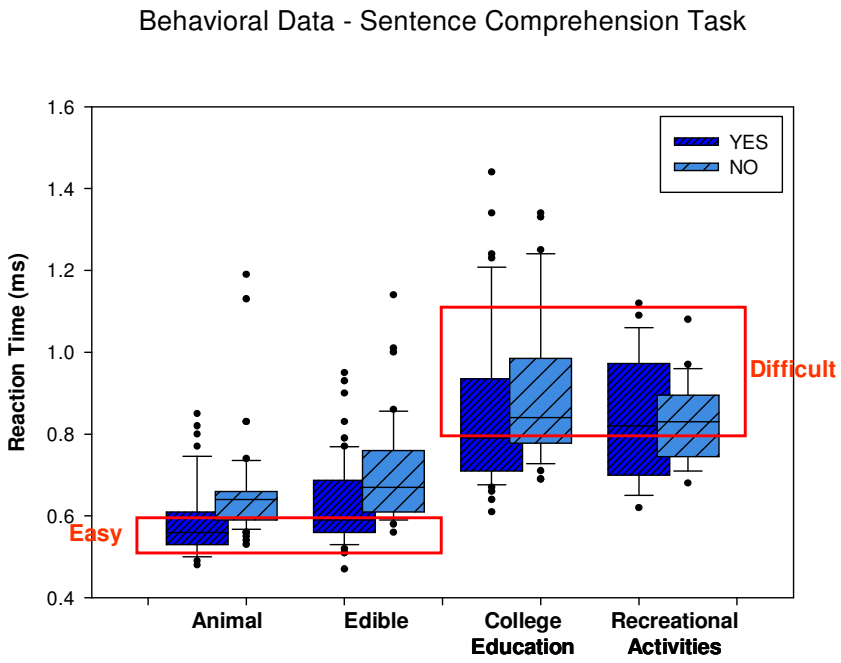

Figure 6.3: Reaction time classification of stimuli for language comprehension task. Red boxes indicate the time window of the stimuli selected.

6.3.2 Task Design

To allow retrospective categorization of task difficulty, an event related design would be required to separate trials based on their reaction times. Also using a jittered form of event related design would be a better suited approach for fMRI analysis for estimating dynamics of the hemodynamic response and at the same time retaining the inherent nature of ERP designs. Keeping this in mind, the tasks in our research were designed as follows. Each task had two runs in both fMRI and ERP sessions.

Picture Naming Task:

A jittered event related task design [98] was generated using the OPTSEQ2 program [99]. Each task run consists of 34 picture stimuli (17 from the "Easy to name"

and 17 from the “Difficult to name” category) and 13 control stimuli. The picture stimuli were not repeated within or between the runs. Each stimulus was displayed for 3s with an inter stimulus interval (ISI) varying from 1 to 12s. A fixation cross was displayed during the ISI. The total duration for each task run was 3min 12s.

Verb Generation Task:

The task design for the verb generation task was exactly the same as the picture naming task. Similar to the picture naming task, each task run consisted of 17 “easy to generate verb” nouns, 17 “difficult to generate verb” nouns and 13 non-words. Each task run was 3min 12s long.

Language Comprehension Task:

The language comprehension task had a mixed type of design i.e. a block design with events randomized in each block [98, 100]. Each run of this task consisted of 8 blocks: 4 category blocks (one block for each category) and 4 control blocks. Each category block had a category question (displayed for 6s) followed by a list of 10 subcategory options (each option displayed for 1.8s and with an ISI of 0.4s). Similar to the behavioral testing, subjects were instructed to covertly answer the category question with “Yes” or “No” and press a button for the corresponding answer. Each control block, like the category block, consisted of an instruction to view a list of 10 non-words and to press either button after each non-word. The duration of each block was 28s with the total duration of the task equal to 3min 44s.

6.4 Discussion

The behavioral study enabled evaluation of the entire stimuli set for all the language tasks. Using the behavioral study results, the stimuli set for picture naming and verb generation tasks were trimmed to remove too easy or too difficult stimuli and at the same time to provide sufficient separation between the categories of stimuli and enable observation of functional task difficulty differences using fMRI and ERP.

Chapter 7

Evaluation of Task Difficulty in Picture Naming and Verb Generation Tasks

7.1 Introduction

Both picture naming and verb generation have been extensively studied, both from a behavioral and a functional viewpoint [5, 94, 101-108]. The focus of these studies has been to revalidate cortical activation patterns using different functional imaging modalities; study different components of the language production processing stream; assess intersession-intersubject variability, age related changes and differential activation patterns between the two tasks. Some discrepancies in results between language function studies have also been observed. While some picture naming studies show that the classical language areas, the Broca's and Wernicke's areas, are not activated in simple picture naming [108, 109], there are numerous studies which have demonstrated activation in these regions [102, 110]. These discrepancies might be related to the different nature of baseline conditions used, the exact task used (e.g. simple naming, go/no-go tasks, identification of specific object properties), the presentation and/or training used (e.g. first time presentation vs. repeated presentation) and the level of task difficulty. Simplicity, ease of performance and an extensive background available on both these tasks, make them an attractive choice for a task battery designed to evaluate brain plasticity in aphasia patients.

With studies of brain function, including picture naming and verb generation, an important confound most often neglected is the individual difference in difficulty of performing a particular task. These differences in difficulty vary over a wide spectrum and are dependent on a number of factors like education, age, social background and health history of participating subjects. Most often this variability is controlled by careful screening of participants and designing simple tasks which can be standardized for function over subjects. Studies investigating effects of task difficulty over a number of paradigms [111-114] have observed a general brain activation increase with task demand [113-115]. These studies have defined task difficulty in an objective sense, either using some logical separation between easy and difficult tasks [114, 116] or ensuring correct categorization based on apriori collected behavioral data [112, 117]. There have also been a few studies which have explored subjective measures of task difficulty, correlated with functional activation [115, 117]. An obvious advantage of using a subjective definition of difficulty is its ability to categorize individual variability.

This inter-subject variability is a more prominent issue in stroke patients, where the nature and extent of recovered language function depends on 1) the functional architecture of the premorbid brain [25], 2) the degree of spontaneous recovery as well as the location of compensatory recruitment, and 3) the extent of the stroke-induced lesion [35, 40]. Understanding of how task difficulty is affected by stroke is critical to make any conclusions with respect to the nature of language recovery in these patients. This also demands for a reliable measure of task difficulty in language function.

The goal of this chapter was to demonstrate task difficulty-related activation effects in picture naming and verb generation using fMRI and ERP. Subject-specific task

reaction times, as a subjective measure of task demand, to predict level of language related functional activation, were evaluated. The effect of age on task difficulty effects was also studied.

7.2 Methods

7.2.1 Subjects

Ten young (5 male, 5 female; mean age = 24.4 ± 6 yrs) and ten old (5 male, 5 female; mean age = 57.8 ± 9 yrs) healthy adult subjects were recruited for this study. All subjects were native English speakers and had no history of neurological disease or stroke. Right-handedness was confirmed for all subjects with the Edinburgh Handedness Inventory [118]. The study was approved by the Institutional Review Board of Stony Brook University, and all subjects provided informed consent prior to participating. The study protocol consisted of two sessions: a functional MRI session and an electroencephalography session with the same functional tasks. The two study sessions, however, were performed at least one week apart, and were counterbalanced so that half of the subjects viewed the functional stimuli once before participating in the fMRI session. All subjects completed the fMRI session, while eighteen of the twenty subjects completed the EEG session (one subject decided not to participate in the EEG section and EEG data for one subject was unuseable due to technical problems in data collection).

7.2.2 Functional Tasks

Subjects completed 2 runs of all the three language tasks described in the previous chapter in each session of the study. The data from the picture naming and verb generation tasks are presented in this chapter. Similar to the behavioral study, subjects covertly generated a name for each picture or an action verb associated with each noun. Control stimuli were passively viewed without attempting a covert response. Subject responses were collected and reaction times calculated for each stimulus. Stimuli for which the task was not performed (i.e. no button press was recorded) or reaction times were longer than the 3 second stimulus presentation were assigned a zero reaction time. This check prevented the overlap of reaction times from consecutive stimuli. Recorded reaction times were used to categorize the entire set of picture or word stimuli into "Easy" and "Difficult" items. Stimuli with reaction times less than the median reaction time for that subject were labeled *"Easy"* and stimuli with reaction times greater than the median were labeled *"Difficult."* To ensure sufficient separation between the "Easy" and "Difficult" categories, three stimuli with reaction times above and below the median were not included in the analysis.

7.2.3 Functional MRI

7.2.3.1 Imaging Parameters

Functional images were collected on the Philips Achieva 3T MR Scanner at Stony University Hospital using an eight channel SENSE head coil. An echo planar imaging sequence with the following parameters was used: TE/TR = 30/2000 ms, flip angle = 90°,

SENSE factor 2, scan matrix = 64*64 and a field of view of 20cm. Thirty contiguous 4mm transverse slices were used to cover the entire brain. A total of 96 frames were collected for each session. The functional task was programmed using EPRIME software (Psychology Software Tools, Inc.) and was run using a computer outside the scanner room. Task instructions and stimuli were projected onto a screen at the back of the magnet bore from a projector inside the MR scanner room. Subjects viewed the screen from a mirror positioned above the head coil. To minimize subject movement, the subject's forehead was secured with tape to the base of the coil.

7.2.3.2 Data Analyses

Data Preprocessing, Single Subject and Random Effects Analyses:

All fMRI preprocessing and statistical analyses were done using the statistical parametric mapping package (SPM2) (Wellcome Department of Imaging Neuroscience; http://www.fil.ion.ucl.ac.uk/spm). The first four volumes of each scan were discarded to account for the signal reaching equilibrium. Motion correction was first performed by realigning all the raw functional volumes to the first volume of each scan. All subjects showed correctable motion artifacts with motion within 3mm in any direction and 3 degrees of rotation and hence were retained for further analysis. Sinc interpolation was then applied to correct each scan for differences in slice acquisition times by temporally realigning all volumes to the middle slice. Next, functional scans were registered to MNI (Montreal Neurological Institute) space using the EPI template provided with SPM. An

affine transformation with a set of 7 x 8 x 7 basis functions was used to spatially normalize the data into 3 x 3 x 3 mm^3 voxels [119]. The normalized images were then smoothed with an isotropic 8mm full-width half maximum (FWHM) Gaussian kernel.

Individual subject data were modeled using a General Linear Model (GLM) [120] on a voxel by voxel basis (first level analyses). For both tasks, easy, difficult, control and invalid event types were modeled. Invalid trials were those with either no button press or reaction times greater than 3 seconds and stimuli with RT in between the easy and difficult event types. In addition, the six movement parameters from the realignment stage were entered as regressors in the design matrix. A session-wise grand mean scaling of all voxels and a high pass filtering of 1/128Hz was applied. The BOLD response for each event type was modeled using the canonical hemodynamic response function (HRF) and its temporal and dispersion derivatives. T-contrast maps for each subject were generated from the amplitude of the HRF using all pictures (or nouns) vs. control, difficult vs. easy and easy vs. difficult contrasts.

First level contrast images were entered into a second-level random effects analysis done separately for each age group using a one sample t-test. An uncorrected threshold of $p<0.001$ and > 10 contiguous-voxel clusters was used to extract the group statistic functional maps for all pictures/nouns vs. control (difficulty independent) contrast and a less conservative threshold of $p<0.005$ and > 10 contiguous-voxel clusters was used for difficult vs. easy and easy vs. difficult (difficulty dependent) contrasts. While use of an uncorrected threshold can lead to false positives and care should be taken in interpretation of the results, the uncorrected threshold was used for an initial *qualitative* assessment of functionally active regions only.

Region of Interest (ROI) Analyses:

All ROI analyses were performed using MARSBAR [121]. Based on previous language functional neuroimaging studies [122, 123], the following *apriori* cortical ROIs were used (left and right): BA 44 (pars opercularis), BA 45 (pars triangularis), BA 47 (pars orbitaris), inferior temporal gyrus (ITG), middle temporal gyrus (MTG), superior temporal gyrus (STG), supramarginal gyrus (SMG), angular gyrus (AG) and the anterior cingulate cortex (ACC).

ROI analysis was performed using functional localizer ROI's (fROI) [124]. All stimuli, irrespective of difficulty level or reaction time, were used to define the fROI, as follows: The WFU Pick Atlas tool [125] and the Anatomical Automatic Labeling Atlas [126] were first used to select the anatomical ROI. Next, subject-specific fROI's were defined from functionally activated clusters within the anatomical ROI, with a threshold of $p<0.05$, uncorrected for multiple comparisons. Within the fROI, the principal eigenvariate was used to extract the percent BOLD signal change values (%BOLD). The principal eigenvariate was used, as opposed to the mean BOLD signal, to account for the spatial inhomogeneity of the BOLD response and minimize dilution of signal within the fROI [124]. Hemodynamic responses for all the stimuli types (i.e., easy, difficult and control tasks for both PN and VG) were also generated. Fitted evoked responses, peak latency and peak half width (FWHM) were calculated. A repeated measures analysis of variance (ANOVA) with age group as a between subjects factor was used to evaluate significant task difficulty differences and age related associations in the %BOLD, peak latency and FWHM between the easy and difficult conditions.

Linear Mixed Model Analysis to evaluate effectiveness of reaction time categorization:

To evaluate the effectiveness of using individual reaction times for categorization of task difficulty, a separate analysis using the data from the young group of subjects and comparing two types of categorizations of task difficulty was done: 1) categorization based on individual subject reaction times (subject-specific RT) and, 2) apriori categorization based on reaction times for each stimulus averaged over the young group of subjects (group-averaged RT). As the young group of subjects showed the maximum task difficulty effect using the ROI analysis for VG, data from only this group was used for comparison of task difficulty categorizations.

Separate GLM analyses were used to model the individual subject data for each type of categorization. GLM analyses used the same methodology described above. Items were arranged in order of reaction time and divided into four sets of increasing RT, each containing an equal number of stimuli. The choice of four sets was to ensure that there were enough stimuli per set to model the BOLD response and at the same time allowing enough statistical power to model the BOLD-RT relationship across the blocks. Each block was defined as a separate regressor in the model. The %BOLD values for the four blocks and for all individuals were then entered in a separate linear mixed model analysis for each task difficulty categorization. To study individual subject variability of task difficulty, regression analysis was performed to obtain the regression slopes for each individual.

To evaluate sensitivity of the subject-specific RT categorization to age effects, the four block GLM analysis was also done for the old group of subjects. Age-related

differences between the modeled relationship between %BOLD and RT were then evaluated using age group as a between subjects factor.

Lateralization with Task Difficulty:

Studying lateralization with task difficulty is important especially for application to stroke patients where the outcome of recovery can be predicted based on which hemisphere is recruited [40]. Contralateral hemispheric recruitment is also considered as a compensatory mechanism in healthy subjects [20].

Hemispheric specialization based on all tasks vs. control contrast and based on the task difficulty contrast for both tasks was evaluated using laterality index calculations (LI = (L – R)/(L + R), where L and R are number of voxels in the left and right hemispheres respectively) i.e. LI of 1 indicates strong left and -1 strong right lateralization. A bootstrap algorithm was used to calculate LI [127, 128]. In short, the algorithm iteratively calculates 10,000 LI values at different activation thresholds. Thresholds with activation in < 10 voxels in either hemisphere are excluded from LI calculations. For each threshold, a mean LI was calculated. A weighted mean of the LI values over all thresholds (higher thresholds with higher weights) was then calculated to give the final bootstrapped LI value. This approach was used to reduce threshold dependency and the influence of statistical outliers in LI calculations.

LI calculations were performed for the inferior frontal (BA 44/45/47), entire temporal lobe and parietal lobe, using all pictures vs. control and all nouns vs. control contrasts to calculate LI for difficulty independent language production. The difficult vs.

easy contrast was used to calculate task difficulty LI based on subject-specific categorization. A repeated measures ANOVA was used to evaluate differences in hemispheric recruitment between difficulty-independent word production and the difficulty dependent word production. Age as a between subjects factor was used to evaluate age related differences in hemispheric recruitment between difficulty-independent word production and difficulty-dependent word production. Post hoc pair wise contrasts comparing the two LI values separately for each age group were also performed.

Functional Connectivity with Task Difficulty:

Modulations of functional connectivity between language regions with experimental conditions – particularly between language productions as compared to passive viewing of controls and difficult as compared to easy stimuli were evaluated using correlation modulation (CM) networks [129] and psycho-physiological interactions (PPI) [130]. Differences in these condition-specific modulations of connectivity between young and old subjects were also evaluated.

Correlation Modulation Networks:

CM networks were generated for all pictures/nouns vs. control and difficult vs. easy for both the young and old subjects. The fMRI time-course for each condition using the principle eigenvariate was extracted for each ROI as described earlier. Functional connectivity networks for a particular condition were next generated by computing a

weighted correlation between the time-courses of every pair of the defined ROIs. All ROI paired correlations were carried out at the neuronal level after generating the neuronal time-series by using a Parametric Empirical Bayesian formulation for hemodynamic de-convolution of the fMRI time-course [131]. The weighting for the correlation is condition dependent and hence results in a network specific to the condition. The weighted correlation between two regions with time-courses $x = (x_1,..,x_n)$ and $y = (y_1,..,y_n)$ is given by:

$$c_p(x,y) = \frac{\mathrm{cov}_p(x,y)}{\sqrt{\mathrm{var}_p(x)\,\mathrm{var}_p(y)}} \quad where, \ \mathrm{cov}_p(x,y) = \sum_{t=1}^{n} p_t x_t y_t \quad \& \quad \mathrm{var}_p(x) = \mathrm{cov}_p(x,x)$$

$p = (p_1,..,p_n)$ is the condition-specific weight function (one for condition present and zero elsewhere). Next, a CM network, showing variations in functional connectivity between two conditions, was obtained by subtracting the respective pair-wise correlation values between the two conditions. This subtraction removes artifactual correlation confounds due to cardiac, respiratory or MR noise, which are all common to both conditions.

Each component of the CM network was tested for significance across subjects using the Wilcoxon signed rank test. Comparison of CM networks between the young and old groups were done using the Wilcoxon rank sum test. Network links were considered significant at 5% level of significance.

Psycho-Physiological Interactions:

Psycho-physiological interactions between two ROIs for a particular condition were calculated using a GLM approach. The fMRI time-course for one ROI was used as the data and the fMRI time-course for the second ROI, the condition and second ROI*condition time-courses were modeled as separate regressors. This model was solved

using a least square fit to obtain parameter estimates for each regressor. The estimate of the ROI*condition regressor gives the psycho-physiological interaction between the two ROIs for that condition. PPI values were obtained for all ROI pairs and for each condition.

Repeated measures ANOVA using the PPI estimates, condition as within-subjects factor and age group as between-subjects factor was used to evaluate the significance of these interactions. Post hoc pair wise contrasts comparing the three condition estimates and their age interactions were also performed.

7.2.4 Event Related Potentials

7.2.4.1 EEG Data Collection

The EEG recordings were conducted in a sound proof recording chamber with subjects seated on a comfortable reclining chair in front of a monitor screen. Subjects were instructed to remain as still as possible and minimize eye blinks throughout the experiment. Continuous EEG was recorded using a 64-channel electrode cap (Neuroscan Inc., Sterling USA) according to the International 10-20 system of electrode placement (Figure 7.1) [132]. The fronto-central electrode was used as ground and the linked mastoid electrodes as the reference. The ocular electrodes at the outer canthi of the eye were used to monitor the horizontal electrooculograph (EOG) whereas the vertical EOG was monitored by electrodes placed above and below the orbital region of the left eye. Impedances for all electrodes were kept below 10 KΩ and electrodes with impedances

greater than this level were labeled as “bad electrodes” and excluded from the analysis. A digitization rate of 500Hz and amplification gain of 1000 was used.

7.2.4.2 Data Analyses

Ocular artifact rejection from the EEG data was done using Independent Component Analysis (ICA). EEGLAB v5.03 software package (based on the MATLAB platform) was used to run ICA [133, 134]. The continuous EEG data was first visually scanned to remove time-intervals with large movement-related artifacts (e.g. a sneeze or too much wiggling). Bad channels were identified and excluded before running the ICA analysis. The output of ICA is a component array with a 2D scalp map, trial time plots and frequency spectrum for the individual components. The artifactual components in this component array were then identified.

Vertical eye artifacts (blinks) were identified as components with the following characteristics: 1. the scalp map showing a strong far-frontal projection typical of eye-artifacts; 2. smoothly decreasing EEG frequency spectrum with an initial peak; and 3. irregular short voltage bursts representing individual eye movements in the trial time plots. Lateral eye movement artifact components were identified as those with: 1. the scalp map showing bilateral frontal changes in polarity; 2. smoothly decreasing EEG frequency spectrum and 3. irregular extended voltage drifts (as compared to vertical movements) corresponding to eye movements in the trial time plots. EOG artifact rejection for most EEG analyses is usually done by rejecting epochs with EEG voltage beyond a set threshold. The size of our epochs restricted us from using such an approach,

which would result in discarding a large number of trials for every subject. Using the independent component analysis approach not only helped us to remove the ocular artifact components from our data, but also increase the statistical power of our task by allowing to us to retain all trials.

Using the artifact free EEG data, epochs were then defined from 100ms prior to stimulus onset and continued to 2000ms after stimulus onset for each stimulus. A baseline correction using the 100ms prior to stimulus onset for each epoch was also applied. Stimuli were divided into easy and difficult types in the same manner as done for the fMRI. EEG epochs for each event type i.e. all stimuli (easy & difficult), easy, difficult and control were then averaged to obtain their respective ERPs. For analogous comparisons with the fMRI data, in addition to the averages, difference waveforms i.e. all stimuli vs. control and difficult vs. easy similar to the fMRI contrasts were also generated. Grand averages, i.e. ERPs averaged over all the subjects, were also obtained for each contrast.

7.2.4.3 Statistical Analyses

The grand average ERPs for all stimuli vs. control and difficult vs. easy comparisons were used as a guide to define their respective time intervals. Average voltage for each electrode was extracted from these intervals for each of the respective conditions for every subject. Individual electrodes were grouped into four regions: anterior-left (F1, F3, F5, F7, FC1, FC3, FC5, FT7), anterior-right (F2, F4, F6, F8, FC2, FC4, FC6, FT8), posterior-left (CP1, CP3, CP5, TP7, P1, P3, P5, P7) and posterior-right

(CP2, CP4, CP6, TP8, P2, P4, P6, P8). To statistically evaluate effects seen in the grand averages, a separate 3-way repeated measures ANOVA with condition (All Stimuli/Control or Difficult/Easy), Anterior-Posterior (AP) (4 levels) and laterality (8 levels) as within-subject variables was performed for both the difficult-independent and dependent ERPs for each task. To evaluate age related differences, age as a between-subjects factor was also defined. The Greenhouse-Geisser correction was used for all comparisons [135].

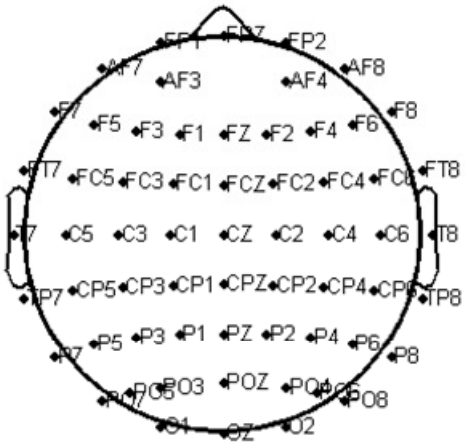

Figure 7.1: International 10-20 system of electrode placement.

7.3 Results

7.3.1 Functional MRI

Results presented in this section are for all subjects for VG and nineteen subjects for PN. Technical problems in recording behavioral responses for one elderly subject caused us to exclude the picture naming fMRI data for that subject from the analysis. In addition, another elderly subject made too few responses in one of the two runs of the picture naming fMRI task and hence data from only one run was used in the analysis.

7.3.1.1 Behavioral Data

Reaction time data collected during the fMRI were analyzed using repeated measures ANOVA to evaluate age related RT differences between the two conditions in each task and between the two tasks. With condition RT as within-subjects factor and age as between-subjects factor, the spread in reaction times for easy and difficult conditions was not significantly different between the two age groups in each task (means for PN – young: E = 1030 ms, D = 1472 ms; old: E = 907 ms, D = 1379 ms & VG – young: E = 1173 ms, D = 1709 ms; old: E = 1112 ms, D = 1626 ms). With task RT as within-subjects factor and age as between-subjects factor, RT was significantly different between the two tasks (main effect) for each condition (easy, difficulty PN<VG: $p<0.001$). However, no age related effects were found. The RT difference between easy and difficult conditions was also significantly different between the two tasks irrespective of age group (mean D - E RT: PN = 457 ± 116 ms, VG = 525 ± 122 ms, $p<0.05$).

7.3.1.2 Language Production Activations

Difficulty Independent Language Production Activations

The brain areas recruited for difficulty independent language production were assessed using the all pictures vs. control and all words vs. control contrasts. Fig 7.2 (PN) & 7.3 (VG) (top) show the cortical rendered activations for these two contrast conditions for each age group. Table 7.1 lists all significant clusters corrected for multiple comparisons.

Region	Side	MNI coordinates			z score	BA
		x	*y*	*z*		
Picture Naming: Task Difficulty Independent Activations						
Young Subjects						
Temporal lobe, sub-gyral	L	-42	-75	-6	4.91	
Middle Occipital Gyrus	L	-30	-93	3	4.87	19
Lingual Gyrus	R	27	-87	-9	4.89	37
Middle Occipital Gyrus	R	33	-96	9	4.83	18
Occipital Lobe, Cuneus	R	18	-102	-3	4.77	18
Old Subjects						
Superior Frontal Gyrus	L	-9	15	57	5.38	
[+]Medial Frontal Gyrus	L	-6	0	60	4.64	6
Cerebellum, posterior lobe	L	-36	-69	-24	4.98	
Fusiform gyrus	L	-42	-63	-18	4.81	37
[+]Occipital lobe, Fusiform	L	-24	-87	-18	4.74	
Verb Generation: Task Difficulty Independent Activations						
Young Subjects						
[+]Frontal Lobe	L	-45	15	6	4.76	44
[+]Extra-Nuclear, Thalamus	R	27	-27	-3	4.71	
Old Subjects						
Inferior Occipital Gyrus	L	-24	-96	-15	5.30	17
Cerebellum, posterior lobe	R	9	-81	-18	4.99	
Cerebellum, anterior lobe	L	-12	-60	-15	4.84	
Superior Frontal Gyrus	L	-3	12	63	5.14	6
Medial Frontal Gyrus	L	-9	12	51	5.07	32
Superior Frontal Gyrus	L	-6	3	60	4.78	6
Midbrain	R	6	-27	-6	5.06	
Verb Generation: Task Difficulty Dependent Activations						
Young Subjects						
Medial Frontal Gyrus	R	6	33	42	4.99	6
Superior Frontal Gyrus	L	-9	18	60	4.88	
Inferior Frontal Gyrus	R	45	15	15	4.84	44

Table 7.1: Task difficulty independent and task difficulty dependent language production activations: Clusters at $p<0.05$ and at $p<0.1$ (+) corrected for family-wise error listed. R = right, L = left. Brodmann's Areas (BA) within 12mm of a cluster focus are listed. Task difficulty dependent language production activations for PN for both age groups and task difficulty dependent activations for VG for old subjects were not significant after FWE correction.

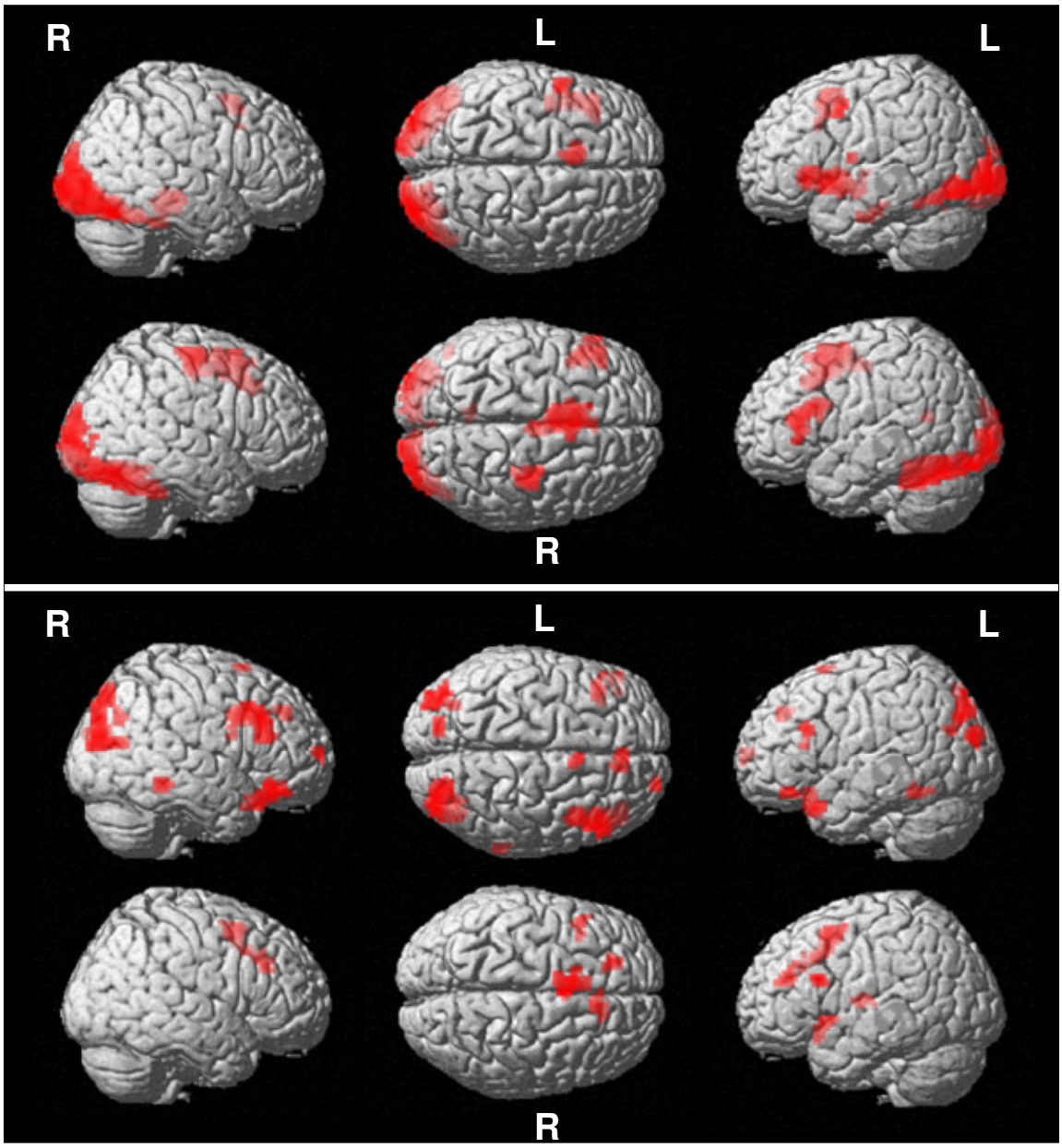

Figure 7.2: Picture Naming Activations: Task difficulty independent language activations ($p<0.001$ uncorrected & >10 voxel clusters, row 1: young, row 2: old) and task difficulty dependent language activations ($p<0.005$ uncorrected & >10 voxel clusters, row 3: young, row 4: old). R = right, L = left.

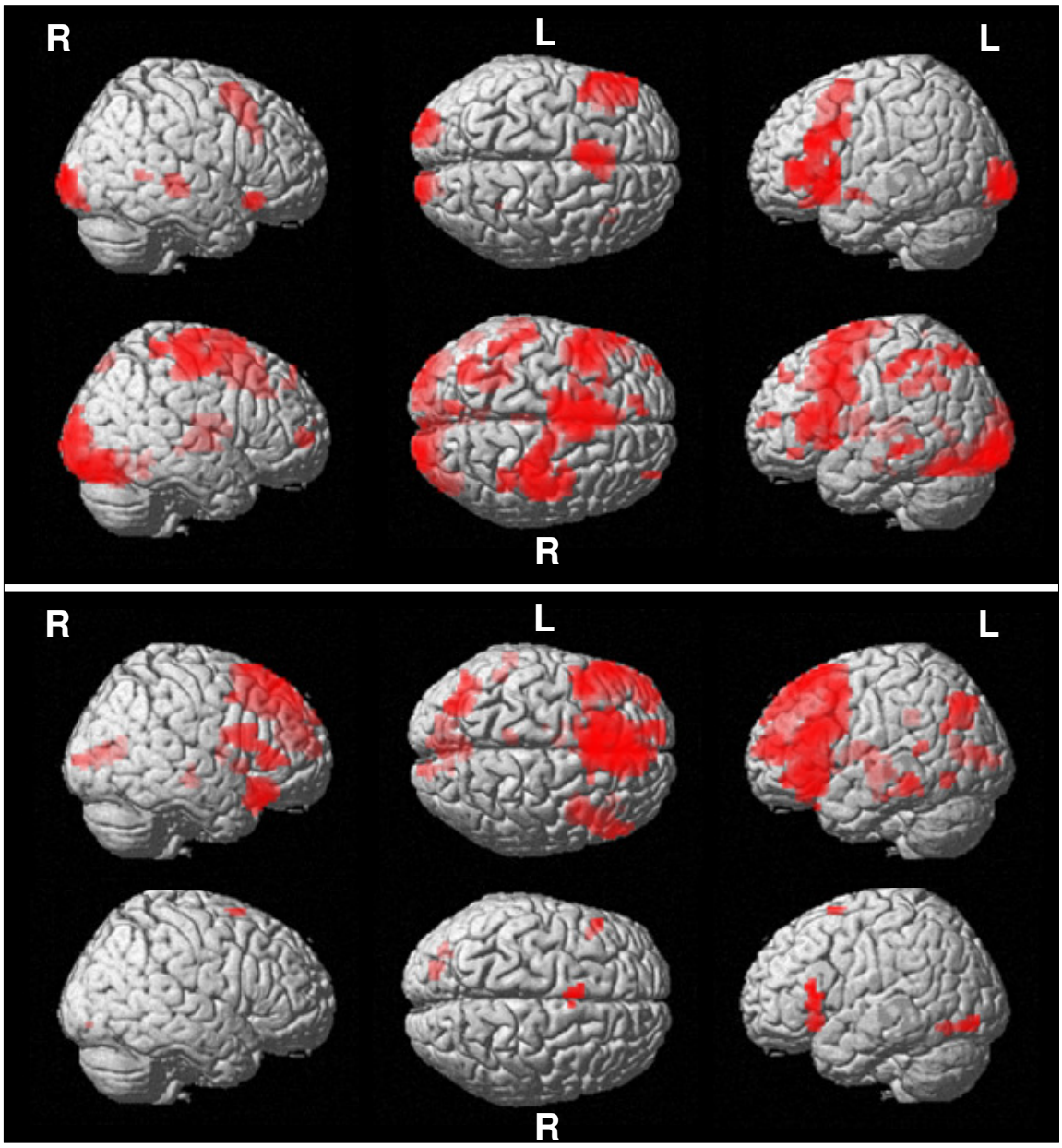

Figure 7.3: Verb Generation Activations: Task difficulty independent language activations ($p<0.001$ uncorrected & >10 voxel clusters, row 1: young, row 2: old) and task difficulty dependent language activations ($p<0.005$ uncorrected & >10 voxel clusters, row 3: young, row 4: old). R = right, L = left.

Difficulty Dependent Language Production Activations

Fig. 7.2 (PN) & 7.3 (VG) (bottom) shows activation based on task difficulty using the difficult vs. easy contrast. Significant activation clusters are listed in Table 7.1. Difficulty dependent activations were significant only for the young group of subjects for

VG. No difficulty dependent clusters were significant for either age group for PN. The reverse task difficulty effect, i.e. easy vs. difficult, did not result in any significant cortical activation clusters.

7.3.1.3 Region of Interest Analyses

The repeated measures ANOVA analysis found a statistically significant within-subjects main effect of condition and condition*age interaction effects, as follows:

Within-subjects main effects (condition):

For VG, % BOLD values for the easy and difficult condition (difficult>easy) differed at $p<0.001$ in the left BA45/47, at $p<0.01$ in the left BA44, left ITG, left MTG, right BA47 and at $p<0.05$ in the left AG and right BA45. Latency differences were observed (difficult peak later than easy) in the bilateral BA47, left BA45, left STG and left MTG ($p<0.01$); and bilateral SMG and right MTG ($p<0.05$). Difficult responses were longer than the easy response (FWHM) in the left BA45/47 ($p<0.01$) and left BA44, left MTG and left AG ($p<0.05$).

For PN, % BOLD (difficult>easy) values were significant only in the left BA47 (difficult>easy: $p<0.05$) and in the left STG (easy>difficult: $p<0.05$). Significant differences for HRF latency (difficult peak later than easy) were found only in the left ITG ($p<0.05$) and HRF FWHM (difficult responses longer than easy) in the left BA45, left ITG and left MTG ($p<0.05$).

*Age related differences in task difficulty (condition*age):*

For VG, %BOLD values between the difficult and easy conditions were significantly different between the two age groups (greater task difficulty differences for young as compared to old) in the left BA45 and right BA47 at $p<0.05$. Trends ($p<0.1$) were seen for left BA44/47 and right BA45. Significant age related differences (young>old) for FWHM values between the two conditions were also found in the right BA45 ($p<0.01$) while trends were seen in the right BA47 and left AG.

No significant age related interactions were found for the HRF latency values from the VG task and any of the HRF measures for PN.

7.3.1.4 Linear Mixed Model Analyses

To evaluate effectiveness of reaction time categorization:

Significant differences between the two RT categorizations, with a larger effect seen using subject-specific RT categorization was found in the left BA47 ($t = 2.72$, $p = 0.023$). As an example the percent signal change values across the four stimuli blocks in the left BA 47 for the young subjects and for each categorization type are shown in Fig 7.4. In addition a trend was also observed in left BA45 ($t = 2.22$, $p = 0.054$) and left BA44 ($t = 1.98$, $p = 0.079$).

Although there were no significant differences between the two categorizations in other ROIs, a significant linear (%BOLD vs. RT) relationship was modeled for both categorizations in the left ITG and right BA45/47 areas; and only for the subject-specific

categorization in the left AG, left MTG and right SMG areas. The results for this analysis are summarized in Table 7.2.

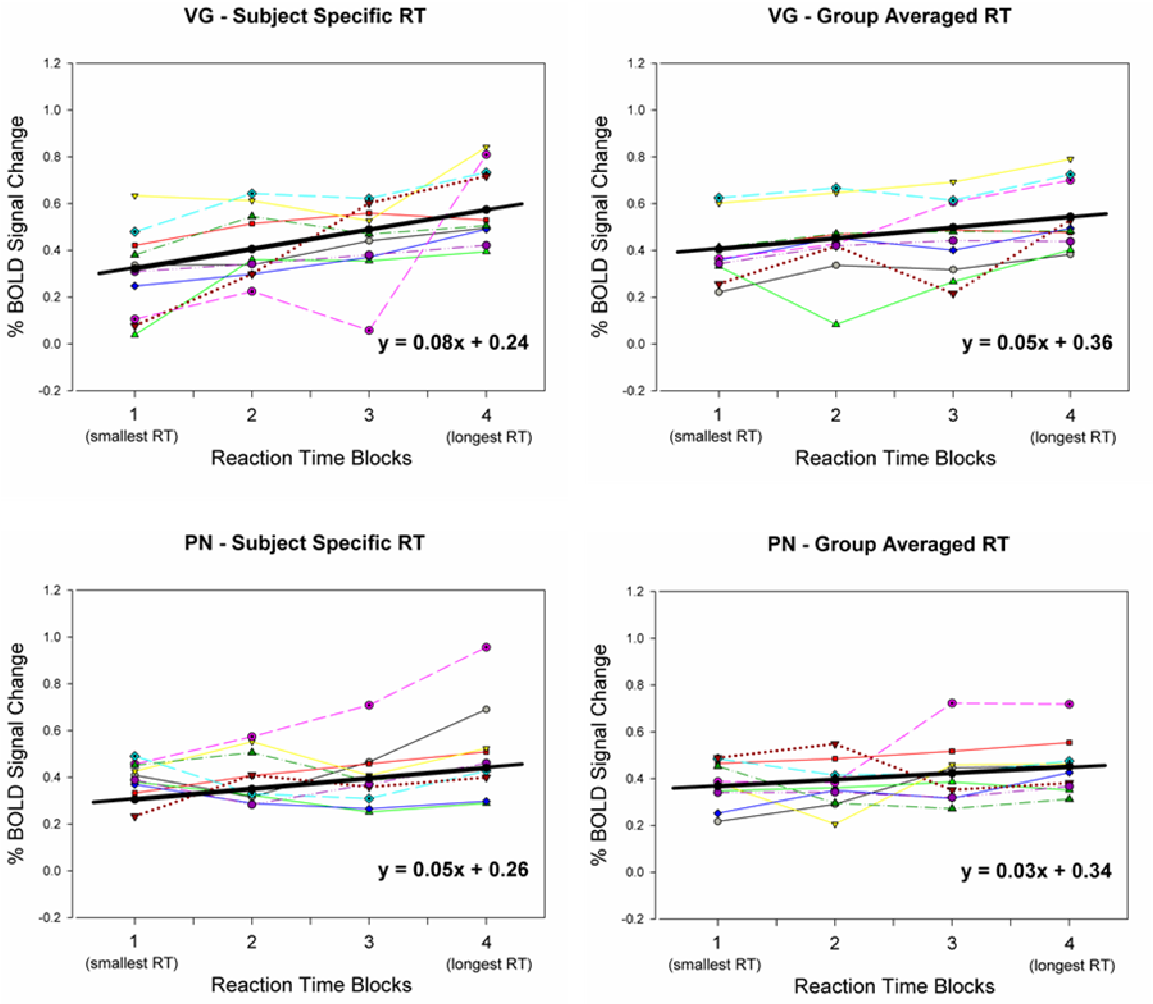

Figure 7.4: Mixed Model Analysis – Subject-Specific vs. Group-Averaged RT: Four block analyses for all subjects in left BA47 for both tasks (top row – verb generation, bottom row – picture naming) and for both RT categorization types (right – group-averaged RT, left – subject-specific RT). Bold line depicts the modeled linear relationship over the 4 blocks and all individuals. Modeled relationships were significant for verb generations only ($p < 0.001$).

ROI	Subject-specific RT		Group-averaged RT	
	Effect ± SE	p	Effect ± SE	p
Left BA45^{+}	0.100 ± 0.016	<0.001	0.069 ± 0.007	<0.001
Left BA47*	0.084 ± 0.020	0.002	0.046 ± 0.009	0.001
Left AG	0.070 ± 0.009	<0.001	0.031 ± 0.014	0.066
Left BA44^{+}	0.067 ± 0.012	<0.001	0.053 ± 0.007	<0.001
Left ITG	0.051 ± 0.005	<0.001	0.029 ± 0.011	0.034
Left MTG	0.047 ± 0.012	0.005	0.020 ± 0.015	0.232
Right BA47	0.036 ± 0.009	0.003	0.054 ± 0.012	0.002
Right BA45	0.030 ± 0.010	0.017	0.047 ± 0.016	0.021
Right SMG	-0.023 ± 0.005	0.002	-0.011 ± 0.007	0.183

Table 7.2: Linear mixed model results comparing subject-specific RT and group-averaged RT categorization for all ROIs - *p<0.05 and $^{+}$p<0.1 indicate significance level for differences between the two RT categorizations. The p-value indicates the statistical significance of the modeled linear relation across all subjects (over the 4 reaction time blocks) and the effect defines the slope of the modeled linear relationship.

Age related differences:

The relationship of %BOLD with RT was found to significantly change with age in a number of ROIs for VG only. Similar to the ROI analysis, age related differences were observed in the left frontal (BA45: $F(1,18) = 16.27$, $p = 0.001$; left BA44: $F(1,18) = 11.25$, $p = 0.004$; left BA47: $F(1,18) = 4.56$, $p = 0.047$), right frontal (right BA45: $F(1,17) = 8.55$, $p = 0.009$; right BA47: $F(1,17) = 5.19$, $p = 0.036$) and left AG ($F(1,14) = 14.08$, $p = 0.002$). In all the ROIs, a stronger linear effect of %BOLD with increasing RT was observed for the young group as compared to their older cohort. As an example, in Fig. 7.5 we show the percent signal change values across the four stimuli blocks in the left and right BA 45 for both groups of subjects. A greater regression slope for %BOLD vs. RT is seen for the young subjects as compared to the old subjects. These ROIs also showed significant main within-subject effects (irrespective of age group) of the modeled relationship of %BOLD with RT (left BA44/45: $p<0.001$; left BA47, left AG, right BA45: $p<0.01$ and right BA47: $p<0.05$). Trends ($p<0.1$) were modeled in the left ITG and

left MTG. A trend for the main effect in the left ITG was also observed for the PN task. The effect sizes of the significant modeled relationship for both subject groups are summarized in Table 7.3.

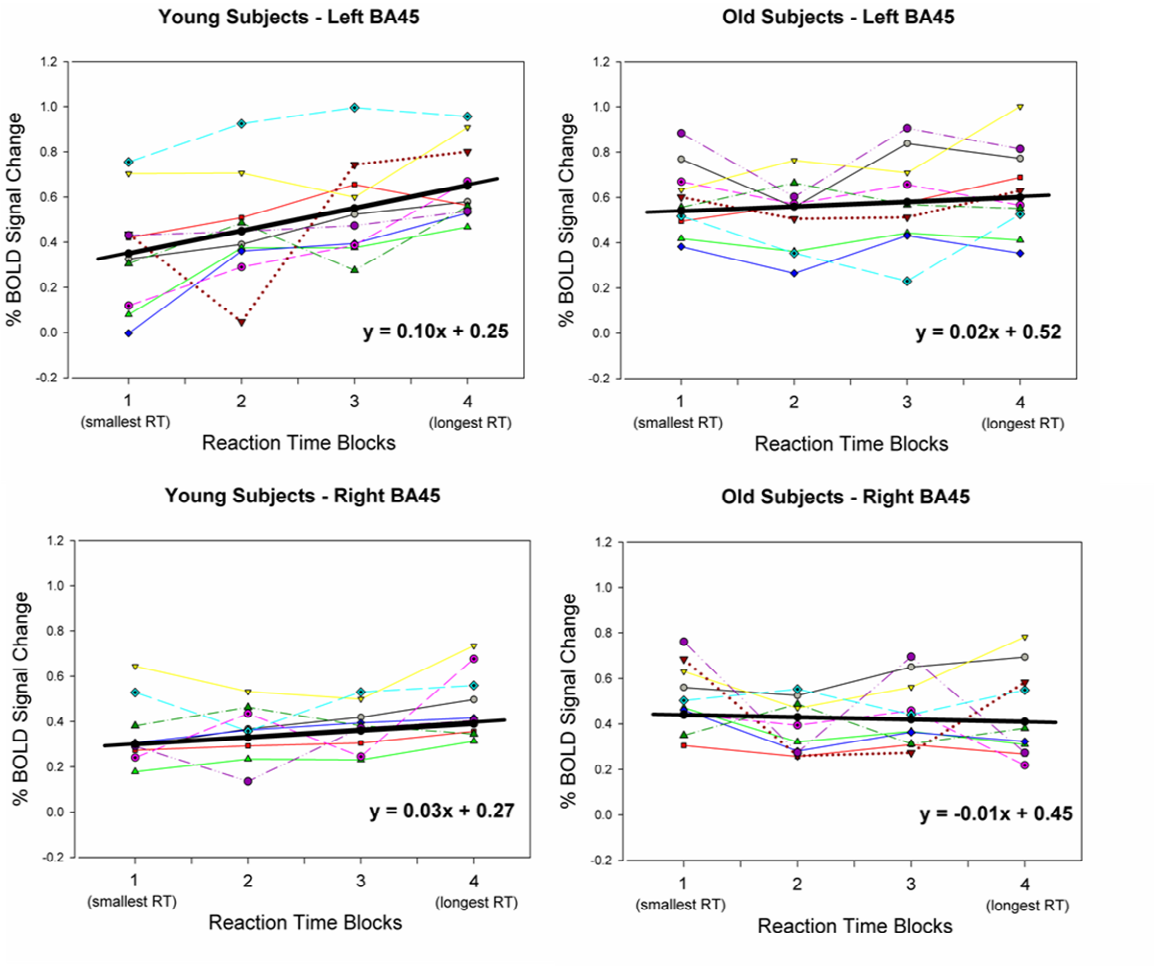

Figure 7.5: Mixed Model Analysis – Young vs. Old Subjects: Four block analyses in BA45 for VG task (top row – left BA45, bottom row – right BA45) and for both subject groups (right – old, left – young). Bold line depicts the modeled linear relationship over the 4 blocks and all individuals in each group. Modeled relationships were significant only for the young group of subjects (left BA45: $p < 0.001$; right BA45: $p<0.05$).

ROI	Young Subjects		Old Subjects	
	Effect ± SE	p	Effect ± SE	p
Left BA45**	0.100 ± 0.016	<0.001	0.021 ± 0.011	0.096
Right BA45**	0.030 ± 0.010	0.017	-0.009 ± 0.012	0.449
Left BA47*	0.084 ± 0.020	0.002	0.025 ± 0.013	0.083
Right BA47*	0.036 ± 0.009	0.003	0.003 ± 0.011	0.774
Left BA44**	0.067 ± 0.012	<0.001	0.025 ± 0.011	0.046
Left AG**	0.070 ± 0.009	<0.001	0.000 ± 0.011	0.993
Left ITG	0.051 ± 0.005	<0.001	0.013 ± 0.014	0.379
Left MTG	0.047 ± 0.012	0.005	0.005 ± 0.007	0.556

Table 7.3: Linear Mixed Model Analysis: Age Effects – ROIs with significant main effects of %BOLD vs. RT for VG - **p<0.01 and *p<0.05 indicate significance level for differences between the two age groups.

7.3.1.5 Lateralization with Task Difficulty

A significant rightward laterality shift with task difficulty was observed in the inferior frontal and temporal regions for both tasks. This shift was not significantly different between the two age groups (i.e., no age interactions). For VG, this shift in the functional hemispheric recruitment of the inferior frontal region ($F(1,18) = 8.14$, $p<0.05$) was from strong left (difficulty independent LI, LI_{all}: young = 0.65, old = 0.72) to weakly left lateralized (difficulty-dependent LI, LI_{diff}: young = 0.25, old = 0.45). In the temporal region, functional specialization shifted ($F(1,18) = 10.98$, $p<0.005$) from left (LI_{all}: young = 0.53, old = 0.57) to bilateral in young and weakly lateralized in older subjects (LI_{diff}: young = 0.04, old = 0.24). However, in the parietal region, LI remained weakly left lateralized (LI_{all}: young = 0.16, old = 0.27; LI_{diff}: young = 0.31; old = 0.31).

Similarly, for PN a rightward shift of functional dominance was found in the left inferior frontal region ($F(1,17) = 13.92$, $p<0.005$; LI_{all}: young = 0.34, old = 0.66; LI_{diff}: young = -0.13, old = 0.17) and the temporal region ($F(1,17) = 6.41$, $p<0.05$; LI_{all}: young

= 0.27, old = 0.38; LI_{diff}: young = 0; old = -0.02). Similar to VG, the shift in hemispheric recruitment in the parietal region was not significant (LI_{all}: young = 0.22, old = -0.08; LI_{diff}: young = 0.09, old = 0.08). As an example of the shift with task difficulty, differences in language lateralization based on difficulty-independent as compared to subject-specific analysis in the frontal regions are shown in Fig. 7.6 for VG for both age groups.

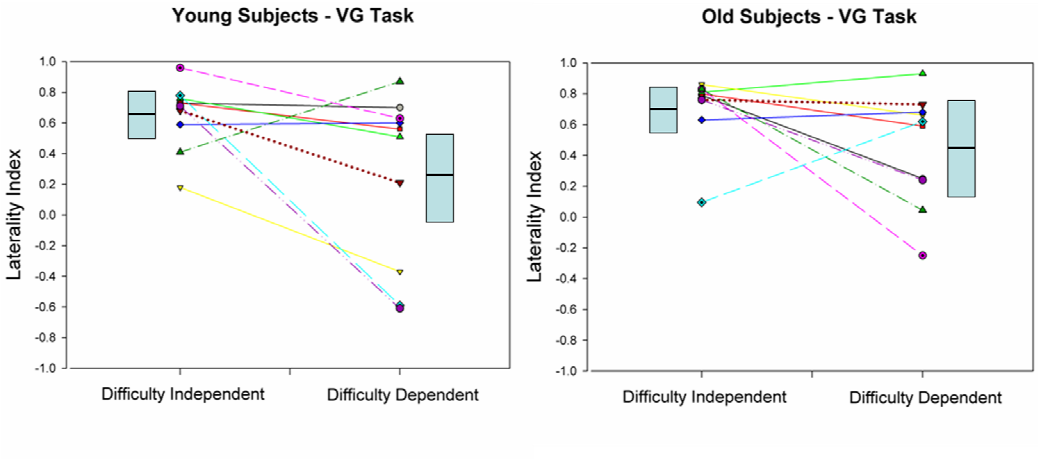

Figure 7.6: Lateralization with Task Difficulty: Pair-wise comparisons between difficulty-independent and subject-specific difficulty-dependent activation maps revealed significant hemispheric laterality shift in the inferior frontal for only the young age group (p=0.05). Boxes indicate mean and ±95% confidence intervals.

7.3.1.6 Functional Connectivity with Task Difficulty

CM Networks:

Functional connectivity differences observed with the VG task are summarized in Fig 7.7 (A&B – All words vs. controls; C&D - Difficult vs. easy). For the all words vs. control network, significant differences in functional interactions between the young and old subjects ($p<0.05$) were present for the L & R-ITG (CM Young = 0.262, Old = -0.024)

and L-AG & R-ITG (CM Young = 0.224, Old = -0.061) network links. For the difficult vs. easy network, the network links between the two groups were significantly different for: L-BA44 & L-BA45 (CM Young = -0.032, Old = 0.032), L-BA44 & L-MTG (CM Young = -0.087, Old = 0.087), L-ACC & R-BA47 (CM Young = -0.096, Old = 0.286) and R-BA44 & R-AG (CM Young = -0.021, Old = -0.145).

PPI Analyses:

To increase statistical power and reduce errors due to multiple comparisons, the ROIs used in this analysis were restricted to (left and right): Inferior Frontal Gyrus (IFG – by combining BA44-45-47), Wernicke's area, AG and ACC. No significant psycho-physiological interactions were significant. However, a trend for condition dependent interactions between the R-IFG and R-Wernicke was found (p=0.054). Post-hoc tests for this interaction revealed significant differences between Difficult vs. Control (p=0.045) and Easy vs. Control (p=0.023) comparisons only. No age related differences between any psycho-physiological interactions were found to be significant.

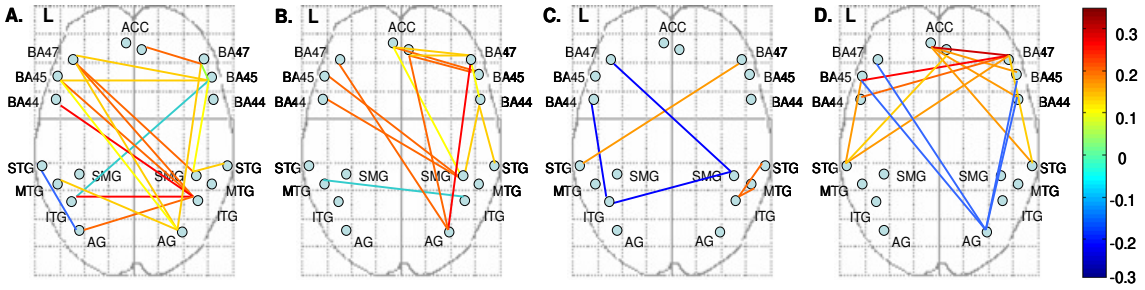

Figure 7.7: Functional Connectivity Analysis - CM networks: All words vs. Control (A – Young; B – Old) and Difficult vs. Easy (C – Young; D – Old). Mean CM value over the group is indicated by color of the links (see color scale).

7.3.2 Event Related Potentials

7.3.2.1 Difficulty Independent & Dependent Language Production ERPs

The voltage distribution maps for the difficulty-independent and difficulty-dependent language ERPs averaged over 40ms time bins for both age groups are shown in Figures 7.8 - 7.11. Boxes indicate the time windows selected for statistical analyses.

7.3.2.2 Statistical Analyses

Difficulty Independent Language Production ERPs:

For PN, the early negativity and late positivity difference on the voltage distribution maps (Figure 7.8) were statistically significant between all pictures and control condition (520 to 640ms: $F = 4.67$, $p<0.05$; pictures > control & 1000 to 1160ms: $F = 17.99$, $p=0.001$; pictures > control). The AP difference (anterior > posterior) seen during the late time interval was significant (main effect AP: $F = 5.94$, $p<0.05$) and different between the two conditions (condition*AP: $F = 9.79$, $p<0.005$). The AP effect was also different between the two age groups in that interval (AP*age group: $F = 5.47$, $p<0.05$; young anterior > old). The laterality levels were significantly different for both conditions (main effect laterality: $F = 9.3$, $p<0.001$; midline electrodes more negative than lateral) and for different AP levels (AP*laterality: $F = 2.68$, $p<0.05$). However the laterality levels were not different between the two conditions or age groups.

For VG, similar to PN, a significant early negative (young = 520 to 640ms & old = 600 to 720ms: $F = 25.8$, $p<0.001$; all words > control) and late positive difference (young = 880 to 1000ms & old = 920 to 1040ms: $F = 8.45$, $p<0.01$; all words > control) between the all words and control stimuli were found. The early negativity was also different over different levels of laterality (condition*laterality: $F = 6.04$, $p<0.005$). Significant AP main effect ($F = 4.73$, $p<0.05$), AP*laterality ($F = 2.94$, $p<0.01$), and condition*AP*laterality ($F = 3.59$, $p=0.001$) effects indicate that a significant left anterior negativity difference was present for the words as compared to controls. In addition, a greater negative effect was observed for old as compared to young subjects (condition*AP*laterality*age group ($F = 2.1$, $p<0.05$). For the late time window, the positivity was more anterior and lateralized over the two conditions (laterality main effect: $F = 3.53$, $p<0.05$: middle levels more negative and Laterality*AP: $F = 3.65$, $p=0.001$). Significant difficult-independent effects for both tasks are summarized in Table 7.4.

Difficulty Dependent Language Production ERPs:

Similar to the fMRI results, no significant difference between the difficult and easy stimuli (main or interaction condition effects) were present for either time window for PN. The only significant effects found were a main AP effect independent of laterality levels ($F = 6.3$, $p<0.05$); an AP*laterality effect ($F = 2.6$, $p<0.05$)) and an AP*age effect ($F = 6.91$, $p<0.05$) for the late positivity.

For VG, significant differences between the difficult and easy conditions were found only for the early time window (960 to 1200ms: $F = 4.84$, $p<0.05$: difficult > easy).

This effect was also found significantly different over different laterality levels between the two conditions (condition*laterality: $F = 3.02$, $p<0.05$). In addition, main effects of laterality ($F = 6.25$, $p<0.005$) and AP*laterality ($F = 4.24$, $p=0.001$) confirmed that the early negativity was more centralized for both easy and difficult conditions. The late positivity was more central and lateral from main laterality ($F = 10.97$, $p<0.001$) and AP*laterality ($F = 3.69$, $p<0.005$) effects. Significant effects for both tasks are summarized in Table 7.5.

	Picture Naming		**Verb Generation**	
TIME WINDOWS **EFFECT**	520 to 640ms (young, old)	1000 to 1160ms (young, old)	520 to 640ms (young) 600 to 720ms (old)	880 to 1000ms (young) 920 to 1040ms (old)
CONDITION (All Stimuli, Control)	F = 4.67 p = 0.045	F = 17.99 p = 0.001	F = 25.82 p < 0.001	F = 8.45 p = 0.009
LATERALITY	NS	F = 9.30 p < 0.001	NS	F = 3.53 p = 0.026
AP	NS	F = 5.94 p = 0.019	F = 4.73 p = 0.025	NS
CONDITION * LATERALITY	NS	NS	F = 6.04 p = 0.003	NS
CONDITION * AP	NS	F = 9.79 p = 0.003	NS	NS
LATERALITY * AP	NS	F = 2.68 p = 0.018	F = 2.94 p = 0.008	F = 3.65 p = 0.001
CONDITION * LATERALITY * AP	NS	NS	F = 3.59 p = 0.001	NS
AP * AGE GROUP	NS	F = 5.47 p = 0.024	NS	NS
CONDITION * LATERALITY * AP * AGE GROUP	NS	NS	F = 2.10 p = 0.045	NS

Table 7.4: ERP Statistical Analysis for All Stimuli vs. Control PN & VG waveforms. NS indicates not significant.

TIME WINDOWS / EFFECT	Picture Naming		Verb Generation	
	600 to 680ms (young, old)	1240 to 1360ms (young) 1520 to 1600ms(old)	960 to 1200ms (young, old)	1360 to 1440ms (young, old)
CONDITION (Difficult, Easy)	NS	NS	F = 4.84 p = 0.040	NS
LATERALITY	NS	NS	F = 6.25 p = 0.002	F = 10.97 p < 0.001
AP	NS	F = 6.30 p = 0.020	NS	NS
CONDITION * LATERALITY	NS	NS	F = 3.02 p = 0.039	NS
LATERALITY * AP	NS	F = 2.60 p = 0.014	F = 4.24 p = 0.001	F = 3.69 p = 0.002
AP * AGE GROUP	NS	F = 6.91 p = 0.015	NS	NS

Table 7.5: ERP Statistical Analysis for Difficult vs. Easy PN & VG waveforms. NS indicates not significant.

N400 Analyses:

In addition to the above time windows, distinct negativity differences between the easy (blue), difficult (red) and control (green) conditions were also observed in the grand averages (360 to 600ms) of the midline electrodes only for the PN task (Fig 7.12). To statistically evaluate this effect, a repeated measures ANOVA with condition (Easy/Difficult/Control) and electrode (Fz/Cz/Pz) as within subject factor and age as between subject factor was used. A significant difference between all three conditions ($F = 9.7$, $p=0.001$) and all three electrodes ($F = 8.84$, $p<0.005$) was observed. The difficult waveform was the most negative followed by the easy and control waveforms. Such a pattern was absent for the VG task for the same interval.

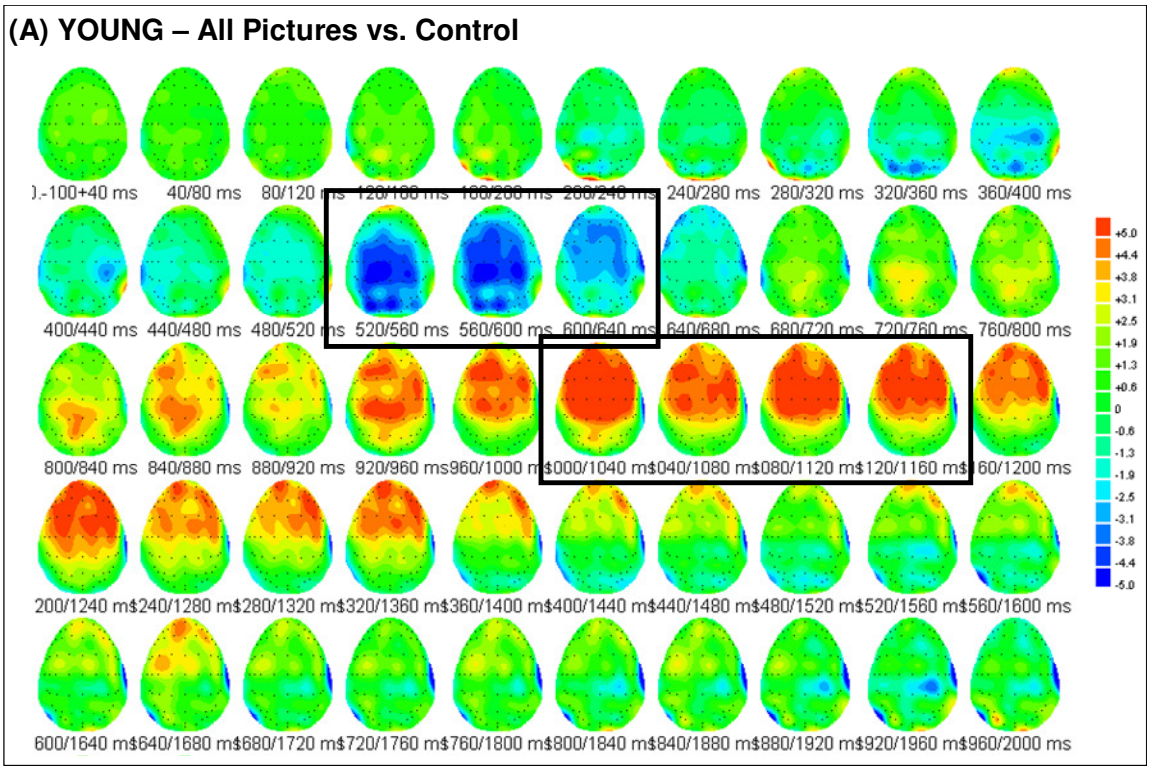

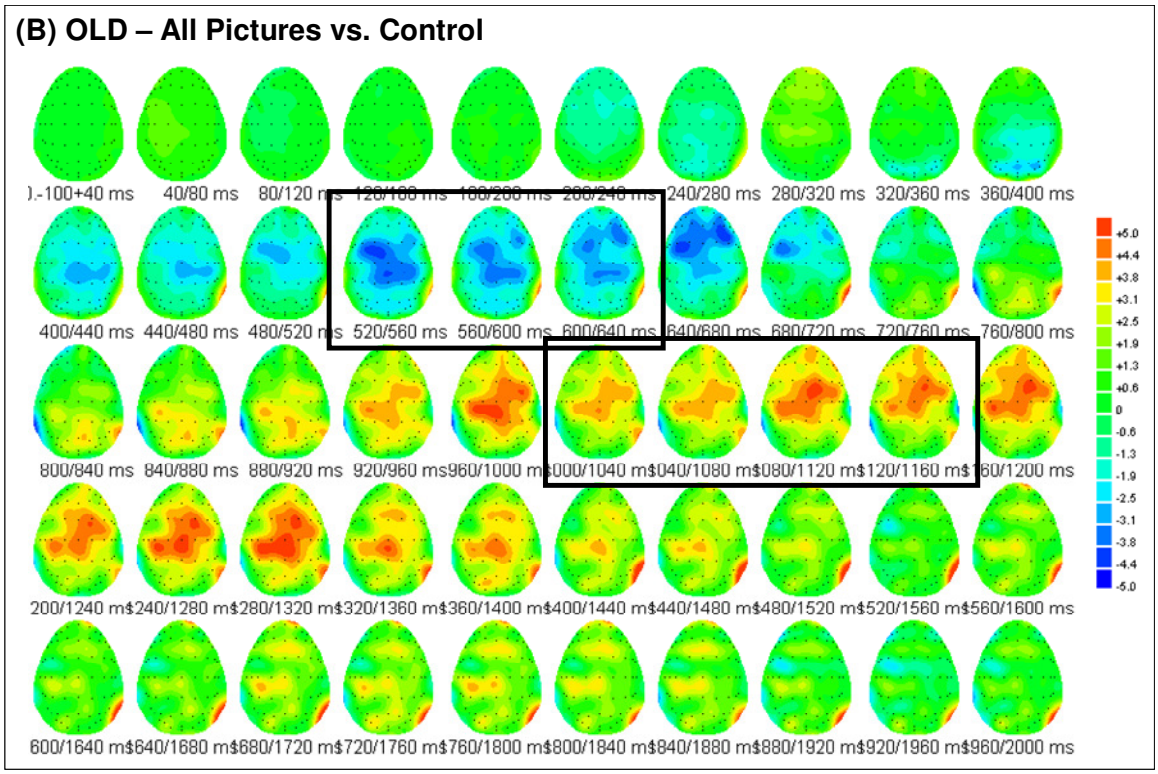

<u>Figure 7.8</u>: Voltage Distribution Maps for Task Difficulty Independent Language ERPs for Picture Naming Task (A – young; B – old groups). Boxes indicate early and late time windows selected for statistical analysis. Central negativity in the early time window and a centro-parietal positivity in the later time window is seen.

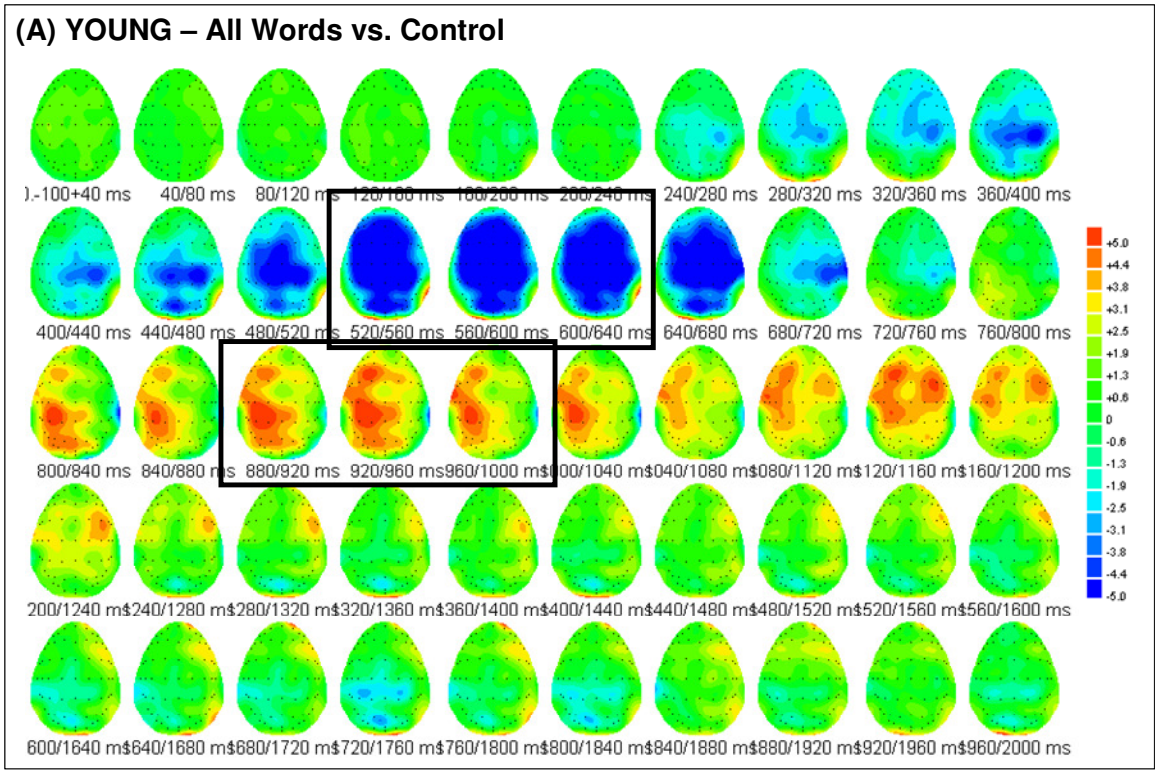

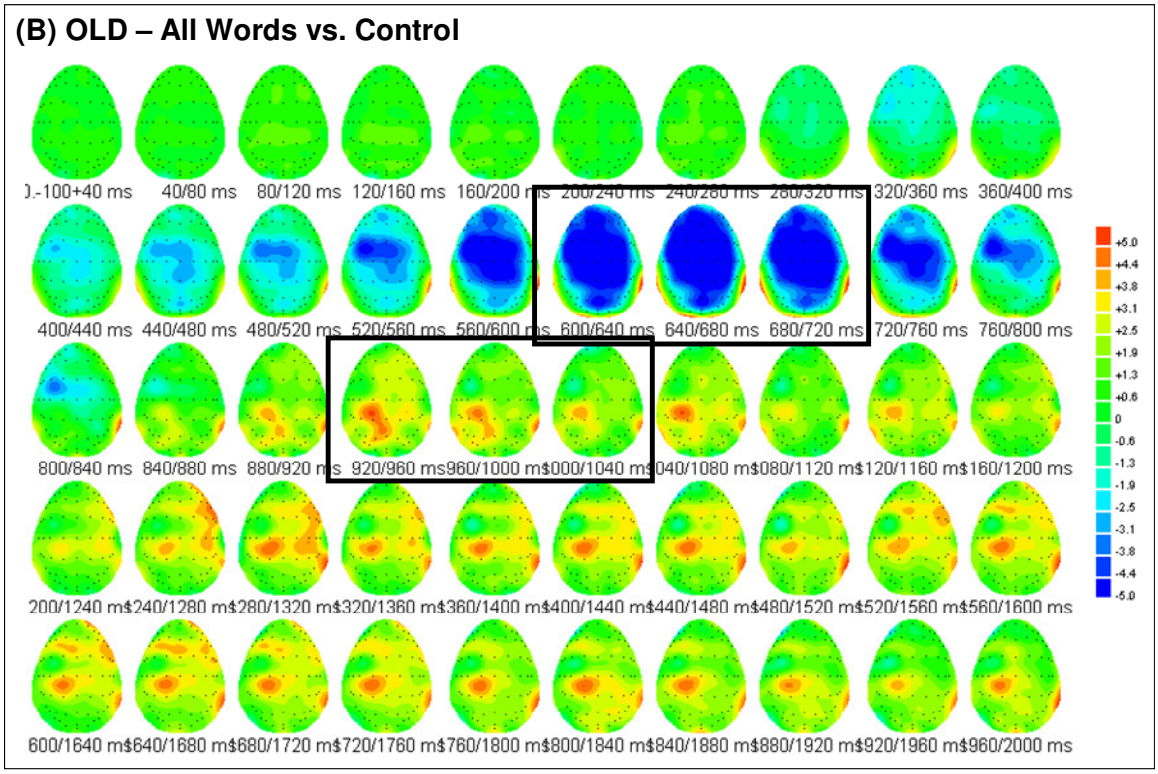

Figure 7.9: Voltage Distribution Maps for Task Difficulty Independent Language ERPs for Verb Generation Task (A – young; B – old groups). Boxes indicate early and late time windows selected for statistical analysis.

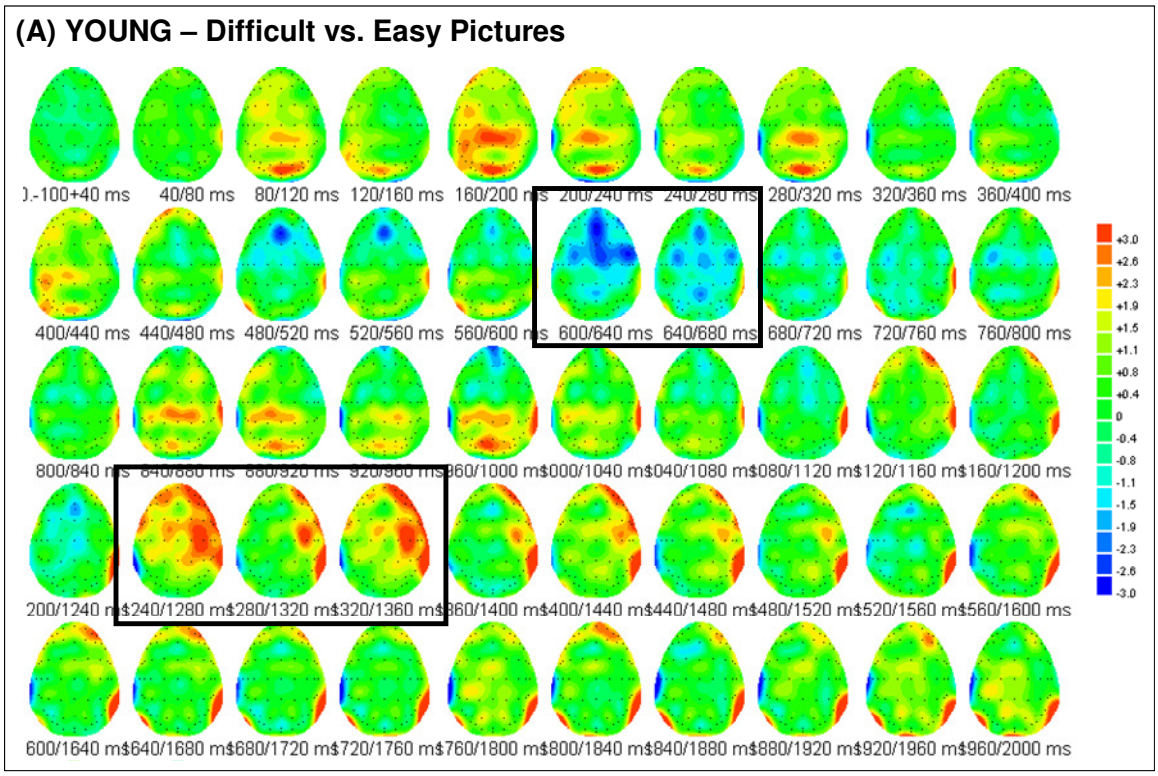

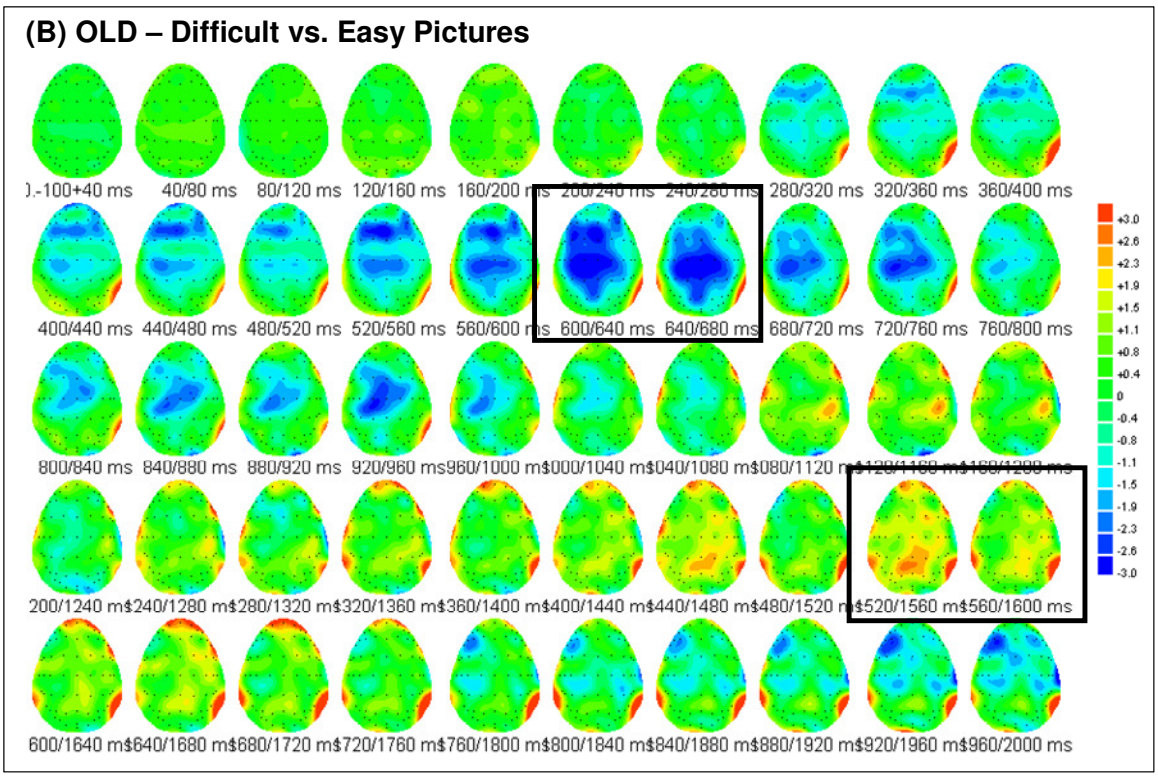

Figure 7.10: Voltage Distribution Maps for Task Difficulty Dependent Language ERPs for Picture Naming Task (A – young; B – old groups). Boxes indicate early and late time windows selected for statistical analysis.

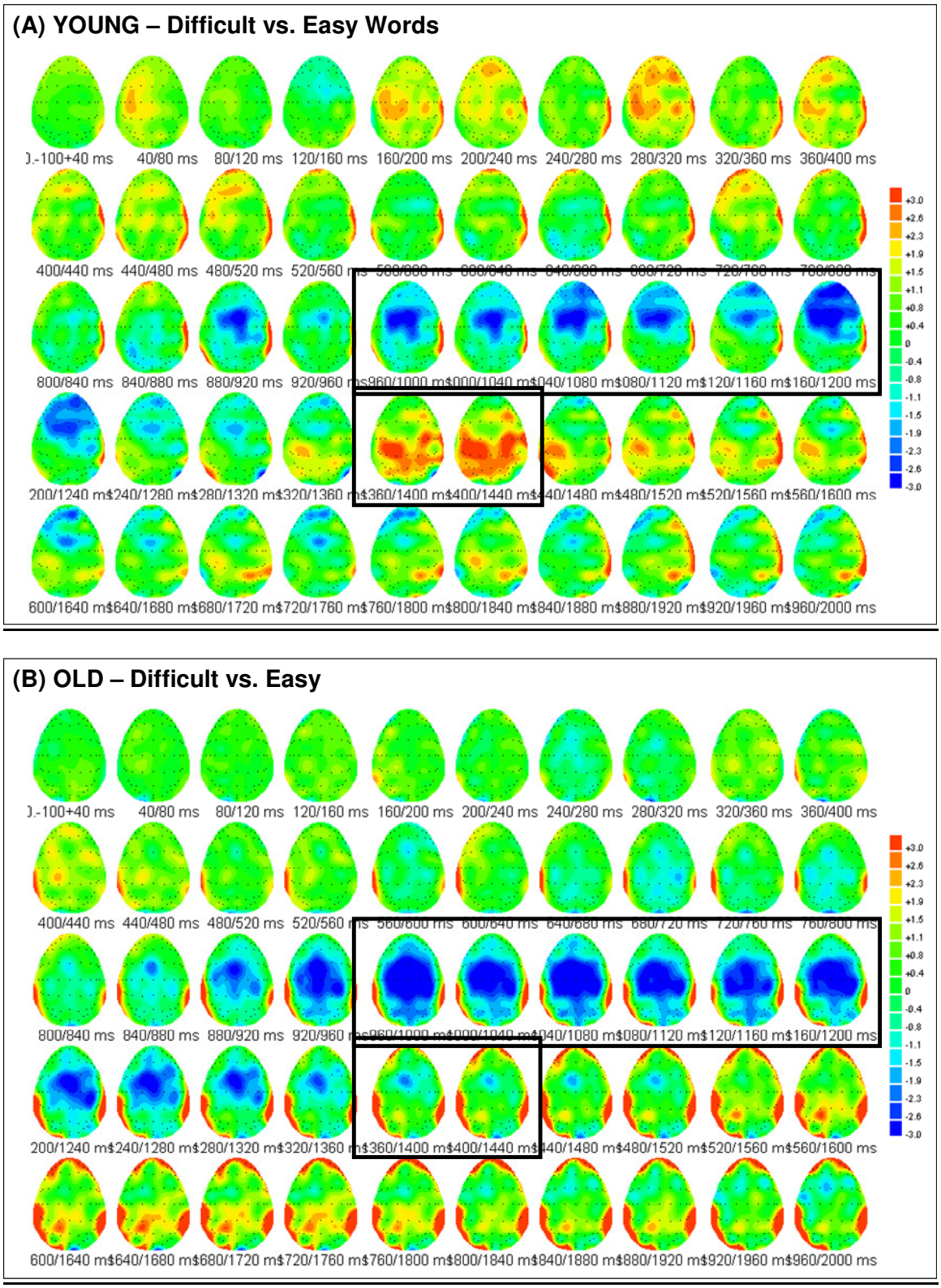

Figure 7.11: Voltage Distribution Maps for Task Difficulty Dependent Language ERPs for Verb Generation Task (A – young; B – old groups). Boxes indicate early and late time windows selected for statistical analysis.

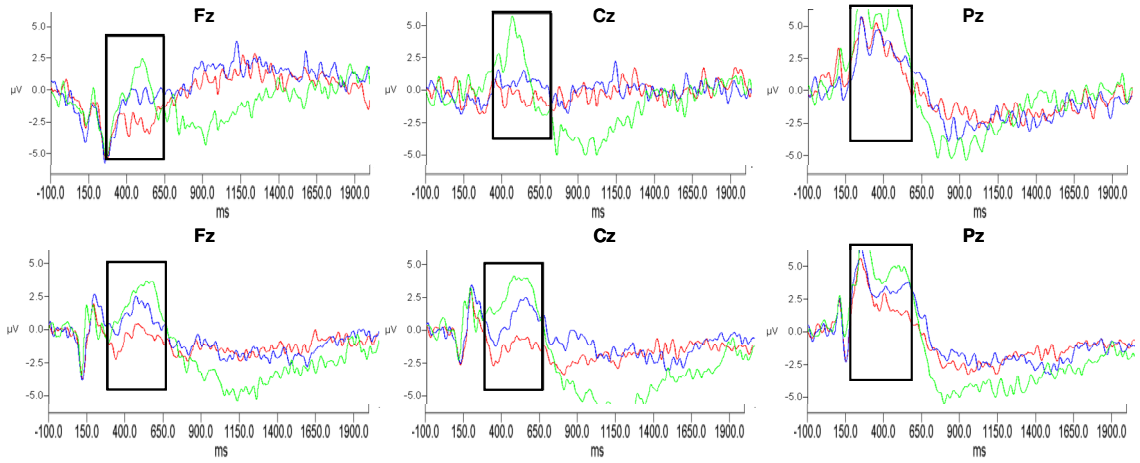

Figure 7.12: Grand Average ERP Waveforms showing the N400 effect in PN at the midline (Fz, Cz, Pz) electrodes. (Difficult (red), Easy (blue) & Control (green) top row – young; bottom row – old groups). N400 effect was found significant (p=0.001)

7.4 Discussion

Picture naming and verb generation tasks have shown great potential in mapping the language functional architecture in healthy subjects as well as in evaluating language deficits and rehabilitation with therapy in aphasic patients [136, 137]. In this chapter, task difficulty – a potential confound of subject-wise variability in healthy and more importantly in aphasic patients, was evaluated using two neuroimaging modalities. A subjective definition of task difficulty was also evaluated in comparison to a more common objective definition.

7.4.1 Functional MRI

Task Difficulty Effects: Using individual subject reaction times as an independent measure of task difficulty, we observed task difficulty effects on functional activations

primarily in the frontal regions, more prominently in the verb generation task. A stronger effect size was recorded for the left-sided activations by using subject RT's to define task difficulty. Qualitatively, this distinction can be appreciated in Fig. 7.4 which shows the strong linear relationship between the BOLD response and RT, across all four blocks and for nearly all subjects. In contrast, the group-averaged RT method was not able to consistently categorize task difficulty of the stimuli for individual subjects, showing a weaker effect across the entire RT range. Presumably there is a larger amount of variability in the subjective degree of the difficulty of the task, and the group-averaged model does not correctly account for subject-to-subject differences. The strong linear relationship of the subject-specific analysis also shows the validity of subject reaction time as measure of task difficulty, not only in general terms, but on an individual stimulus basis. Previous attempts to characterize task difficulty have relied on using objective definitions of easy and difficult tasks inherent to their task designs [111, 114, 138, 139] or used response times as a gauge of task difficulty taken within the scanner [112, 113, 115, 140-143] or from ancillary pilot studies [144, 145] in fMRI block designs to validate easy and difficult blocks. In comparison, there are only a few studies that have used response time information for retrospective categorization of task difficulty [115] [112]. These studies however showed an overall group effect of the dependence of BOLD response on reaction time. Using an event related fMRI design permitted us to evaluate these differences at the individual subject level which are more relevant in rehabilitation studies of stroke patients.

Age effects: Significant age related differences in the effect of task difficulty were also observed in the bilateral frontal regions. Younger subjects showed greater task

difficulty related differences in the BOLD signal as compared to their older counterparts. Using the linear mixed model analysis strategy enabled highlighting these differences more clearly and in more regions as compared to the traditional two condition subtraction (i.e., easy vs. difficult) ROI analysis. Interestingly, the mean BOLD signal for both the easy and difficult tasks for the older group of subjects was comparable to the mean BOLD signal for the difficult tasks for the younger subjects. This increase in BOLD signal level for the easy tasks in the older subjects may indicate age-related changes in cognitive processing as a compensatory mechanism to maintain performance, as has been shown in prior aging studies of language function [146]. Further, the decreased task difficulty effects seen for older subjects may indicate that ease of language performance develops with age and experience. However, the behavioral data did not show a significant age-related difference between the reaction time spread between the easy and difficult stimuli. Thus, the measures of task difficulty seem to suggest a decoupled relationship of the BOLD signal and behavioral data with aging.

Other functional measures: In addition to peak BOLD signal differences, the hemodynamic response peaked later and took longer to return to baseline with increased subject-specific task difficulty in both the frontal and temporal regions for VG and only the left temporal regions for PN. An age related difference was observed only in the width of the hemodynamic function in the right frontal region for VG. Using laterality index analysis, a significant rightward shift in laterality was seen for the task-difficulty modulated contrast as compared to stimulus vs. control contrasts. This shift was evident in both frontal and temporal regions for both the tasks, but not in the parietal lobe for either task. No age related differences in laterality index shifts were observed. This shift

may indicate an overall strategy to recruit additional contralateral cortical areas with increased task difficulty for both tasks.

Functional Connectivity: For the evaluation of functional connectivity differences with task difficulty and these changes with age, two methods of analyses were used. A number of significantly different connections with task were observed between the two age groups using the CM method. However none of these connections were significant when corrected for multiple comparisons. Overall an increase in the right hemispheric connections with age for both difficulty independent and difficulty dependent CM networks was observed (Fig. 7.7), indicating an increased rightward shift in functional connections with age. This observation seems to be in agreement with our laterality index results and the hemispheric asymmetry reduction in older adults observed in a number of other studies [20].

Verb Generation vs. Picture Naming: While the use of reaction time to categorize task difficulty was successful for verb generation, significant activations were not seen in the ROI analysis with this contrast in picture naming. The reaction time spread was smaller for picture naming, and our analysis was also limited to the language-related brain areas, both of which may have limited our success in demonstrating task difficulty effects. Another possible difference is the semantic component of the task. The lack of frontal activation demonstrated in many picture naming studies [108, 147, 148] has been argued as due to the relative lack of a semantic component. The stronger effect sizes seen in frontal as compared to temporal regions in VG, with the strongest task difficulty effect in left BA47, may be related to the strong semantic nature of this task. The robust nature

of this task to map language regions, demonstrated in numerous prior studies [94, 149, 150], may also be the reason for seeing these subtle effects of task difficulty in VG.

7.4.2 Event Related Potentials

Semantic Effects: Differences between the ERPs for control and linguistic stimuli were found both early in the waveforms and late in waveforms, and for both tasks. There was a greater overall negativity for the language stimuli in the first time window and increased positivity in the second time window. For PN, the longer-latency effect was an enhanced positivity over the frontal areas. This may be associated with the increased frontal processing required for naming pictures than for passively viewing of unnameable control stimuli. For VG, in the earlier time window, a greater central negativity was observed. This may be analogous to N400 effects reported in many situations, reflecting greater semantic processing for words as compared to control stimuli.

Difficulty effects: Both early and late effects were observed for item difficulty as well, but these effects differed for picture naming and verb generation. For PN, the earlier time window (360 to 600ms) showed the greatest negativity for the difficult condition, followed by the easy and then the control condition. Difficulty effects were not observed for the VG task in that time window. Instead, a much later (960 to 1200ms) central negativity difference between the difficult and easy condition was observed for VG.

Age effects: Latency differences were observed between the young and old groups for VG (Figure 7.11). For both the difficult-independent and difficulty-dependent

difference waveforms, the older subjects showed later or more extended processing as compared to the young subjects. This extended processing may be an indicator of additional compensatory temporal processing in the older subjects as compared to their younger counterparts.

In summary, language processing dependence on task difficulty was evaluated using fMRI and ERP. Subject specific categorization of task difficulty and an event related verb generation task highlighted significant task difficulty related effects in both neuroimaging modalities. Age related differences were also observed. The linear mixed model analysis strategy is an effective approach to model both individual and group level relationships between BOLD signal and subject reaction times. This may be a more relevant approach in studies of stroke patients where a considerable subjective variability in performance is expected.

Chapter 8

Integration of fMRI and ERP to study Language Function and Task Difficulty

8.1 Introduction

Understanding functional organization requires knowledge of functional neuroanatomy, time course of the processing, the type of processing and interaction between various functional components. Most of the currently existing neuroimaging techniques are limited in the nature of information they can provide. While the hemodynamic based neuroimaging techniques (fMRI/PET) provide good spatial resolution (few mm), they are limited in the temporal nature of information they can provide (1s). Neuronal based modalities (EEG/MEG) on the other hand provide excellent temporal information (0.001s) but are limited in the spatial identification of sources. To integrate the complementary information provided by these two techniques, many groups in the neuroimaging community have attempted numerous efforts directed at combining these two modalities (For a review see [151, 152]). These attempts have relied on the main assumption that the signals detected by each method correspond to the same set of underlying neural generators. In a review of these attempts, Horwitz and Poeppel [152], have categorized three classes for these approaches:

Converging Evidence:

The most common, but qualitative approach has been to converge evidence from different studies with a common finding that supports one's result. However, given the

complexity of the brain networks involved in a particular function, it is extremely difficult to comment about the correlation of results from the two different techniques without a thorough understanding of how each of these methods probe the underlying physiology.

Direct Data Fusion:

As the name suggests, this approach mainly attempts to combine the two imaging data sets using mathematical or statistical algorithms. The source of brain activity measured at the surface of the skull is determined by modeling the conductive current source distribution in the head. These methods are divided based on the assumptions that either only a few underlying equivalent current dipoles generate the EEG/MEG data [153], or there exists a uniform spatial distribution of sources with temporally continuous EEG/MEG values throughout the brain [154]. The fMRI/PET data is integrated with the EEG/MEG data by using the foci of the fMRI/ PET-derived hemodynamic activations as constraints to localize the EEG/MEG sources. This has been one of the most popular approaches towards data fusion.

Computational neural modeling:

In addition to the above methods, a modeling approach to solve this data fusion problem has been proposed [155]. The underlying basis of such an approach is to construct a neural model which would allow comparison of simulated fMRI/PET and EEG/MEG data within the model. A similar approach has been implemented by Pflieger *et al.* using a non-linear system identification approach in which separately acquired fMRI and EEG/MEG datasets were temporal aligned to simulate "virtually simultaneous" datasets [156].

In this chapter, direct data fusion was used to combine fMRI and ERP data from a language comprehension task highlighting contextual semantic processing. fMRI and ERP results for this task are presented. fMRI constrained dipole analyses were performed to determine the relationship between observed fMRI activations and specific ERP components.

8.2 Methods

8.2.1 Data Collection & Preprocessing

Functional MRI and ERP data from the language comprehension task for the same set of 20 subjects (10 young and 10 old) was used in this section. Subjects performed two runs of the task during each imaging session. Details about the task have already been discussed in chapter 6. In short, during each run subjects viewed 4 types of category questions followed by a number of options. Subjects covertly responded for each option with a 'yes' or 'no' and a corresponding button press, depending on whether or not the item presented fit the category. Based on the behavioral study, two of these categories were classified as easy and two as difficult.

Functional MRI and EEG data for the task was collected in the same manner as described in chapter 7. Preprocessing steps for both modalities were the same as those for the picture naming and verb generation tasks.

8.2.2 Data Analysis

8.2.2.1 Functional MRI

Single subject fMRI data was modeled using the same GLM data analysis strategy used for PN and VG tasks. For every subject the following trial types were defined: easy-yes, easy-no, difficult-yes, difficult-no, control, instructions and invalid trials. For the two easy categories (i.e. animal/non animal and edible/non edible), Yes-No option types were predefined and incorrect or no subject responses were labeled as invalid trials. The difficult category options (i.e. recreational activities and professions requiring college education), because of their subjective nature, were defined as 'difficult-yes' or 'difficult-no' based on individual responses. As before, trials with no subject response were included as invalid trials. All options within the control blocks were defined as 'control' and all instruction questions for each block as 'instruction' categories. Because of technical problems in collecting responses for this task in the MRI, subject responses from the ERP session were used for this analysis (reaction times were not used for these analyses).

Two types of ROI analyses were performed to extract %BOLD values. The first type of analysis was based on the traditional method of using complete anatomical ROIs to extract %BOLD values. The second type of ROI analysis was similar to the fROI analysis used for PN and VG. An F-contrast of the main effect of yes and no trial types, irrespective of category difficulty, was used to extract the fROIs. Based on previous literature on language comprehension studies [6], the following *apriori* cortical ROIs (left

and right) were used: BA 44, BA 45, BA 47, inferior temporal gyrus (ITG), medial temporal gyrus (MTG), superior temporal gyrus (STG), supra-marginal gyrus (SMG) and cingulate gyrus (CG).

Repeated measures ANOVA were performed for each ROI, with task difficulty (easy/difficult categories) and condition (yes/no) as within-subject factors and age group as a between-subject factor.

8.2.2.2 Event Related Potentials

Epochs, from 100ms prior to stimulus onset and continued to 900ms after stimulus onset, were defined for the preprocessed EEG data. A baseline correction using the pre- stimulus onset for each epoch was also applied. Stimuli were divided into easy or difficult types and yes or no conditions in the same manner as done for the fMRI. EEG epochs for each event type were then averaged to obtain their respective ERPs. Difference waveforms, i.e. each event type vs. control, were also generated. Grand averages for these waveforms (i.e. ERPs averaged over all the subjects) were also obtained.

Individual subject N400 and P600 peak latencies for easy and difficult conditions were determined using a sine-wave correlation method. Sine-wave correlation methods have previously been shown to be robust in identifying peaks in noisy ERP data [157]. The choice of window width for correlation was based on the approximate temporal window for each of these effects observed in the grand averages. More specifically, a half sine-wave of window length 120ms was cross-correlated with the 'no vs. control'

waveforms from 300 to 500ms time interval. The lag with the maximum cross-correlation coefficient in this time window was selected as the latency of the N400 peak. Similarly, a wider half sine-wave window (180ms) was cross-correlated with the 'yes vs. control' waveforms from 450 to 750ms time interval to determine the P600 peak latency. Using these peaks, area of all the ERP waveforms within ± 50ms of the N400 peak and ± 75ms of the P600 peak were calculated and used for statistical analyses. Grand average waveforms showing the N400 and P600 effects at the three midline electrodes (Cz, Fz & Pz) for difficult categories for the old subject group are shown in Figure 8.1. Voltage distribution maps of 'easy-no vs. control' (A) and 'easy-yes vs. control' (B) waveforms for the young group of subjects are shown in Figure 8.2.

Statistical analyses were done by grouping individual electrodes into four regions, as in section 7.2.4.3. A 4-way repeated measures ANOVA was used with anterior-posterior (AP four levels), laterality (8 levels), difficulty (easy/difficult) and condition (yes/no) as within-subject variables and age as a between-subjects factor. The Greenhouse-Geisser correction was used for all comparisons [135]. To spatially localize each of the two ERP components and to evaluate for spatial differences between task difficulty categories and between age groups, the same repeated measures analysis was also performed using only the condition waveforms on which the N400 and P600 components could be identified (i.e. No minus Control condition for N400 and Yes minus Control condition for P600).

Since both these effects were expected to be maximum at the midline electrodes, an additional 3-way repeated measures ANOVA was also performed using only the three

midline electrodes (Fz, Cz & Pz) with difficulty and condition as within-subject factors and age as between-subject factors.

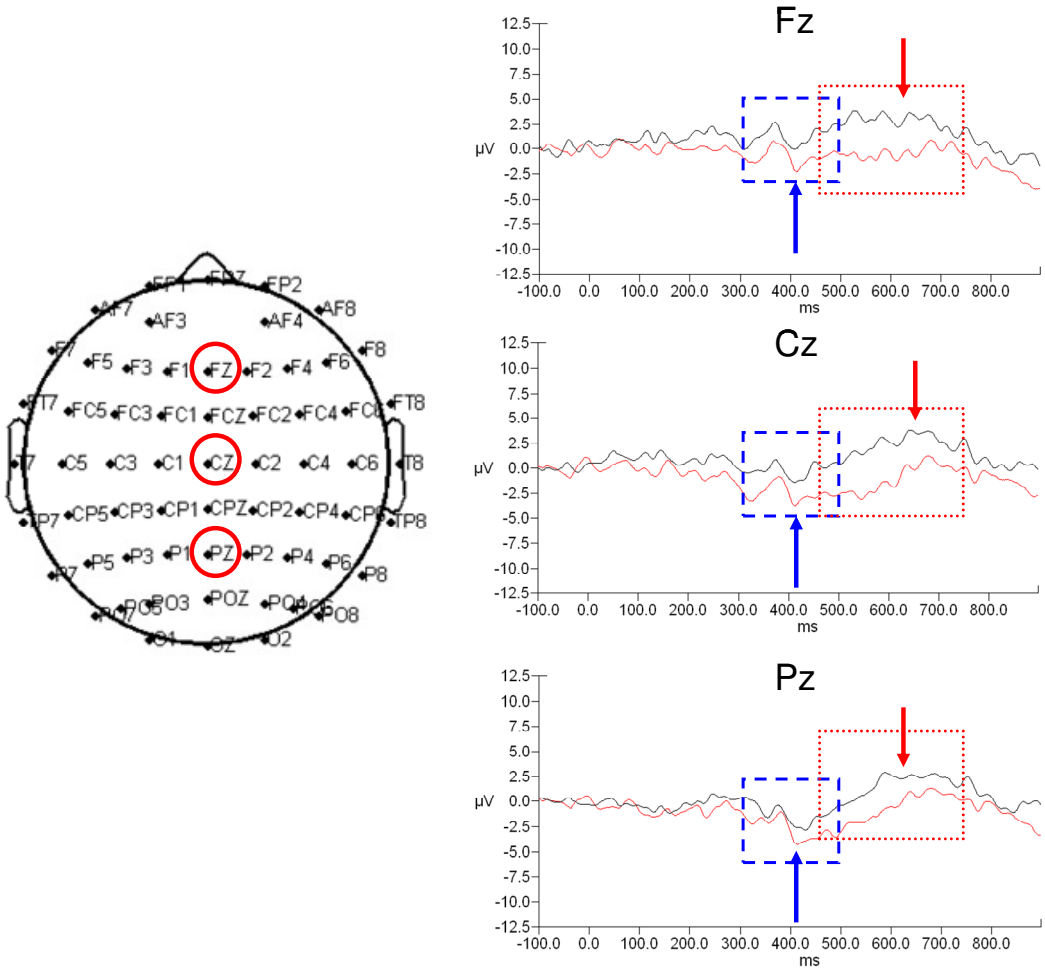

Figure 8.1: ERP grand averages for difficult categories in old subjects showing the N400 (blue arrow) and P600 (red arrow) components at the three midline electrodes (FZ, CZ & PZ). ERP waveform for Yes (black) and No (red) options are shown. Greater negative peak at 400ms (N400) for the semantically unrelated condition and greater positive peak at 600-650ms (P600) for semantically related condition are seen. Blue (300-500ms) and red (450-750ms) boxes indicate time windows selected to identify individual subject N00 & P600 component peaks.

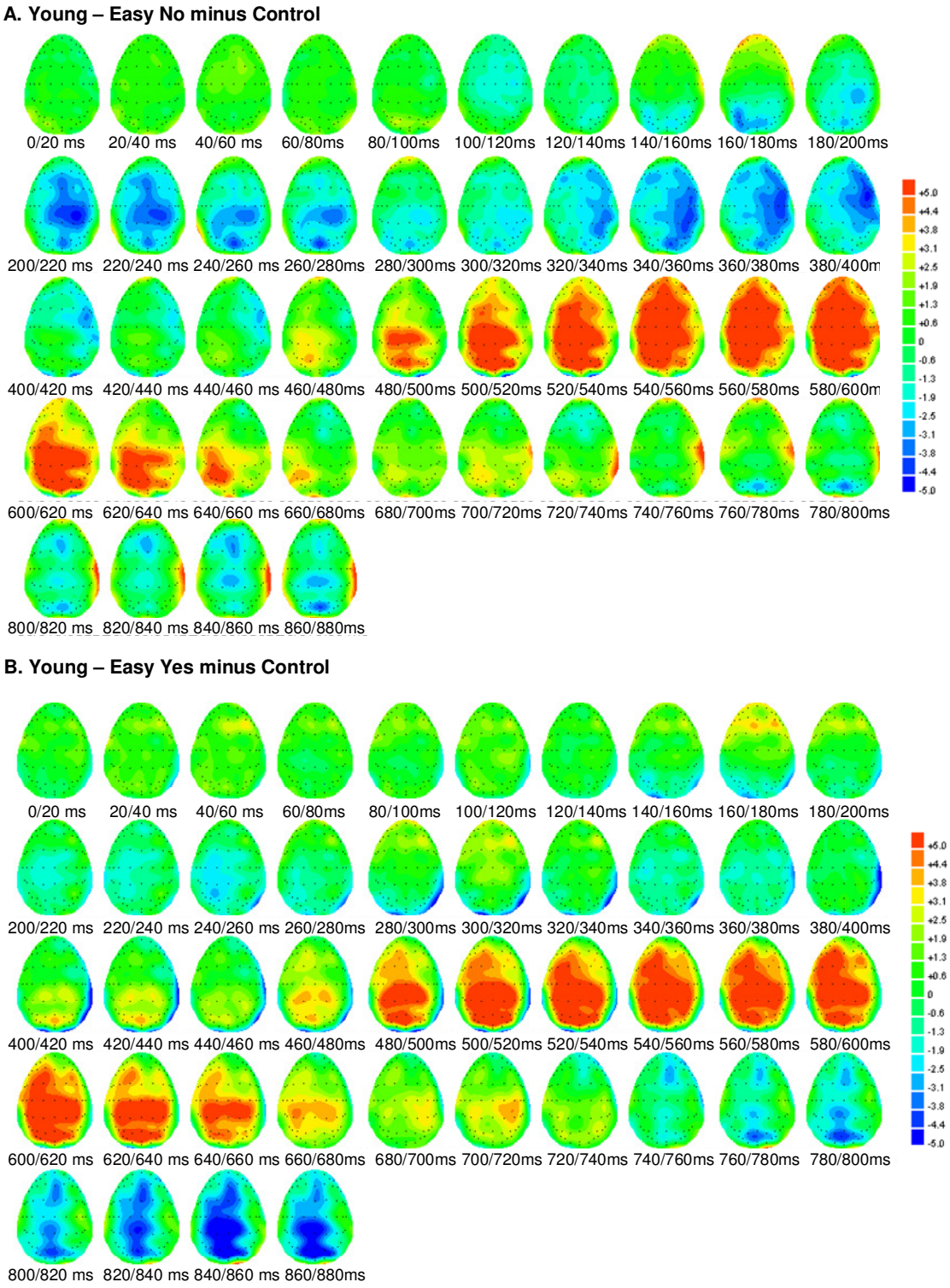

Figure 8.2: Group averaged voltage distribution maps for A. semantically unrelated (No minus Control), and B. semantically related (Yes minus Control) for the objective categories in young subject group. N400 associated negativity is seen for the semantically unrelated ERP and not for the semantically related ERP ($p<0.05$). P600 associated positivity is seen for both options with greater amplitude for the semantically related options ($p<0.005$).

8.2.3 Source Analysis

CURRY v.4.5 software package was used for performing source analyses (http://www.neuroscan.com/curry5). A realistic three component head model was first defined for every individual subject using the boundary element method (BEM) [158] and the subject's T1 MR anatomical image. Using the MR image, scalp, skull, CSF, grey and white brain matter surface segmentation was performed. Conductivities of 0.33 S/m for the CSF and the scalp and a conductivity of 0.0042 S/m for the skull were used to define the model [159]. The BEM model method assumes a homogeneous isotropic conductivity within each compartment and uses approximately 3000 nodes to represent all the compartments. Anatomical reference points were identified on the individual subject MR image: nasion, inion, left-right preauricular points, anterior commisure (AC) and posterior commisure (PC). Using the nasion, inion and preauricular reference points and the segmentation results, an international 10/20 system montage of electrode locations was defined for every individual. The AC-PC reference points were used to transfer the MR image space into the Talairach based coordinate system before doing any further analyses.

An anatomically constrained dipole analysis was then performed over the entire averaged EEG waveforms for all stimuli types for each individual. For each of these waveforms, activation foci identified from the fMRI ROI analysis were used as seeds. A rotating dipole was seeded at each of these activation foci with a 1mm freedom of movement, for every seed separately. This analysis solves for the inverse problem and calculates how much of the measured data can be explained by a dipole source located at

the selected seed point. This is also called the explained variance by the source at each time point. Time courses of these explained variances for the averaged ERP data were extracted and used to interpret the results. Mean explained variances over the same time windows for the N400 and P600 conditions using the 'no minus control' and 'yes minus control' waveforms were calculated for both task difficulty categories. To evaluate differences between explained variance for the different ROIs, a repeated measures ANOVA using condition (yes/no), task difficulty level (easy/difficult) and ROIs as within-subject factors and age as between-subjects factor, was performed.

8.3 Results

8.3.1 Functional MRI

Anatomical ROI Analyses:

Using the anatomical ROI method, significant differences between %BOLD values for the easy and difficult categories and trends between semantically related and unrelated conditions (yes vs. no) were observed. %BOLD values between the easy and difficult categories (main effect of task difficulty; %BOLD difficult>easy) were significantly different in the left BA45 ($F = 7.488$; $p=0.015$). A trend of %BOLD values for the No condition higher than the Yes condition was found in the left BA44 ($F = 4.32$; $p=0.054$).

Semantic unrelated-related processing differed with question category difficulty (task difficulty*condition interaction) in the right SMG ($F = 5.89$; $p=0.027$). In this

region, the %BOLD value for the Yes condition was higher than the No condition for the easy categories, while the No condition had higher %BOLD values for the difficult categories. However, posthoc analyses did not reveal significant differences between the Yes-No conditions when the easy and difficult categories were analyzed separately. In addition, a difficulty*condition*age group effect was found in the left ITG ($F = 8.25$; $p=0.012$). Posthoc analyses revealed that only the young group showed a significant task difficulty effect in processing No vs. Yes conditions (easy – No>Yes significant at $p=0.039$ & no significant difference between the No & Yes condition for difficult categories.).

fROI Analyses:

Similar to the anatomical ROI analysis, this method of ROI analysis resulted in significant differences between %BOLD values for the easy and difficult categories. However no significant differences or trends between the semantically related and unrelated options were observed with this method. Main task difficulty effects (i.e. %BOLD difficult > easy) were observed in the left BA47 ($F = 6.3$; $p=0.023$), left BA45 ($F = 5.82$; $p=0.028$) and the left ITG ($F = 5.18$; $p=0.037$).

In addition, left ITG showed differences in task difficulty between age groups (task difficulty*age group – $F = 6.57$; $p=0.02$) and differences in semantic unrelated-related processing with task difficulty and with age groups (task difficulty*condition*age group – $F = 7.57$; $p=0.014$). Posthoc analyses done separately for the two age groups with %BOLD values in the left ITG revealed that the task difficulty effect was significant only for the older group (difficult > easy; $p=0.011$). In addition, only the young group showed

a significant task difficulty effect in processing No vs. Yes conditions. However further posthoc analyses looking at condition effects separately in each difficulty category revealed no differences between the semantic related and unrelated stimuli (easy – No vs. Yes & difficult – No vs. Yes for young not significant).

8.3.2 Event Related Potentials

N400

N400 amplitude was significantly different between the semantically related (Yes) and unrelated (No) condition, with more negative amplitude for the No condition (main effect condition – $F = 6.35$; $p=0.022$; No<Yes). This effect was consistent over both age groups and over both easy and difficult categories (no age group or task difficulty interactions with condition were significant). The N400 peak was significantly later for the difficult categories (406ms) than the easy categories (384ms, $F = 5.11$; $p=0.037$). N400 voltage spatial distribution was found significantly different between the two age groups and between the two difficulty conditions (laterality*age group: $F = 4.05$, $p=0.017$; task difficulty*AP*laterality: $F = 2.65$, $p=0.017$).

Using only the midline electrodes (Fz, Cz, Pz)

Similar results were obtained only the midline electrodes. N400 amplitude was more negative for the unrelated condition than the related condition over the three

midline electrodes (main effect condition - F = 6.95; p=0.017). No age group or task difficulty category interactions with condition were observed.

P600

There were significant differences in the P600 amplitude between the semantically related (Yes) and unrelated (No) condition (main effect condition – F = 11.99; p=0.003; Yes>No) and between the two difficulty categories (main task difficulty effect – F = 4.52; p=0.048; easy>difficult). The P600 amplitude difference between the No and Yes conditions was also found to be significantly different between easy and difficult categories (task difficulty*condition – F = 10.1; p=0.006). Posthoc analyses revealed that the amplitude difference between the Yes and No conditions (Yes>No – p<0.001) was significant only for the difficult categories. The P600 peak was significantly later for the difficult category questions (646ms) as compared to the easy categories (589ms, F = 13.16; p=0.002). Central positivity seen in P600 voltage distribution maps was significant (main effect Laterality: F = 16.12, p<0.001). P600 spatial distribution was significantly different between the two categories for the two age groups (task difficulty*age group: F = 4.44, p=0.05 and AP*task difficulty*age group: F = 6.99, p=0.007).

Using only the midline electrodes (Fz, Cz, Pz)

Using the three midline electrodes, the same results were observed. P600 amplitude was significantly different between the semantically related and unrelated

conditions (F = 14.24; p=0.002; No<Yes) and between the two difficulty levels (F = 5.77; p=0.028; easy>difficult). Similar to the earlier results, the P600 amplitude difference between the Yes-No conditions also found to be significantly different between the easy and difficult category levels (task difficulty*condition – F = 10.95; p=0.004) with posthoc differences seen only for the difficult categories (Yes>No; p<0.001).

8.3.3 Source Analysis

Based on the fMRI ROI analyses, seed points in five ROIs - left BA44, left BA45, left BA47, left ITG and right SMG, were selected to perform source analyses. The biggest cluster location in each ROI for every individual subject was selected as seed location. Repeated measures ANOVA analysis using the explained variances for each ROI resulted in no significance difference between the ROIs. No single seed point was found to be specific to the N400 or P600 time window. To check if poor SNR in our data could have limited the outcome of this analysis, a free dipole with no seeding constraints was fit to the data for a single subject with a well defined N400 peak. However, this dipole still was able to explain only a minimal amount of variance in the data. The mean explained variance over all subjects for each time window and for each ROI are plotted in Figure 8.3.

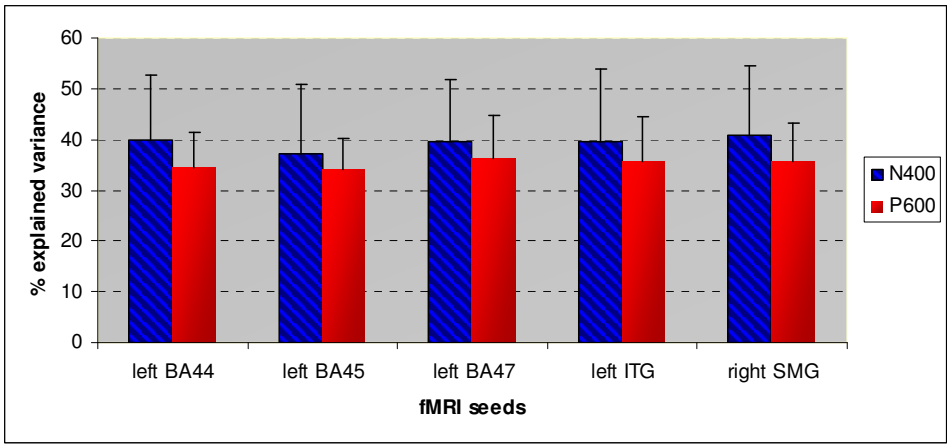

Figure 8.3: Percentage of variance explained by each of the selected fMRI seeds. All five selected seeds explained less than 50% of the variance in the data. No significant difference between ROIs was observed.

8.4 Source Analyses using PN & VG data:

An important finding using our ERP data was the differences in negativity (N400) across conditions seen during the 360 to 600ms time window in PN (See section 7.3.2). These differences were associated with the N400 effects previously seen in studies of semantic processing of picture stimuli [160-162]. This effect was also sensitive to task difficulty, with increase in negative amplitude with difficulty in naming pictures. For the VG ERP data, a central negativity effect was observed in approximately 520 to 720ms (young: 520 to 640ms & old: 600 to 720ms) time window for processing all words in comparison to controls and in a much later window (960 to 1200ms) for difficult as compared to easy words. Although these differences were not in the expected time window commonly observed for the N400 effect (between 300-500ms), it was discussed that the latency of this negativity may suggest a delayed semantic processing for VG. Also, difficult VG tasks were found to have delayed and prolonged semantic processing as compared to easy tasks.

The goal of source analysis was to qualitatively confirm that the central negativity effects seen for PN and during the delayed time intervals for VG are in principle related to the same semantic processing. If this was true, the sources from all three data sets (i.e. all pictures vs. control, all words vs. control and difficult vs. easy words) should converge to the same cortical locations. For solving this inverse problem, minimum norm least squares (MNLS) current density source reconstruction technique was used (Details about current density source analysis can be found in section 4.1). Current density methods, unlike limited source dipole methods, require no a priori assumptions about the nature of source current distributions and are the best choice when activity distribution is poorly known in advance. Age-group averaged ERP waveforms for all stimuli vs. control for PN & VG and for difficult vs. easy for VG were selected for this analysis. As we did not see any task difficulty related effects in PN, the difficult vs. easy waveform for PN was not used. The averaged waveforms were first filtered with an 8Hz low pass filter to improve SNR for source reconstruction. Realistic three component BEM head model was defined as described in the previous sections. A standard space T1 weighted MR image of a standard brain was used to model the different layers of BEM. Current density methods search for the best estimate of a distributed primary current by making an assumption of existence of a grid of sources in 3 dimensional spaces. This grid of sources was restricted to the cortex extracted from the MR image for all analyses. Minimum norm estimates were then calculated in steps of 2ms during the respective time windows for each waveform. A χ^2 criterion was used to estimate the regularization parameter. Current density maximum and sources within 30% of the maximum estimate were used to identify location of sources.

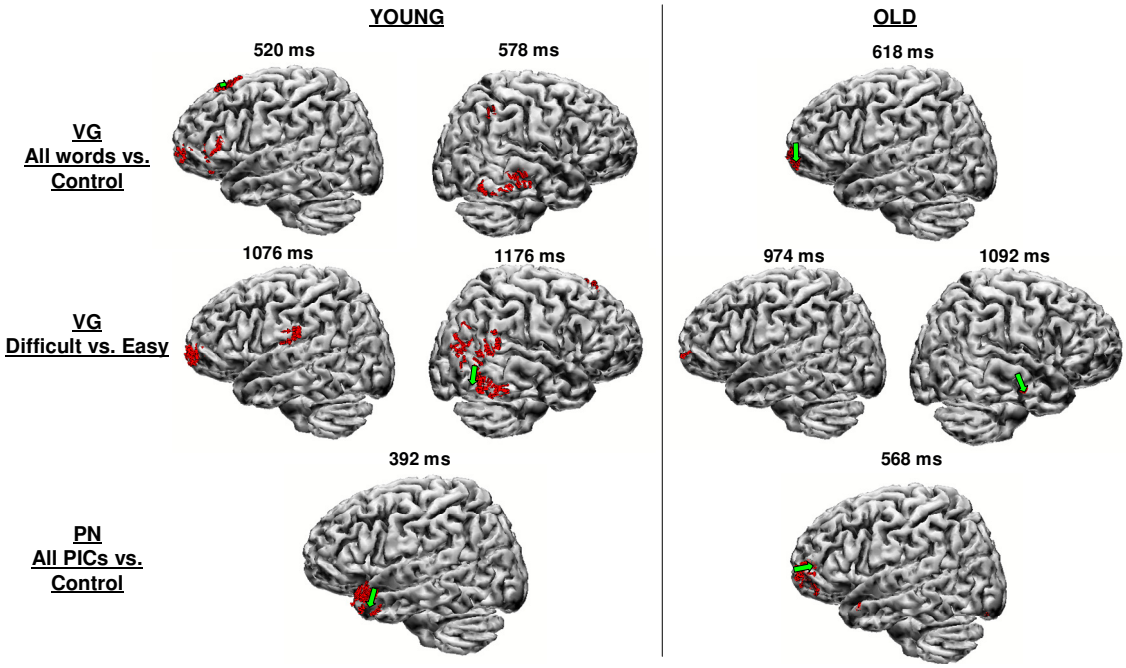

Figure 8.4: Current Density Source Analysis for PN & VG – top row – VG: All words vs. Control; middle row – VG: Difficult vs. Easy; bottom row – PN: All PICs vs. Control. Green arrow indicates location of maximum current density estimate & red arrows represent sources within top 30% of the maximum estimate. Consistent sources in the left inferior frontal region are seen for VG in both young and old groups of subjects and for both comparisons. Same source location observed for old subjects for PN.

Results:

The maximum source locations and sources within 30% of the maximum source estimate for each of the waveforms are shown in Fig 8.4. A consistent source is observed in the left medial inferior frontal region for both all words vs. control and difficult vs. easy VG data and present for both young and old groups of subjects. The same source location is also observed for only the old subjects for the all pictures vs. control waveform for the PN data. These results seem to indicate that the observed central negativity observed in all three data sets is linked to the same underlying neural processing. Moreover, the inferior frontal region was also found activated for the same comparisons using the fMRI data. An additional source location in the right inferior

temporal region was present for both comparisons for VG in the young subjects and the difficult vs. easy comparison for the old subjects.

8.5 Discussion

Successful language comprehension depends on the correct semantic and syntactic integration of information. Electrophysiology studies of language comprehension have identified two markers for violations in processing semantic and syntactic information: N400 – a negative peak at roughly 400ms post stimulus typically seen in response to words which do not fit semantically in the context of a sentence and P600 – a positive peak seen roughly around 600ms in response to syntactic anomalies in a sentence. Although these markers have been identified in separate studies of semantic and syntactic violations, there have been arguments and observations that have shown evidence that these two processes may be linked in a more complicated manner [163]. In a review of these findings, Kuperberg has proposed two competing neural processing streams of language comprehension: a semantic memory-based mechanism and a combinatorial mechanism that assigns structure to a sentence based on morphosyntactic rules, but also on the basis of semantic-thematic constraints.

In this chapter, the fMRI and ERP results from a language comprehension task designed to highlight semantic processing in a contextual sense are presented. Most studies of semantic processing, using both these modalities, have used tasks which evaluate semantic violations in a sentence [164, 165] or word priming [16, 166]. In addition, there have been a few attempts to evaluate semantic violations in a broader

context rather than simple sentences [167]. Our task is unique from these previous attempts and evaluates semantic processing for single words/options in reference to a particular semantic context, represented by each of the four categories in our task.

We found a significant difference between ERPs for options which fit the semantic context and those which do not. Options with semantic context violations showed a greater negative peak during the 300 to 500ms time window (N400). This result is consistent with previous studies of semantic processing, where a negative peak has been observed for semantic violations in sentences [165] or for mismatched semantic priming between words [16]. Using our task, we have shown that the same N400 effects can be reproduced in words which do not fit the semantic context (yes vs. no) of both objective (easy) and subjective (difficult) categories in our task. Although, there were no differences between amplitudes of the N400 effect between the two difficulty category types, peak latency for the subjective categories was later than the objective ones. Aging studies of sentence or word level N400 semantic effects have found reduced N400 peaks with age [166]. Both subject age group recruited in our study showed no difference between amplitudes of the effect but had different spatial voltage distribution patterns with the N400 effect more lateralized on the right for the young and on the left for the old group.

The P600 effects seen with our ERP data were not expected. P600 effects have previously been observed in studies of syntactic violations with comprehension [7, 168]. Our task was designed to elucidate only semantic violations. The presence of this effect (greater P600 amplitude for the semantically related options as compared to the unrelated options) can be related to previous findings of P600 peak modulation with semantic

expectancy [169]. P600 effects between the subjective and objective categories were found significantly different, with a greater amplitude and latency observed for the subjective categories. Similar to the N400 results, only spatial voltage distribution differences were observed between the two age groups, with no differences in amplitude of the effect.

Different semantic processing for the yes and no options was also reflected as hemodynamic differences in BOLD fMRI signal. Two types of ROI analysis methods were used with our fMRI data, both methods showing only little agreement. Using ROIs defined anatomically, greater BOLD signal for the semantic context violations was found only in the left BA44 over both category types and in the left ITG only for the young subjects for the easy categories. These results are in agreement with frontal and temporal regions previously shown to be associated with semantic information processing [170]. Differences in BOLD signal between the semantically related-unrelated options and between the two difficulty categories were found in the supramargnial gyrus. Enhanced BOLD values for the semantically related options in this region for the objective category is consistent with previous findings [16]. Using functional definition of ROIs for analysis, only differences between the category types (greater BOLD values for difficult compared to easy categories) were found in the left BA45-47 & inferior temporal gyrus. Older subjects showed greater difficulty category differences in the inferior temporal region as compared to young subjects. However, no differences were found for semantic context violations. Both ROI analysis methods showed an absence of a significant effect in superior temporal gyrus, an area commonly seen with fMRI tasks of semantic violations. This was unexpected considering the role of this region in semantic processing [171].

Another important focus of this chapter was to integrate results from fMRI and ERP using source analysis. Dipole analysis was used to solve the inverse problem of identifying neural sources. To reduce the solution space for this inverse problem, five fMRI regions showing significant category and yes-no effects using the ROI analyses were selected as seed locations to constraint the dipole analysis. This ROI constraint dipole analysis method, allowed us to calculate the amount of variance in the measured data explained by each of the seed ROIs over a selected time window. The use of explained variance to evaluate correlation of results from fMRI & ERP has been previously shown in novel stimulus processing [172]. Using our data, no clear relationship between any of the selected fMRI seeds with the ERP time windows was found. All fMRI seeds were able to explain only minimal amount of variance in the data (<50%). A possible reason for this result is the poor signal to noise ratio of our data sets. Filtering the data improved the SNR by almost a factor of two; however this still did not improve the amount of explained variance by the fMRI seeds precluding us from making any specific conclusions from the source analyses. Another reason could be the presence of more than one focal source for the effects seen in our data. If this is the case, then a single dipole model will always be limited in explaining maximum variance in the data. Our results nevertheless indicate that our task is successful in evaluating semantic processing of word stimuli in a contextual sense and these results can be seen with both fMRI and ERP modalities.

Chapter 9

White Matter Connectivity and Structure-Function Associations

9.1 Introduction

Diffusion tensor imaging and functional MRI provide complementary information in terms of studying neural organization. While fMRI allows mapping the functional architecture of the brain, DTI has the ability to image white matter (WM) pathways and provide useful insight on the anatomical connections of these functional regions. An inherent requirement of DTI based tractography techniques is the need to define a hypothesis based seed region of interest (ROI) to initiate fiber tracking. Appropriate criteria for selection of these seed ROIs have a significant effect on the validity of DTI results. Selecting these seed ROIs based on anatomical knowledge has been the popular approach to identify fiber bundles in healthy subjects [59, 173, 174]. However this selection may be operator biased and also may not be able to account for changes in anatomical pathways in the presence of clinical pathology [54]. An alternate obvious choice would be to use fMRI activations directly as seeds for tractography. However, the loss of fiber orientation in cortical grey matter due to a characteristic low anisotropy limits the extension of WM fiber bundles to these activation voxels and often results in tracking only a few fibers part of the complete tract. This has led to a more practical approach of using functional information from fMRI as a guide to selecting seed ROIs within the WM. The intersection of these two techniques have expanded the utility of

each of these techniques used alone and have shown potential to further our understanding of how the brain works.

Integration of these two imaging techniques have been attempted using numerous approaches: 1. qualitative evaluations by means of simple overlay of images from these modalities [175] or using more advanced 2D and 3D visualization techniques [176, 177]; 2. statistical evaluations by establishing relationships between quantitative measures from the two techniques [178, 179]; 3. selection of seed voxels for tractography located in WM regions adjacent to functional activations [180-182]. A number of groups have modified the seed voxel techniques to improve seed selection. Toosy *et al.* have used a robust two step seed voxel selection process using anatomical guidelines to control for the inter-subject variability of traced fibers attributed to variability in seed selection [183]. By segmenting the visual pathways using DTI, significant structure-function correlations were observed between the measures from these tracts and visual functional activations. Instead of fMRI assisting the seeding of DTI, Dougherty *et al.* have assigned fiber tracts to particular cortical ROIs only if the end-points of the fibers were within 2mm of the cortical ROI [184]. Schonberg *et al.* have shown the significance of using fMRI with DTI by selecting seed ROIs from a sphere of 15 voxels around the fMRI cluster and depending on the directions of fibers approaching the fMRI activation [54]. Using this method they successfully mapped deformed WM architecture in patients with space occupying lesions.

Although these attempts to integrate the two techniques have been fairly successful, Kim *et al.* have pointed out challenges and problems associated with these integrations [182]: 1. Selection of appropriate threshold to be used for selecting compact

seeding ROIs from patchy BOLD activations, and whether or not voxels in these ROIs should be treated as homologous regardless of their p-values; 2. Limitations of conventional DTI algorithms in extracting fiber tracts for ROIs placed exclusively in the cortical grey matter (resulting in very few or zero fibers), which demand a need for an automated search algorithm for the closest fiber termination points to be included as part of seeding ROI; and 3. Relating typical large voxel sizes from fMRI images to the underlying hundreds of thousands of axonal fibers. Although the solution to the last challenge is limited by achievable resolution using MRI, the first two problems can be resolved by careful post processing algorithms. A few post processing approaches towards these problems have been applied with main focus to avoid the manual selection of ROIs. Using a Brodmann's area template containing both cortical GM and sub-cortical WM regions as seeds for tractography, Thottakara *et al.* have used the functional relevance of these areas to compartmentalize underlying WM pathways [185]. However, this method is limited by its assumption that the functional areas for a subject are restricted to the standard anatomical boundaries of the used template. This may not hold true for patients where functional areas are often displaced beyond the standard anatomical boundaries. Another approach using sophisticated probabilistic techniques have been successful in tracking fibers directly from GM cortical ROIs thus requiring no manual ROI definition or prior user knowledge of fiber anatomy [53, 64]. While the probabilistic tracking algorithm may seem to be robust against most earlier mentioned limitations, the main shortcoming of the method is the computation complexity and time involved to estimate the probability density function at every voxel, making this approach impractical for clinical applications.

In this chapter, an automated and less computational intense approach to combine DTI-fMRI is proposed and evaluated. Optimization of DT-MRI for tractography on the Philips 3T scanner was performed and quantitative measures for GM-WM associations were extracted for a group of healthy subjects.

.

9.2 Optimization of Diffusion Tensor Imaging

The DT-MRI sequence parameters were optimized on the Philips 3T Achieva Scanner at Stony Brook University Hospital. Sequence optimization was done for b-value, number of diffusion encoding directions and number of signal averages. Effects of cardiac noise on diffusion tractography were also evaluated.

9.2.1 Methods

9.2.1.1 Imaging Parameters

Four healthy, right handed subjects participated in this study. DT-MR Imaging was done using an 8-channel SENSE head-coil. An echo planar imaging (EPI) spin echo sequence with a SENSE factor of 2.4 and flip-angle of 90° was used. A non-cardiac gated DT-MRI sequence at b = 800 s/mm^2 and 3 cardiac gated DT-MRI sequences at b = 800, 1000 and 1200 s/mm^2 were obtained using a medium (15 direction) diffusion encoding resolution for all the subjects. For 3 of the 4 subjects, high (32 direction) diffusion encoding DT-MRI scans were obtained at b = 800 & 1000 s/mm^2. The echo times (TE)

for the scans corresponding to the respective b factor were as follows: 58ms for 800 s/mm^2, 60ms for 1000 s/mm^2 and 63ms for 1200 s/mm^2. A repetition time (TR) of 2.7s for the non-cardiac gated scans and 4s for the cardiac-gated scans was used. All scans were collected using a matrix size of 112*112. Thirty contiguous axial slices each 4mm thick and a FOV of 22cm were used to cover the whole-brain. Three runs of the medium resolution scans and two runs of the high resolution scans were collected to match for scan time at the two levels of diffusion encoding resolutions. The scan time for a medium resolution non cardiac gated scan was 52s and for a cardiac gated scan was 1min 16s. Scan time for each high resolution non cardiac gated scan was 1min 40s and for a cardiac gated scan was 2min 24s.

9.2.1.2 Data Analysis

DT-MRI data analysis was done offline using a diffusion tensor computation and fiber bundle tracking tool - DTIstudio [186]. The fiber tracking algorithm implemented in DTIStudio is based on the Fiber Assignment by Continuous Tracking (FACT) and brute-force reconstruction approach. Fiber tracking was done for voxels with fractional anisotropy (FA) values > 0.3 and stopped at voxels with FA < 0.18 or if the fiber turning angle was > 40°.

Two sets of fiber bundles were tracked: the pyramidal tract and corpus callosum. For the pyramidal tract visualization, a multiple ROI seed-target approach was used. Seed ROIs in the bilateral cerebral peduncles were defined and all fibers originating from these ROIs and passing through the bilateral precentral gyrus (target ROI) were assigned as the

pyramidal tract. For the corpus callosum, frontal and posterior "U" fibers were tracked using single ROIs placed in the splenium and genu respectively.

9.2.1.3 Sequence Evaluation

For sequence evaluations, fiber tracking results were qualitatively and quantitatively evaluated. Qualitative evaluations were done by judging the integrity of the tracked fiber bundles and identifying spurious fibers, while the number of fibers tracked and fiber density were used for quantitative evaluation. Fiber density was calculated as the total number of tract fibers arising from the seed ROI and reaching the target ROI as compared to the total number of fibers arising from the seed ROI alone. Fiber density evaluation was done only for the pyramidal tract (since a seed-target approach was not used for U-fibers).

$$Fiber\ Density = \frac{\#tract\ fibers}{\#total\ fibers\ from\ seed\ ROI}$$

9.2.2 Results

9.2.2.1 Cardiac vs. Non-Cardiac Gating

Effect of cardiac noise was evaluated at b=800. Non-cardiac-gated DT-MRI showed more spurious fibers (Fig. 9.1) in 3/4 subjects for the pyramidal tract and 2/4 subjects for the U-fibers (of the remaining two subjects, one showed no spurious fibers while spurious fibers were seen for both the scans for the other subject).

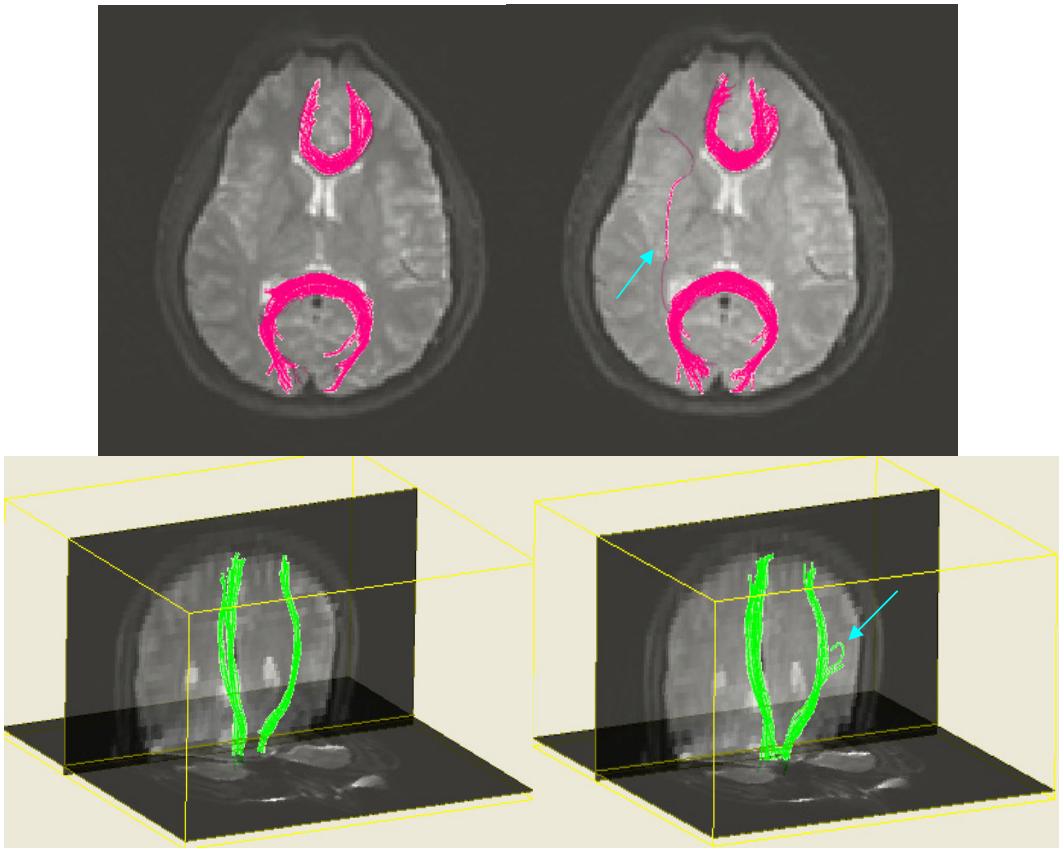

Figure 9.1: Cardiac-gated (left) and Non-cardiac-gated (right) DT-MRI evaluation for one subject. U-fibers (pink) and fibers belonging to the corticospinal tract (green) are shown. Spurious fibers (marked with blue arrows) seen for the non-cardiac gated data.

9.2.2.2 Optimization of b value

Fiber density and # fibers were compared for b=800, 1000 & 1200 with medium and at b=800 & 1000 with high resolution. Significant differences for fiber density were found between b800 & b1000 at high ($p=0.035$, b800<b1000) (Fig. 9.2) and for # fibers between b800 & b1000 at medium ($p=0.002$, b800<b1000) encoding (Fig. 9.3). Pyramidal tract visualization was better or comparable for b1000 than b800 at both encoding resolutions. The b1000 scan was comparable or better than b1200 for 3 of the 4

subjects (except subj1). U-fiber visualization was equivalent or worse for b1200, whereas both b800 and b1000 had equivalent fiber visualization.

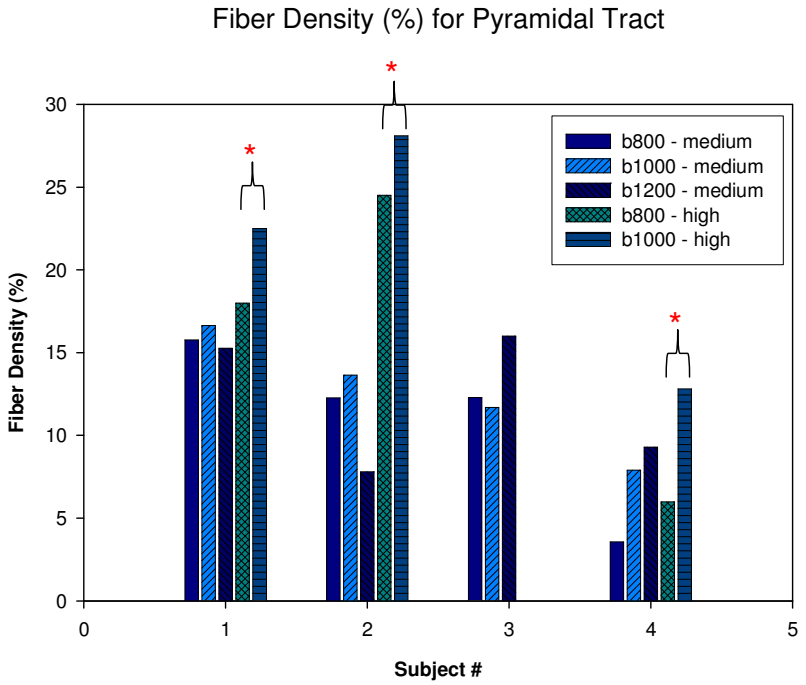

Figure 9.2: Comparison of Pyramidal Tract Fiber Density values for the DT-MRI sequences. * p=0.035, b800 high <b1000 high

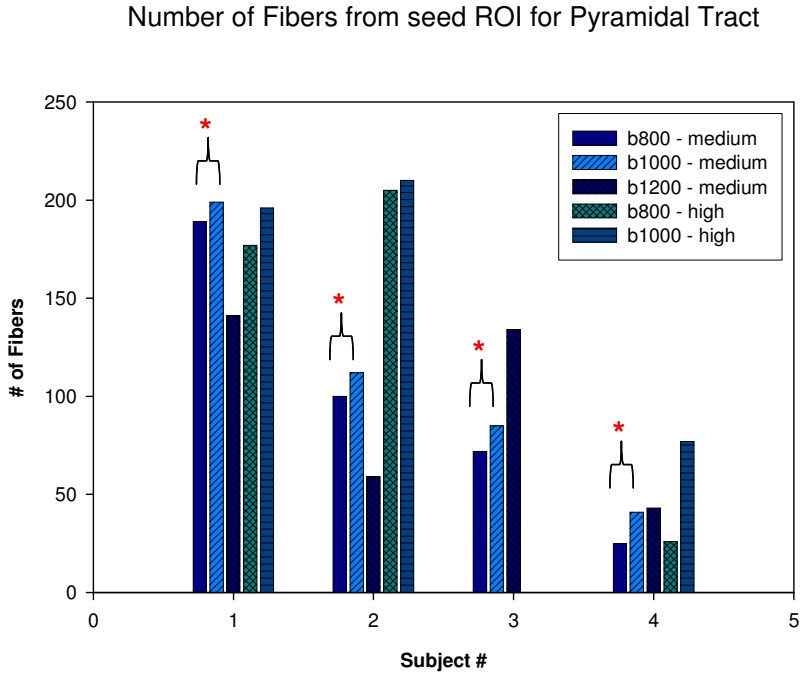

Figure 9.3: Comparison of Number of Fibers from seed ROI for Pyramidal Tract for the DT-MRI sequences. * p=0.002, b800 medium <b1000 medium

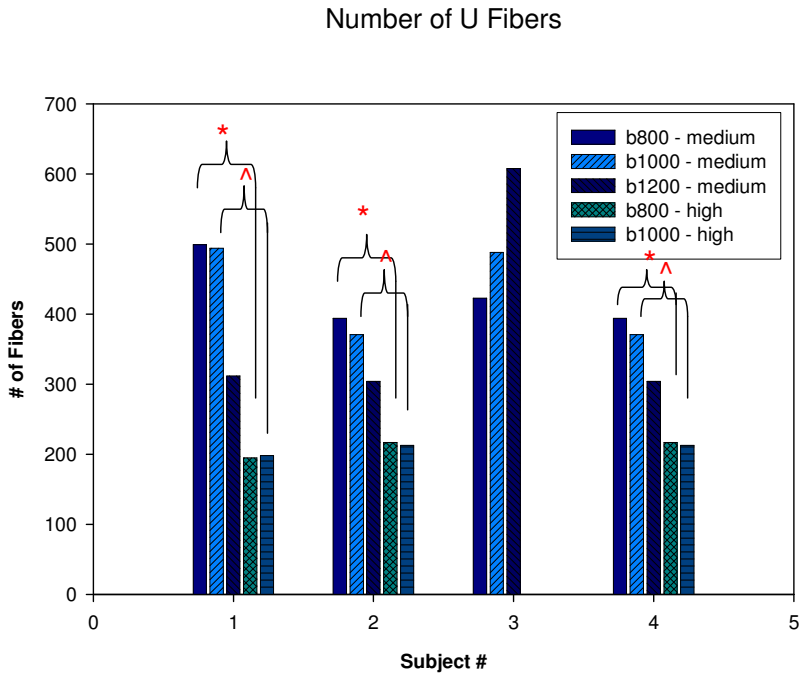

Figure 9.4: Comparison of Number of Fibers from seed ROI for U fibers for the DT-MRI sequences. * p=0.035, medium > high at b800; ^ p=0.047, medium > high at b1000.

9.2.2.3 Optimization of diffusion encoding directions

Significant differences for # fibers (medium>high) were found at b=800(p=0.035) & b=1000(p=0.047) only for the U-fibers (Fig. 9.4). A careful interpretation of this result is required as subj1 which showed the maximum difference between # fibers for medium and high encodings, also had the most spurious fibers for the medium data sets. For the pyramidal tract, better visualization was obtained for the higher resolution for all subjects at b1000 and 2/3 subjects for b800. Although not significant, mean fiber density for the pyramidal tract was higher for the high resolution encoding as compared to the medium resolution encoding for both b = 800 & b = 1000 (Figure 9.2).

9.2.3 Conclusion

Our results show that optimum diffusion tensor imaging can be done using a cardiac gated DT-MRI sequence with 32 directional diffusion-weighted encoding at a b value of 1000 s/mm^2 with a total scan time of 4min 48s (two averages).

9.3 Algorithm to integrate DTI/fMRI

9.3.1 Methods

9.3.1.1 Algorithm

An inherent assumption for integration of structure and function is that the WM structure associated with GM functional activations lies in close proximity to regions recruited for function. This algorithm is also based on the same assumption that the language WM pathway (called *arcuate fasciculus (AF)*) connecting the frontal activation (Broca's area) and the temporal activation (Wernicke's area) seen in language functional tasks lies in the WM close to these regions. Using different size combinations of frontal (seed) and temporal (target) ROIs with DTI tractography, it is possible to estimate the appropriate combination of the two ROI sizes which will result in extraction of fibers belonging only to the WM pathway connecting these two regions.

Rationale for the validity of the proposed algorithm:

The rationale for existence of such a combination of ROI sizes can be understood by considering how the anatomy of fibers tracked changes with iterative increments of combinations of the two ROIs. Every iteration step, for which the size of one seed point is increased, basically involves the addition of fibers to the number of fibers tracked in the previous iteration. The number of fibers added depends on the relative increase in sizes of the two ROIs for that iteration. As an example, a plot of the number of fibers tracked (y-axis) for different combinations of frontal (F-'n'voxels) and temporal ROI sizes (T-'n'voxels on x-axis) for one representative subject are shown in Fig. 9.5. Here 'n' represents the radii of the ROI in number of voxels. The graph is divided into different sections and description how the fibers tracked change with iterations in each section in provided below:

Section A: For ROI size combinations marked by section A (F-1voxel to F-3voxels & T-1voxel to T-18voxels), the size of the frontal seed ROI is minimal and only a minimum number of fibers are tracked from this ROI. Since this ROI size is small, presumably all fibers tracked belong to the AF. Next the size of the target ROI is iteratively incremented. For the first few increments in target ROI size (T-1voxel to T-7voxels), limited target ROI size allows only a few fibers tracked from the seed ROI to reach the target ROI. Any further increments in sizes of the target ROI (T-8voxels to T-10voxels) will add more fibers arising from the seed ROI to reach the target ROI. When the size of the target ROI is big enough (T-11voxels to T-18voxels) to allow all fibers tracked from the seed ROI

(F-3voxels) to reach the target ROI, any further increments in size of the target ROI do not change the number of fibers tracked. This can be seen as a plateau in section A (plateau 1) in Fig 9.5. Figure 9.5.a shows the fibers tracked for combination of F-3voxels & T-15voxels.

Section B: Consider the combinations of ROI sizes in section B (F-4voxels to F-13voxels & T-7voxels to T-11voxels). For combinations of seed and target ROI less than the optimum value (F-4voxels to F-9voxels and T-7voxels to T-11voxels), these iterations will result in a drastic increase in the number of fibers tracked (as compared to Section A) with all tracked fibers belonging to the AF fiber bundle. For combination of seed-target ROIs, where the size of the seed ROI is greater than optimum but target ROI is less than optimum (F-10 voxels to F-13voxels & T-7voxels to T-11voxels), iterations will result in tracking of additional fibers not belonging to the AF (e.g. other fibers going frontal or fibers of the inferior fronto-occipital fasciculus running parallel and adjacent to the AF). This can be seen as a large slope in the plot (slope 1).

Section C: Consider section C, where the size of both the ROIs is very close and less than the optimum value (F-6voxels to F-9voxels & T-12voxels to T-14voxels). When the number of fibers tracked is very close to the total number of fibers belonging to the AF i.e. seed and target ROI sizes are close to optimum, successive increments in the target ROI will result in a plateau. The highest plateau point gives the optimum combination of seed-target ROI sizes (plateau 2 & Figure 9.5.b).

Section D: Consider section D, which contains iterations where the size of the seed ROI is below the optimum value and that of the target ROI is beyond the optimum value (F-4voxels to F-9voxels & T-14voxels to T-18voxels). As the size of the target ROI is further increased beyond the optimum seed-target size, the target ROI will be large enough to include fibers from the neighboring fiber bundles thus resulting in again a drastic increase in the number of fibers tracked (slope 2 & Figure 9.5.c, additional fibers marked with red arrow).

Section E: This section contains iterations where both the seed and target ROI sizes are beyond optimum values (F-10voxels to F-13voxels & T-12voxels to T-18voxels). For iterations with increments of the seed ROI beyond the optimum seed size, the size of the seed ROI is large enough that even a small increment in target ROI will result in tracking of neighboring fibers in addition to those belonging to the AF (Figure 9.5.d, additional fibers marked with red arrows). This results in a progressive increase in slope of the plot for increments in seed size (slope 3 & Figure 9.5.e).

Proposed Algorithm:

Practically, the integration of fMRI and DTI was done using the following steps:

Step1: Defining the functional activation areas

To define the two functional activation areas, the verb generation task included in our study was used. Functional activation clusters in both the areas were identified using all words vs. control contrast at an uncorrected level of p=0.05. For the Broca's area,

activations were restricted to the BA44 ROI, while the Wernicke's area ROI was used to define the temporal activations. These fMRI activation clusters were transferred from normalized MNI space to the individual subject diffusion space using the image registration tool (FLIRT) in FSL [187].

Step 2: Segmentation of WM

For extracting the WM for every subject, the high resolution T1 weighted SPGR data was used. The sagittal anatomical data was first resliced in the same orientation as the DT-MR images (axial) using the Multi Planar Reconstruction (MPR) tool available on the Philips MR scanner. The axial anatomical images were then resampled and registered to the DT-MR images using the FLIRT tool. Segmented white matter image for every subject was then obtained using the segmentation routine provided with the SPM2 package.

Step 3: Identification of centers of ROI for fiber tracking

The main problem in using fMRI activation clusters to track the WM pathways is that the activation ROI is located in the low anisotropic GM area preventing the WM fiber tracts from extending into the seed ROI. To overcome this problem, new seed and target sphere ROIs were defined. The centers of these ROI spheres were determined as points on the WM/GM boundary nearest to the functional ROI. To determine these points, the center of mass for the activation cluster was calculated and the WM/GM boundary point at the shortest Euclidean distance from this center of mass was identified

as the center of the sphere. New centers were identified for both the frontal and temporal functional ROIs.

Step 4: Determining the optimum radii for the seed and target ROIs

An iterative approach was used to identify the optimum radii for these new, extended seed and target ROIs. At each iteration step, the radius of the seed ROI was incremented from the previous step and then held constant while iteratively increasing the radius of the target ROI. The initial radius for each ROI was 1 voxel dimension (1.72mm). A total of 18 iterations with a step size of 1 voxel dimension were performed. Fiber tracks for all combinations of the seed and target ROI radii were extracted. Fiber tracking was performed using a streamline tracking algorithm based on the FACT method [50] and 4^{th} order Runge-Kutta [51] integration. A stopping criterion of FA < 0.18 or fiber turning angle > 40° was used. Since a seed-target approach was used, only fibers generated from the seed ROI and reaching the target ROI were included as part of the tract. The numbers of fibers for all combinations of seed-target radii were then plotted. The optimum radii for the seed and target ROI were determined from the highest plateau point in the plot (plateau 2, Figure 9.5).

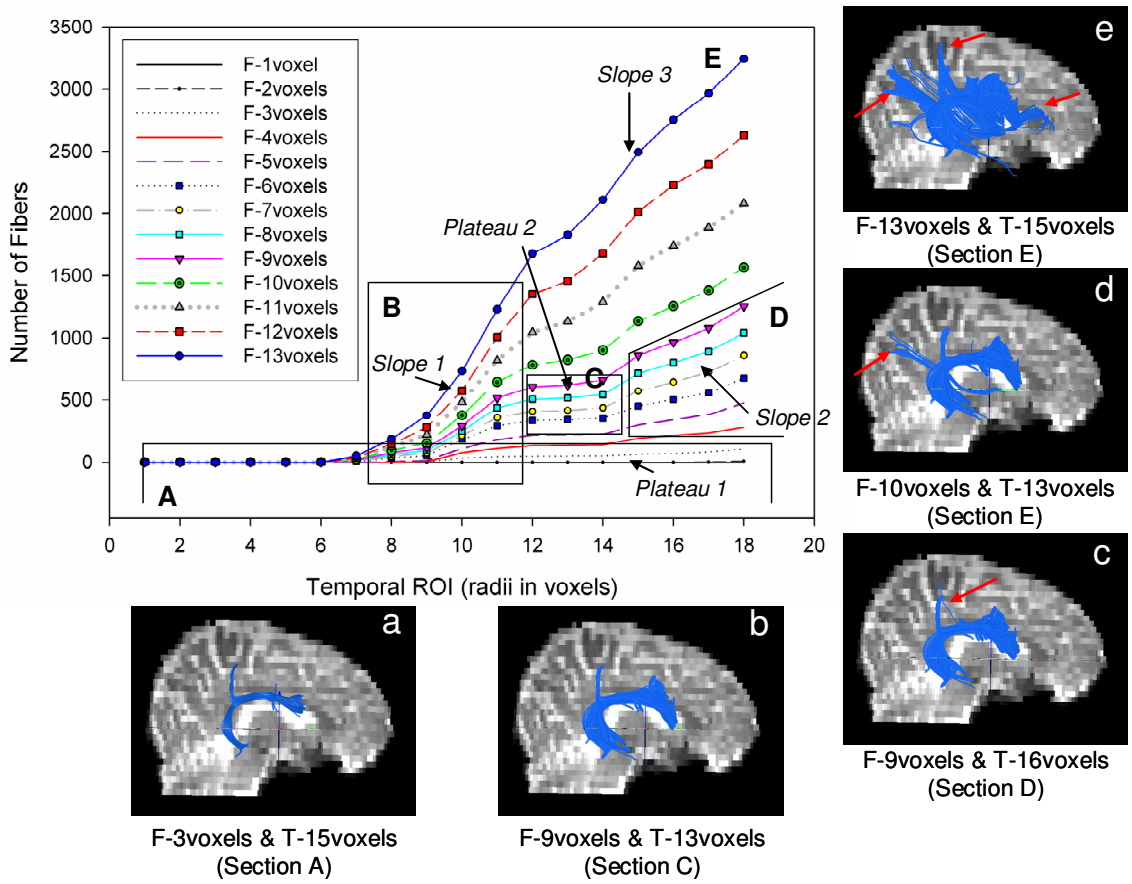

<u>Figure 9.5</u>: DTI-fMRI Algorithm Plot for all combinations of seed (frontal: F-'n'voxels) and target (temporal: T-'n'voxels) radii for one subject. Numbers indicate size of ROI in mm. a – Fibers for seed-target combination in Section A; b – Fibers for optimum seed & target size (Section C); c – Fibers for optimum seed ROI, but target ROI size > optimum target size (Section D); d – Fibers for optimum target ROI, but seed ROI size > optimum seed size (Section E); e – Fibers for both seed & target ROI size > optimum seed-target sizes (Section E). Slope 1,2,3 & Plateau 1,2 are features identified in the plot. Spurious fibers (fibers other than AF) are marked by red arrows.

9.3.1.2 Evaluation of Algorithm

Subjects & Data Collection

DTI data was collected for eighteen of the subjects who participated in the fMRI study. Data from sixteen subjects was used for evaluation of the DTI/fMRI algorithm. No

significant Wernicke's area activations were present for the remaining two subjects and hence were excluded from this analysis. DT-MR Imaging was done using the optimized sequence for 9/16 subjects. For the remaining 7 subjects, scanning was done before the DTI optimization study and had the following parameters: b = 800 s/mm^2, medium diffusion encoding resolution (15 directions) and 3 NEX. The total scan time for these scans was 2min 18s.

Data Analyses

All DT-MRI scans were first corrected for eddy current induced image distortions using a 3D affine registration algorithm from the AIR package [188]. New DTI gradient tables for individual subjects were generated after correction for slice angulations, slice orientation and co-registration parameters (due to eddy current correction) using the DTI gradient table creator software [189].

AF Fiber tracts in both hemispheres from three analysis methods were extracted and compared to evaluate our proposed DTI-fMRI algorithm: 1. Complete AF tract using the proposed algorithm, 2. Section of this AF tract restricted to within and between the frontal and temporal ROI (this would allow to exclude sections of the track continuing beyond the two ROIs and restrict only to the tract section physically connecting the two ROIs) and 3. AF tracked using a manual two-plane approach.

The manual two-plane approach used for comparison is based on the method proposed by Wakana and colleagues [173]. In short, this method is based on using RGB color maps and defining two planes for selection of ROIs to track the fiber bundle (See

Fig. 9.6). For the first ROI, the lowest axial slice in which the fornix can be identified is selected. Then a coronal slice is selected at the middle of the posterior limb of internal capsule (Fig. 9.6.a). In this slice, the first ROI is defined to include the core of the superior longitudinal fasciculus (SLF) (seen as a green triangular section) and all branches coming out from this area (Fig. 9.6.b, c, d). For the second ROI, a coronal slice at the middle of the splenium of the corpus callosum using the mid sagittal plane is selected. The second ROI is then chosen to include all the labeled fibers (Fig. 9.6.e&f).

Both qualitative and quantitative comparisons of the three sets of tracked fiber bundles were performed. Qualitative comparisons were done to ensure that the tracked fiber bundles contained only fibers belonging to the arcuate fasciculus and no neighboring fiber bundles. Checks were also performed to ensure that the proposed algorithm was able to track the complete arcuate fasciculus. For quantitative comparisons, mean values of FA, ADC, axial ADC (λ_1) and radial ADC ($(\lambda_2+\lambda_3)/2$) measures over each fiber bundle were extracted. A repeated measures ANOVA with laterality (left/right) and fiber tracks (3 sets of fiber bundles) as within-subject factors and age group as between-subjects factor was used to compare each of the quantitative measures extracted for the three fiber bundles and also to compare the left vs. right hemispheric fiber tracts.

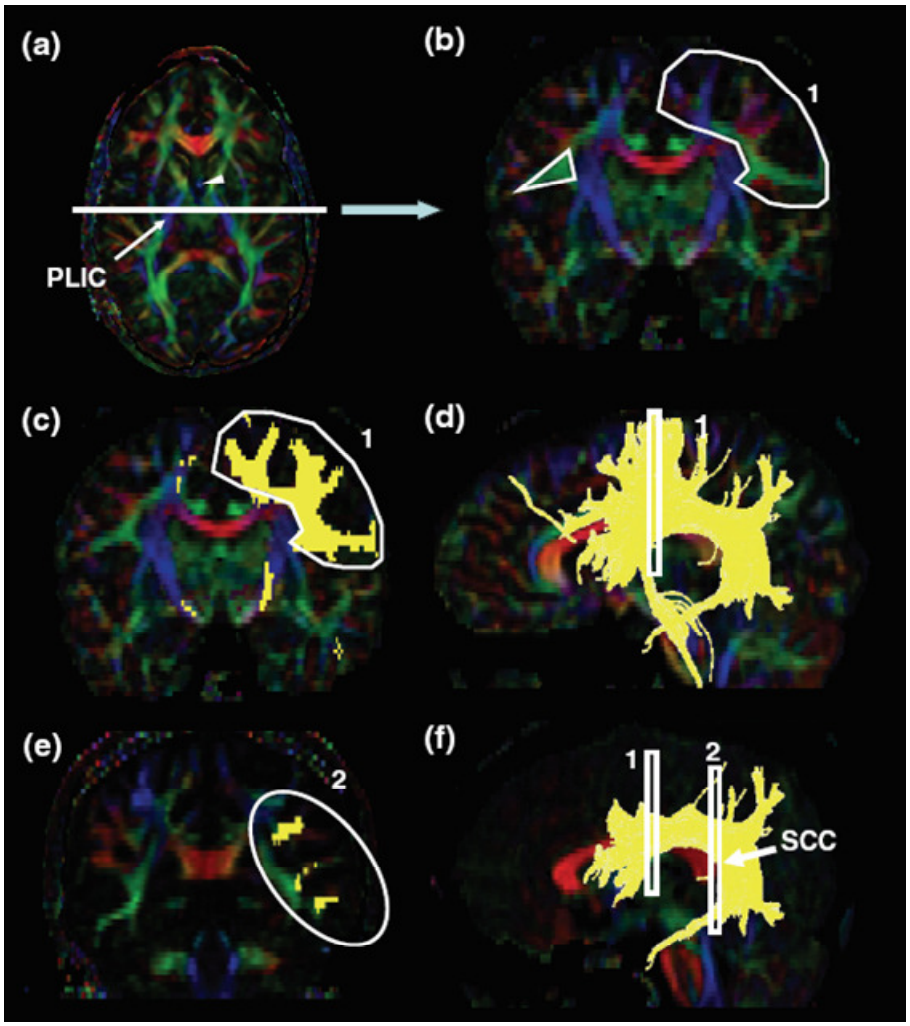

Figure 9.6: Manual two-plane approach for tracking the Arcuate Fasciculus. Figure taken from [173]. At the middle of the posterior limb of the internal capsule (a, PLIC), a coronal slice is selected (b). The SLF can be identified as an intense triangle-shape green structure. The first ROI is shown in (c: coronal) and (d: sagittal). For the second ROI, a coronal slice (e) is selected at the splenium of corpus callosum (SCC) (f).

9.3.2 Results

Qualitative Evaluation:

Qualitatively, the left AF bundle was tracked successfully in 13 of 16 subjects using both the proposed algorithm and the manual two-plane approach. For the remaining 3 subjects, either method was not successful in tracking the complete AF bundle.

- Proposed algorithm superior: 2/13 subjects.
- Equal performance: 6/13 subjects.
- Manual method superior: 5/13 subjects. For 3/5 subjects, additional spurious fibers were tracked using the proposed algorithm in comparison to the manual approach. However, most of these spurious fibers were reduced or eliminated after restricting the fiber tracks to only between the seed and target ROIs. For 2/5 subjects, the fiber density was visually less for the proposed method than the manual method.

The right AF fiber bundle comparison was performed for 14 of the 16 subjects. The remaining 2 subjects did not show right Wernicke's area fMRI activation and were excluded. Tracking of the right AF bundle was successful for 12/14 subjects using the two-plane approach and for 11/14 subjects using the proposed algorithm.

- Equal performance: Successful equal performance in 5/14 subjects for both methods.
- Manual method superior: 7/14 subjects. For 5/7 subjects, the fiber density was visually less for the proposed algorithm. For 1/7 subject, additional spurious fibers were observed using the proposed algorithm, which were eliminated after using the cut operation. For 1/7 subjects, proposed method failed completely.
- Both methods failed: 2/14 subjects.

Overall the density of the AF track was less in the right as compared to the left hemisphere.

Quantitative Evaluation:

No significant main effects for differences between the three sets of tracked fiber track bundles i.e. complete AF and section of AF using the proposed algorithm, and AF tracked using the manual two-plane method were found for any of the quantitative DTI measures. A significant main effect of laterality was found for mean FA (left > right; $F(1,10) = 54.9$, $p<0.001$) and mean radial ADC values (left < right; $F(1,10) = 14.6$, $p=0.003$). A greater difference between left and right fiber bundles was found using the proposed algorithm as compared to the manual approach (laterality*fiber bundle set effect: using mean FA: $F(2,20) = 14.5$, $p=0.002$; using mean radial ADC: $F(2,20) = 24.4$, $p<0.001$). Similar trends ($p<0.1$) for main laterality effect (left < right) and laterality*fiber bundle set was observed for mean ADC values.

	Complete AF (proposed algorithm)		**AF section (proposed algorithm)**		**Manual two-plane method**	
	left	*right*	*left*	*right*	*left*	*right*
mean FA						
young	0.428 ± 0.013	0.380 ± 0.027	0.432 ± 0.012	0.380 ± 0.034	0.415 ± 0.021	0.390 ± 0.007
old	0.428 ± 0.025	0.396 ± 0.034	0.428 ± 0.026	0.390 ± 0.031	0.412 ± 0.037	0.407 ± 0.041
mean ADC (um^2/msec)						
young	0.759 ± 0.037	0.790 ± 0.024	0.758 ± 0.039	0.789 ± 0.026	0.762 ± 0.029	0.781 ± 0.031
old	0.760 ± 0.051	0.771 ± 0.057	0.759 ± 0.052	0.770 ± 0.056	0.762 ± 0.060	0.766 ± 0.062
axial ADC (um^2/msec)						
young	1.130 ± 0.052	1.125 ± 0.010	1.130 ± 0.055	1.122 ± 0.016	1.121 ± 0.043	1.126 ± 0.037
old	1.125 ± 0.052	1.105 ± 0.055	1.124 ± 0.052	1.097 ± 0.059	1.111 ± 0.057	1.114 ± 0.067
radial ADC (um^2/msec)						
young	0.574 ± 0.033	0.622 ± 0.035	0.572 ± 0.034	0.622 ± 0.039	0.582 ± 0.028	0.609 ± 0.029
old	0.577 ± 0.051	0.604 ± 0.060	0.577 ± 0.053	0.606 ± 0.057	0.589 ± 0.064	0.592 ± 0.065

Table 9.1: Mean ± SD for quantitative DTI measures obtained from the three analysis methods. There were no significant differences (i.e. main effect) found between the three tested tracking algorithms.

The only age-group effect observed was a trend between age-related laterality differences (laterality*age group) in mean FA value ($F(2,20) = 3.56$, $p=0.089$). The mean

DTI quantitative measures for the left and right fiber bundles for both age groups are summarized in Table 9.1.

9.4 Quantification of WM Tracts and their associations with function.

Next, the DTI quantitative parameters obtained in the previous section were tested for changes with age and associations with GM fMRI activations. We also present results from the Brodmann's area template approach [185]. This method was used as an initial attempt to extract quantitative measures from fiber bundles associated with BA44-45 areas and was replaced by the newly developed algorithm method for future analyses.

9.4.1 Methods

9.4.1.1 DTI/fMRI Algorithm

DTI quantitative measures obtained in the previous section were used: mean values of FA, ADC, axial ADC, radial ADC, all of which were evaluated over the section of AF, derived from the proposed algorithm and from the manual two-plane method. A laterality index value for each of these measures was also calculated. Similarly, LI using pixel counts for all words (LI_{All}) and difficult minus easy (LI_{DE}) in the frontal and temporal regions (see section 7.2.3.2) and LI values using %BOLD values for BA44, BA45, BA47, ITG, MTG & STG were also separately calculated and correlated with DTI LI values using a Pearson's correlation.

9.4.1.2 Tractography using Brodmann's area template

DT-MRI data (medium diffusion encoding and b=800 s/mm^2) from nine healthy subjects was used for this method (4 females; mean age, 31; range, 19-64). A Brodmann's area template was used to compartmentalize the underlying white matter pathways and obtain a probabilistic tractography connectivity map of the white matter pathways specific to a particular Brodmann's Area [185]. Similar to the algorithm method, no manual intervention was required. The main limitation of this method is that all fibers associated with the BA are tracked with no distinction between specific fiber tracks. Hence prior anatomical knowledge of fiber pathways is necessary to separate different tracks.

The BA template available with MRIcro software was used for definition of each area. This template consists of forty six discrete cortical divisions (each representing a BA) and includes cortical grey as well as part of the subcortical white matter. This template is aligned to the T1 weighted brain image normalized in MNI coordinate space, also available with MRIcro. The Multi Planar Reconstruction (MPR) tool available on the Philips MR scanner was used to reslice the individual subject 3D anatomical data at the same orientations as the DT-MR images (axial). To avoid rotating diffusion tensors, tractography was performed in the diffusion space for each individual subject. Individual subject MPR images, BA template and T1 brain image from MRIcro were transferred to individual subject diffusion space. Registration was performed using the FLIRT tool from FSL. Next, tractography was performed to extract all WM fiber tracts using the BA44-45 ROI as seed points. Fiber tracking was done using DTI Studio [186] for all voxels with

FA>0.3 and was terminated at voxels with FA<0.15 or when the turning angle was greater than 45°. A binary mask of the white matter fiber tracts was then generated. This binary tract mask and the individual subject FA maps were then transformed back into MNI space for remaining analysis. The binary tract mask was averaged over all subjects and thresholded to include voxels demonstrating fibers in at least 25% of individuals, resulting in a high probability WM pathway (Fig. 9.7). Two anterior-posterior pathways were highlighted: the arcuate fascicle (AF) and the superior longitudinal fascicle (SLF) (Fig. 9.8). The high probability WM pathway was then divided into 18 parts along the length of the pathway for both the left and right hemispheres.

Left and right hemisphere nonparametric comparisons of mean FA (Wilcoxon Signed Test) were done for: 1) whole brain WM; 2) all WM from axial slices covering the language areas; 3) WM pathway for each individual using the high probability WM pathway mask; 4) WM from the axial slices covering the language areas but not part of the high probability mask; and 5) the separate eighteen parts of the WM probability pathway. Similar to the earlier method, structure-function associations were evaluated by correlating the L-R difference for each of these FA measurements with VG fMRI laterality index.

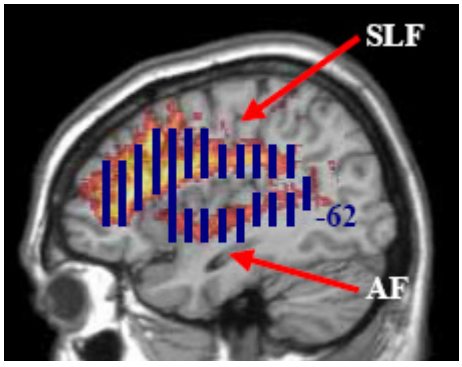

Figure 9.8: Arcuate fascicle (AF) and the superior longitudinal fascicle (SLF) pathways from the High Probability Map and its division into 18 parts. The last coronal slice for division in MNI space is marked.

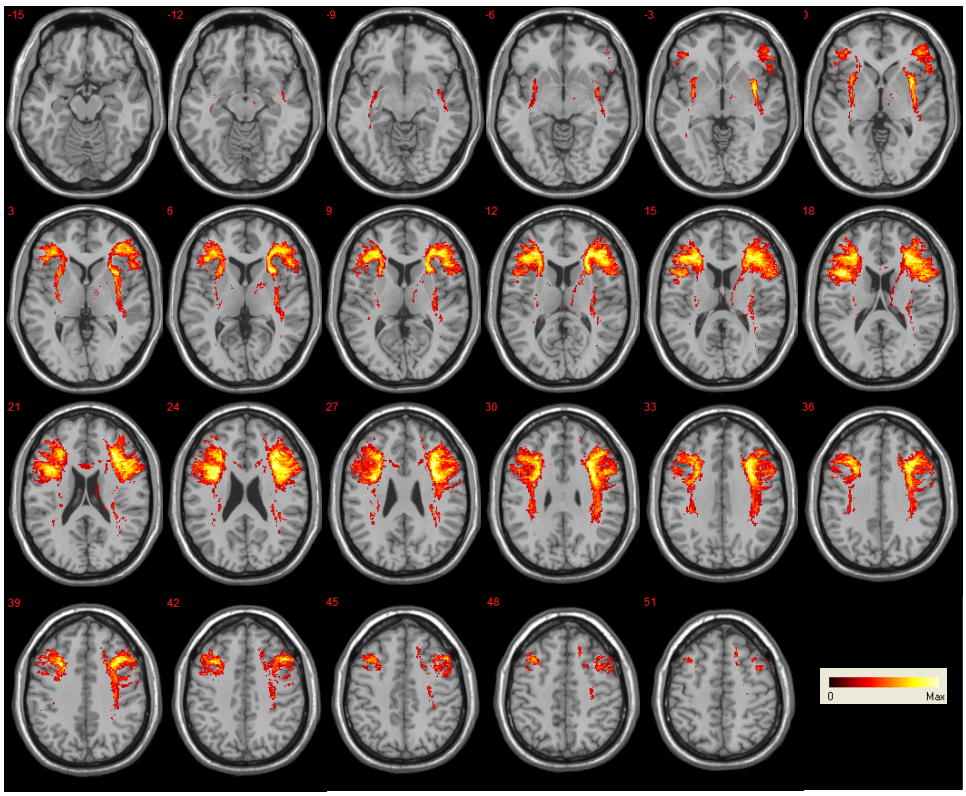

Figure 9.7: High Probability Map of the White Matter Pathways arising or terminating in the BA44-45 area. Color scale value at a voxel indicates number of subjects for which the generated fiber tract passed through that voxel. High probability map for WMT generated by only including voxels demonstrating fibers in atleast 25% (2 out of 9) of all individuals. Images are in radiological convention.

9.4.2 Results

9.4.2.1 DTI/fMRI Algorithm

Mean FA: A significant correlation of the mean FA LI using the proposed algorithm and LI_{DE} in MTG was obtained ($r(12) = 0.665$; $p=0.018$).

Mean ADC: Correlations of mean ADC LI value using the proposed algorithm were significant with LI_{All} in MTG ($r(12) = 0.788$; $p=0.002$) and LI_{DE} in frontal region ($r(12) =$

0.581; p=0.047). Mean ADC LI value using the manual approach correlated significantly with LI_{All} in MTG (r(14) = 0.711; p=0.004), LI_{DE} in MTG (r(12) = -0.6; p=0.023) and ITG (r(10) = -0.662; p=0.037).

Axial ADC: Axial ADC LI values for both methods correlated significantly with LI_{All} in MTG (proposed algorithm: r(12) = 0.7; p=0.011 and manual approach: r(14) = 0.572; p=0.033).

Radial ADC: Correlations of radial ADC LI values using the proposed algorithm were significant with LI_{All} (r(12) = 0.771; p=0.003) and LI_{DE} (r(12) = -0.63; p=0.028) in MTG. Radial ADC LI values using the manual approach had significant correlations with LI_{All} (r(14) = 0.729; p=0.003) and LI_{DE} (r(14) = -0.635; p=0.015) in MTG, LI_{DE} in ITG (r(10) = -0.708; p=0.022) and LI_{DE} in BA45 (r(14) = -0.57; p=0.034).

9.4.2.2 Tractography using Brodmann's area template method

Differences between mean FA (left>right) were observed in all brain WM (z=2.666; p=0.008), WM from axial slices covering the language areas (z=2.666; p=0.008), AF part of the high probability WM pathway (z=2.073; p=0.038), WM outside the high probability WM pathway (z=2.666; p=0.008), and parts of the AF – coronal -62 to -52 (vicinity of Wernicke's area, z=2.192;p=0.028), coronal -12 to -2 (vicinity of Broca's area, z=2.666;p=0.008) & coronal -2 to 8 (z=2.073,p=0.038). No significant statistical differences between the left and right were seen for the SLF. Figure 9.9 shows a comparison of mean FA values in both the hemispheres. Finally, no significant

correlation was observed between fMRI laterality index and the FA difference for the AF pathway.

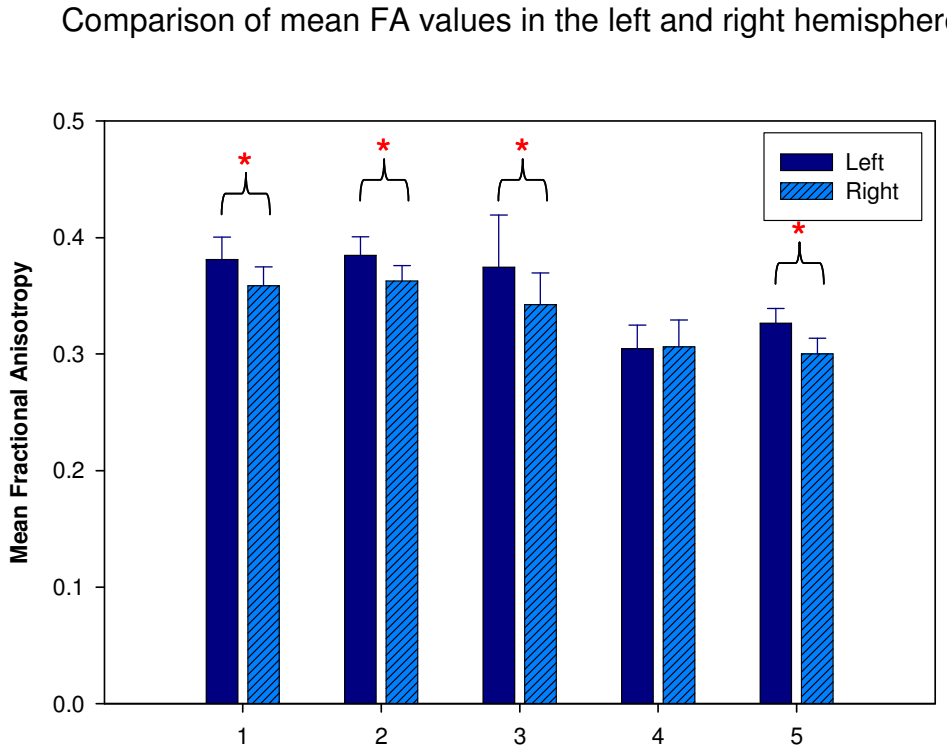

Figure 9.9: Comparison of Mean FA values in the left and right hemisphere: 1 – All brain WM (z=2.666; p=0.008); 2 - WM from axial slices covering the language areas (z=2.666; p=0.008); 3 – AF (z=2.073; p=0.038); 4 – SLF; 5 - WM not part of the WM pathway (z=2.666; p=0.008).

9.5 Discussion

In this chapter, a completely automated algorithm for extraction of DTI measures was developed and tested to study the association between DTI and fMRI imaging modalities. Although DTI and fMRI are different in terms of the nature of information each modality can provide, studying underlying WM structure (using DTI) can provide useful information about development of cortical function (using fMRI). This is relevant in studying recovery of language in stroke patients where the dynamics of language

recovery vary over a wide range and can provide useful hints of the final outcome of functional recovery [30, 40]. As discussed in the introduction, a number of methods to combine these two techniques have been proposed earlier. Most of these methods have been based on appropriate selection of an initial seed point, with potential operator dependent bias. Probabilistic tractography algorithms on the other hand are completely automated and accurate [53]. These methods however are computationally intense requiring an initial processing time of more than a few hours to calculate the probabilistic density functions at every voxel and then an additional time (depending upon the number of seed voxels selected) to perform tractography, thus making them impractical for clinical settings. The proposed algorithm is an attempt to bridge the two types of methods by removing operator dependence and reducing computational time considerably, making it appropriate for use in clinical applications.

The proposed algorithm is based on the assumption that the WM structures associated with fMRI activations should be present in close proximity to the activations. This is a reasonable assumption based on post mortem studies which have shown that WM structures are connecting axonal pathways between functional cortical areas [1]. The method uses the focal point of the fMRI activation to determine an initial seed point as center of sphere ROIs in the WM, thus overcoming the problem of WM fibers terminating before reaching the GM and avoiding the issue of quantification of fMRI activations as seed points [182]. The method worked reasonably well in comparison to a manual approach to extract the AF fiber bundle, selected as gold standard for comparison. The manual method selected has been shown to be reliable in extracting fiber bundles reproducibly [173] but requires careful selection of planes to avoid

selecting fibers from adjacent fiber bundles. In some subjects with this method, additional spurious fibers had to be clipped off in order to extract fibers only belonging to the AF bundle.

Although there were few qualitative differences (decrease in fiber density) in the fiber bundles tracked using the proposed algorithm as compared to the gold standard (especially in the right hemisphere), quantitative measures were not found statistically different. Spurious fibers observed with the proposed algorithm were reduced and in most cases eliminated by restricting the fiber bundle to only between the seed and target ROIs. Although this seed-target approach of the proposed method allows the added flexibility of studying only the section of the fiber bundle between fMRI activations, it necessitates that both seed and target activations are present to track the fiber bundle. The proposed method completely failed in comparison to the manual approach only for one subject. A careful investigation for that subject showed that both the seed-target fMRI activations for that subject were too far from the AF fiber bundle, thus violating the main assumption of the method. An additional iterative step to determine a new seed point closer to the fiber bundle could help in resolving such a problem. However, it is important to note that out of all subjects only one subject showed this problem and could be classified as a possible outlier. The method nevertheless was robust and performed well even in subjects with one of the fMRI activations quite far from the fiber bundle.

Using both approaches, mean FA, mean ADC and radial ADC values were significantly different between the left and right fiber bundles. The right fiber densities were also visually smaller using both methods. This is in agreement with previous studies of left-right asymmetry of the AF fiber bundle in right handed individuals [62, 190-192].

FA was higher while mean ADC and radial ADC values lower in the left fiber bundles. Higher FA values indicate better orientation of the fiber tracts, while lower radial ADC value is an indicator of increased mylination commonly seen with brain development. In addition, this left-right asymmetry difference was more enhanced with the proposed method as compared to the manual method ($p<0.01$). Interestingly, although not significant, a trend ($p<0.1$) was observed in FA laterality differences with age. Reduction in FA asymmetry in the older group of subjects is in agreement with reduced hemispheric asymmetry commonly observed with age in functional [20] and diffusion tensor imaging studies [193].

The left-right laterality of the DTI measures also correlated significantly with the fMRI laterality values calculated using both pixel counts as well as %BOLD signal, thus validating WM-GM associations. These correlations were significant mainly in BA45 and temporal regions (MTG & ITG). Task difficulty dependent laterality (Difficult minus Easy) in the MTG correlated significantly with FA laterality and negatively with mean and radial ADC. Difficulty dependent laterality in ITG correlated negatively with mean and radial ADC values and in BA45 a negative correlation was present only with radial ADC values. This is in agreement with our hypothesis that laterality shifts observed with task difficulty have associations with the underlying WM structure. However surprisingly positive correlations between mean and radial ADC values and task difficulty independent %BOLD MTG values were also observed. Both these results together seem to reiterate the importance of consideration of task difficulty effects when studying language development.

Our initial attempt to study structure-function relationships using a Brodmann's area template to obtain a probabilistic mask of the fiber pathway was unsuccessful in establishing any relationships with the fMRI data. As mentioned in the introduction, the main limitation of this method is its underlying assumption that the fMRI activations are restricted within the boundaries of the template. Also, the method was unable to account for individual variability between fiber tracks of subjects, potentially precluding from establishing any associations with GM. Considering the large amount of variability expected in terms of fiber tracks and location of functional activations, this method may not be a good choice for studying stroke patients.

In summary, a novel automated algorithm to combine DTI and fMRI modalities was proposed and evaluated and GM-WM associations were established for a group of healthy subjects.

Chapter 10

Study and evaluation of functional connectivity and low frequency fluctuations in resting state brain activity with BOLD fMRI

10.1 Introduction

'What does the brain do during rest?' has been a recent topic of interest in neuroimaging research. Understanding neural dynamics when the brain is *not doing any particular activity* can help advance our understanding of results from neuroimaging studies which in general quantify brain function in comparison to a state of rest. Low frequency fluctuation Blood Oxygenation Level Dependent (BOLD) fMRI signal changes (0.012-0.1Hz) in the resting brain have been identified to give useful information of functional connectivity [69, 75, 83]. Studying regional coherence of these fluctuations has led many groups to identify spatial resting state networks related to various functions [81, 82]. In addition, many groups have attempted to establish relations of these low frequency fluctuations with brain pathophysiology. To illustrate a few, Quigley *et al.* studied the effect of focal and diffuse cerebral lesions on both resting state and task-related functional connectivity in patients [194]. Li *et al.* were the first to define mental synchrony using cross correlation coefficients of resting state fMRI within the hippocampus and show its potential as a diagnostic marker in Mild Cognitive Impaired and Alzheimer patients [195]. Another study has shown decreased default resting state activity in the posterior cingulate and hippocampus as useful biomarkers of incipient Alzheimer's disease [196]. Using resting state fMRI, a reduced functional connectivity

between right and left primary motor cortices was observed for MS patients as compared to their control cohorts by Lowe and colleagues [197]. In an initial attempt to evaluate changes in resting state fluctuations following motor stroke and after recovery, Golestani *et al.* found resting state connectivity decreased immediately after stroke, and resolved to normal following recovery [86].

With respect to language function, a few groups have attempted to study language networks in the resting brain. Hampson and colleagues investigated low frequency temporal correlations both in resting state and continuous listening task [75]. They found similar patterns of correlations suggesting that resting state data reflect connectivity between regions of higher order functional networks. In another study, Bartels and Zeki studied interregional correlations in the brain while subjects viewed a continuous movie [198]. Using independent component analysis, they found significant correlations between anatomically connected language areas during both natural viewing and rest with stronger correlations during natural viewing.

Until recently, studies of low frequency BOLD fluctuations have mainly concentrated on developing analysis strategies for resting state data [199], establishing resting state networks in healthy controls [81] and evaluation of how these networks differ in patient populations [195, 197, 200]. There have only been a few attempts in studying the potential of resting state fluctuations as markers of cerebral organization [86]. Resting state fMRI may prove to be a useful addition to study responsiveness to aphasia therapy especially since it does not require any task performance from the subject unlike traditional functional connectivity study measures. This chapter is an initial step towards realizing resting state application to brain plasticity. In this chapter, the resting

state network related to language was identified using different data analysis strategies in a group of healthy senior subjects. Both hypothesis driven and data driven techniques for analysis were evaluated. Data for this group of subjects will be used as control norm in future studies of brain plasticity in patient populations.

10.2 Methods

10.2.1 Data Collection

Resting State MRI data was collected for 10 subjects (4 male, 6 female; mean age = 61.3yrs; SD = 8yrs). An echo planar imaging (EPI) sequence with the same parameters as those for the functional task runs was used: TE = 30ms, TR = 2000ms, flip angle = 90°, SENSE factor of 2, scan matrix = 64*64 and a field of view (FOV) of 20cm. The slice orientation was kept the same as the other functional scans using thirty transverse contiguous slices of thickness 4mm each. A total of 184 frames were collected, resulting in a total scan time of 6min 8s. Prior to any analyses, the first four frames were excluded to allow for equilibrium of the magnetization.

Subjects were instructed to refrain from any cognitive or mental effort while keep their eyes closed for the entire duration of the resting state scan. At the end of the imaging session, all subjects went through an informal interview to judge how successful they were in following these instructions.

10.2.2 Data Analysis – Correlation Analysis Approach

The correlation analysis approach is a hypothesis driven functional connectivity analysis method where temporal correlations of the BOLD fMRI signal fluctuations are evaluated on a voxel by voxel basis with respect to a seed ROI. Regions within a tightly coupled neural network have been shown to have high temporal correlations of BOLD signal fluctuations [75]. Data preprocessing and statistical inferences were carried out using the SPM2 software package.

Data Preprocessing:

Motion correction, spatial normalization and smoothing were done as described in Chapter 7.2.3. To correct for possible scanner drift or fluctuation, all voxel intensities were scaled by dividing the value at each time point by the mean brain image intensity for that time point. The data was also filtered using a band pass filter of 0.012-0.1Hz. The specifications of this filter were chosen from experiences of previous studies which have identified the resting state BOLD fMRI signal oscillations to take place within this band of frequencies [69, 74].

Mapping the language resting state network:

To map the language resting state network, a voxel based correlation analysis using the left Broca's area as the seed ROI was performed. This analysis was performed for two definitions of the Broca's area: 1. the complete anatomical ROI defined by left BA44 & 45; 2. functional ROI defined by using the task difficulty independent VG task

(see Chapter 7.2.3). The second analysis was used to evaluate the sensitivity of functionally-defined seed points compared to anatomically-defined seed points. For both analyses, a mean time series over the defined seed ROI was extracted from the resting state data and defined as covariate of interest in a GLM based regression analysis. In addition, time series from ventricles and a white matter region were selected to regress out any noise fluctuations in the data which would be common to all regions. In addition, motion parameters were also added as regressors to regress out any effects due to motion. Individual subject contrast images corresponding to positive correlation with the left Broca's area were determined (first level analysis) and entered into a second level random effect analysis to test for group effects. A threshold of $p<0.01$ and extent of 5 voxel clusters were used to identify brain areas which are functionally connected to the seed ROI.

Correlation between language resting state connectivity and DTI measures from arcuate fasciculus:

Hemisphere specific correlations between the Broca's and Wernicke's area were calculated to evaluate hemispheric differences and relate these differences to underlying WM tracts. Individual subject GLM analysis was performed using motion parameters, ventricles and WM time series as covariates of no interest. The residuals from this analysis were used to extract left and right Broca's and Wernicke's time series. Similar to the above, analysis was performed for both anatomical and functional definitions of all ROIs. A paired t-test was used to test for hemisphere specific differences in Broca's – Wernicke's area correlations. Laterality indices for the correlation values were also

calculated and correlated with the DTI laterality index values for the arcuate fasciculus tract (see section 9.4) using a linear regression analysis.

10.2.3 Data Analysis – Independent Component Analysis Approach

This approach uses the Probabilistic Independent Component Analysis (PICA) to characterize resting state networks [199]. This method is completely data driven and is not limited to prior expectations of resting state patterns associated with predefined ROI. All data analysis were performed using the PICA algorithm implemented in the MELODIC (Multivariate Exploratory Linear Optimized Decomposition into Independent Components) [80] function in FSL.

Probabilistic Independent Component Analysis (PICA):

Independent component analysis (ICA) is a hypothesis driven analytical technique to find independently distributed spatial patterns that depict source processes in the data. The basic goal of ICA is to solve the blind source separation problem by expressing a set of random variables (observations) as linear combinations of statistically independent component variables (source signals). In an fMRI experiment, the fMRI data matrix can be represented as X, a (p x n) matrix, where n is the total number of voxels and measurements at each voxel are collected at p different time points. This matrix can be written as a product of a mixing matrix A and a source matrix S.

$$X = AS$$

Assuming that m independent sources exist, the matrix A can be represented as (p x m), where each column represents the time series associated with an independent source, and the source matrix as (m x n), where each row represents a spatial map for each source. Alternatively, the source matrix can be expressed as a product of an unmixing matrix W and the data matrix as follows:

$$S = W X$$

where, $W = A^{-1}$. The goal of ICA is to estimate the source matrix by iteratively optimizing the un-mixing matrix $\boldsymbol{W}$ in such a way that the source matrix $\boldsymbol{S}$ contains mutually independent rows, representing independent spatial patterns. This classical ICA technique most often makes an assumption that the number of independent sources present in the data is equal to the number of data points measured ($m = p$) i.e. A is a square matrix. It also makes no assumption about the amount of noise present in the data. This often leads to problems of over-fitting a noise-free generative model to noisy observations. In the case of fMRI, in addition to actual fMRI sources, a number of noise sources are present in the data. These noise sources maybe attributed to motion, physiological and MR artifacts, and even Gaussian noise. This necessitates a suitable probabilistic model that controls the balance between what is attributable to 'real effects' of interest and what is simply due to observational noise.

The PICA technique implemented in MELODIC addresses these problems by allowing for non-square mixing process and assuming that the data are confounded by additive Gaussian noise. PICA uses the concept that once the Gaussian noise in the data is estimated, the real source components in the data will be the ones with a distribution significantly deviated from gaussian. In short, PICA first estimates the number of unique

components present in the data using an estimate of the Gaussian noise in the data (instead of assuming the number of sources equal to the number of observations) and then solves for the source matrix. A detailed explanation of the PICA algorithm can be found in [80].

Data Preprocessing:

For all subjects, data preprocessing for this method was done using the tools available as part of FSL software. FSL was used for data pre-processing rather than SPM2 to avoid data compatibility problems. Similar to the correlation analysis, individual subject data were first motion corrected, spatially normalized in MNI space and spatially smoothed using an 8mm Gaussian kernel. Next a mean based normalization of all fMRI data volumes and a high pass temporal filtering at a cutoff of 250s (0.004Hz) was applied. Using PICA, the preprocessed data were decomposed into sets of vectors which describe signal variation across the temporal domain (time courses), the subject domain and across the spatial domain (maps). A total of 42 independent components were estimated. Estimated spatial maps were converted to z-statistic maps by dividing the raw estimate by the estimate of voxel-wise noise standard deviation. A threshold level of 0.5 – which places an equal loss on false positives and false negatives – was used.

Identification of Resting State Components:

An automated two step process suggested by Greicius *et al.* [196] was used to identify the resting state components. Resting state components have maximum power in

the low frequency range i.e. 0.01 to 0.1Hz. In the first step, a frequency filter was applied to remove components in which the high frequency signal (>0.1Hz) constituted more than 50% of the power in the Fourier spectrum. Next, to identify the language resting state network component from the remaining low frequency components, a template of the left and right Broca's area and a z-map of all the components (indicating how well the voxel's time series correlates with the ICA component time series) were used. A template matching procedure was used where the average z score of voxels falling within the template and the average z score of voxels outside the template were calculated. The difference between these two values was used as a measure of the correspondence of the particular ICA component with the Broca's area template. Component with the highest z difference was selected as the best fitting component to the template.

10.3 Results

10.3.1 Correlation Analysis

Mapping the language resting state network:

Using the random effects analysis, similar language resting state networks were identified using both the anatomically and functionally defined left Broca's area (Fig. 10.1). The main regions identified as part of the network were: bilateral inferior frontal gyrus, bilateral pre-motor cortices (precentral gyrus), bilateral superior and medial frontal

gyrus, anterior cingulate cortex, right superior temporal gyrus, left medial temporal cortex and bilateral parietal lobule.

Correlation between language resting state connectivity and DTI measures from arcuate fasciculus:

Using the paired t-test, no significant differences in the Broca-Wernicke's area correlation were found between the two hemispheres. Also, no significant correlations were observed between the resting state correlation measures and any of the DTI measures.

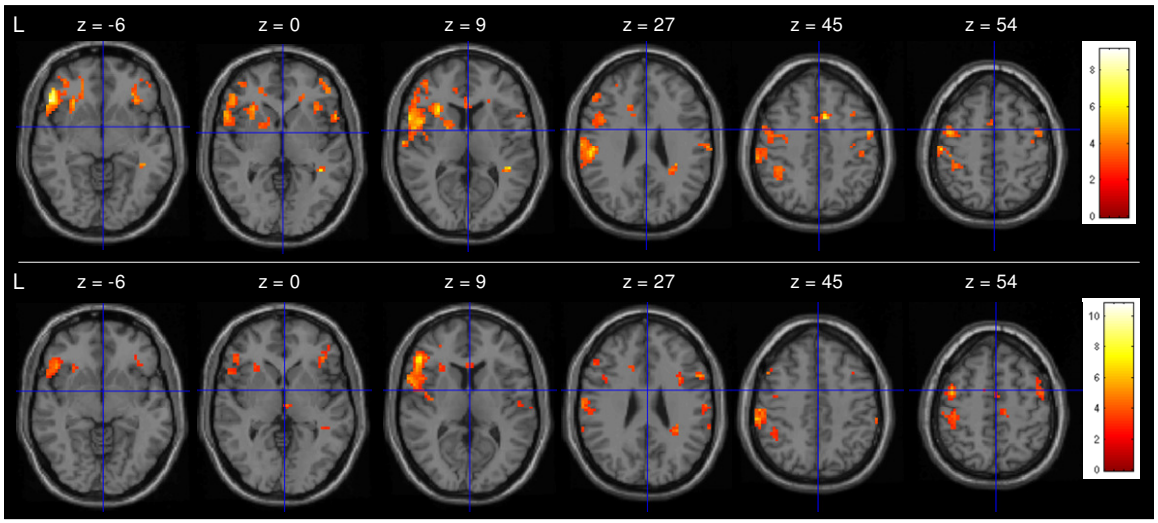

Figure 10.1: Resting language network identified from correlation analysis using anatomical (top row) and functionally (bottom row) defined left Broca's area. Images are in neurological convention (left is left) Slice location in MNI space is indicated above each slice (in mm)**.** Voxels with correlations at $p<0.01$ significant level and within 5 voxel clusters are shown. For both analyses, bilateral inferior frontal gyrus, bilateral pre-motor cortices, anterior cingulate cortex, bilateral superior and medial frontal gyrus, right superior temporal gyrus, left medial temporal cortex and bilateral parietal lobule showed significant correlation with Broca's area..

10.3.2 Independent Component Analysis

Language resting state network:

Out of the 42 components, 22 components were found to have maximum power in the low frequency range of interest. Using the language template matching procedure on these components, the best fit component was identified with a mean z-stat (inside and outside the template) difference of 0.81. However a spatial evaluation of the component revealed no language areas to be a part of the network. The component mainly contained a continuous rim of left frontal voxels, possibly due to some motion or signal dropout artifacts in that region. The second best fit component was identified with a main z-stat difference of 0.55 and included voxels in bilateral frontal, left temporal, medial frontal and anterior cingulate cortex areas. These areas identified as part of the spatial map of the component are similar to the areas of the language network identified using the correlation analysis technique. The spatial map, time series and power spectrum for the component are shown in Fig. 10.2.

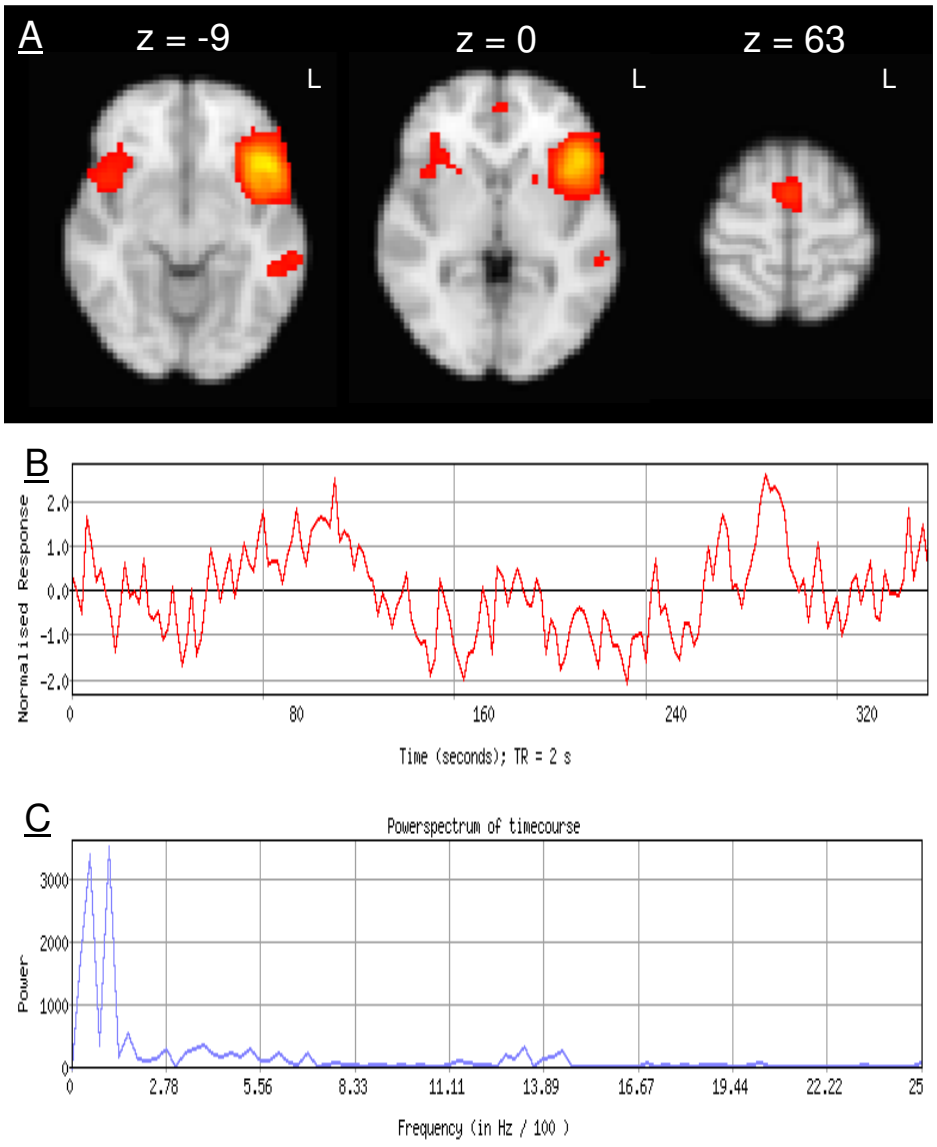

Figure 10.2: Component identified as Language resting network from Independent component analysis. A. Spatial map of the component (Alternative hypothesis threshold p>0.5 was used to threshold the voxels) (radiological convention – L indicates left), Voxels in the bilateral inferior frontal region, medial frontal region, left temporal cortex and anterior cingulate region were determined as part of the network. B. Component estimated time series over 184 fMRI scans, and C. Power spectrum of time course indicating maximum power in the low frequency range (0-0.12Hz).

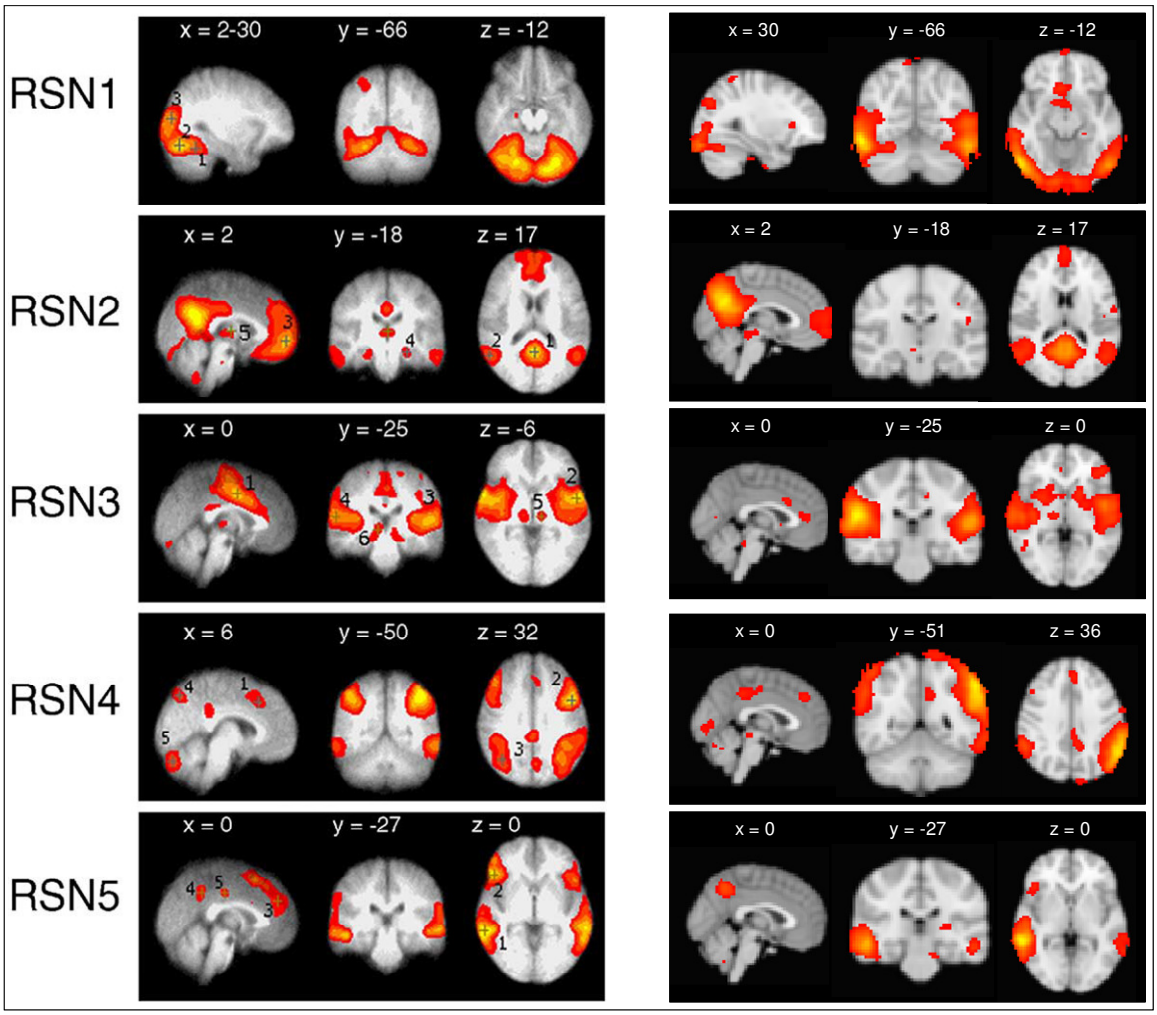

Figure 10.3: Comparison of Resting State Networks identified in the DeLuca study [82] (left) and networks identified in our study (right): RSN1 – Visual Functional Network; RSN2 – Emotion/Visuospatial Network; RSN3 – Sensory & Auditory Network; RSN4 – Dorsal Pathway; and RSN5 – Ventral Pathway. (Images thresholded using an alternative hypothesis threshold p>0.5) (radiological convention)

Other resting state networks:

In addition to language, the remaining components were visually assessed to identify resting state networks previously identified in other studies. The five main resting state networks identified in the study by De Luca and colleagues [82] were also identified in our data:

1. RSN1 – Network mainly including the occipital and temporal-parietal areas and associated with visual function processing;

2. RSN2 – Emotion/visuospatial processing network mainly including the posterior cingulate region, superior temporal gyrus, medial forntal gyrus and thalamus. This functional network has been shown to be related to internal monitoring and states of consciousness (default mode network).
3. RSN3 – Sensory and Auditory system including the cingulate gyrus, precentral gyrus and superior temporal gyrus. This network reflects functional and anatomical interactions relevant to control of action (motor and somatosensation).
4. RSN4 – Dorsal pathway network including the inferior parietal lobule, inferior temporal gyrus and prefrontal cortices. These regions are closely functionally integrated in a wide range of cognitive processes and the pattern of regions in this network has been shown associated to visual perception of action or the 'where' pathway [201].
5. RSN 5 – Ventral pathway including the medial temporal gyrus, inferior frontal gyrus and inferior parietal cortices. The regions of this network are more inferior compared to those in RSN4 and are shown to be associated with the visual perceptual 'what' pathway [201].

Figure 10.3 shows a comparison of networks identified in the De Luca study (left) and those identified using our data (right). The two sets of networks seem to be spatially similar for most cases except for RSN 4 & 5 where the main differences are seen as reduced frontal regions recruited for networks identified using our data. Difference in participant age groups in the two studies (senior age group in our study as against a broader range group 22-51 yrs for the De Luca study) could be one of the reasons for

these differences. In spite of the similarity of regions recruited for RSN1 & RSN4, an additional continuous rim of activated voxels can be seen in the axial slice (RSN1) & coronal slice (RSN4). This observation appears non-functionally related and possibly a motion artifact. More careful investigations to confirm the validity of these networks and their relevance to function are required.

10.4 Discussion

Over the past few years, the neuroimaging community has shown considerable interest in understanding low frequency BOLD fluctuations and how they can be applied to studying functional connections in both healthy and diseased subject groups [69, 74, 75, 81, 200]. Studies testing neuronal origins of low frequency fluctuation have established the validity of using these signals as markers of intact neuronal function [82]. One of the biggest advantages of using low frequency BOLD fluctuations is that they do not require performance of difficult functional tasks unlike those commonly used in functional neuroimaging studies. This is especially beneficial for patients such as stroke-induced aphasics who may have limited understanding of instructions or success in performing desired functional activities in the scanner environment.

In this chapter, we used low frequency fluctuations to establish functional relationships between language regions in an elderly group of subjects. These relationships will serve as norms for comparison in future studies of cerebral reorganization in aphasia stroke populations. There have been only few attempts in studying changes of low frequency fluctuations with brain plasticity [86]. It would be

interesting to test whether or not the spatial nature or inter-regional strength of correlations of these fluctuations changes with functional cerebral reorganization in stroke patients. Two analysis strategies were used to establish these resting state networks: hypothesis driven correlation analysis and data driven independent component analysis. Both of these methods were successful in establishing language resting state networks using our data. Using the correlation based analysis, we also tested the advantage of using correlation seed points defined using a separate functional task in comparison to those defined anatomically. Language resting state networks using both definitions resulted in similar areas and not establishing advantage of one method over the other. However, in comparison to the correlation analysis strategy, the data driven independent component analysis provided an additional advantage in separating noise sources in the data as separate components, resulting in less noisy language resting state maps. In addition using the independent component analysis strategy, we were able to separate different resting state networks previously identified in the literature in the same analysis [82].

There were some differences in the spatial extent of regions recruited in our networks in comparison to the De Luca study. Given that functional networks change with age [20] and the different age groups of participants in both studies, we could associate these differences as age related. The success of using independent component analysis approach lies in the accurate identification of relevant components. Using power spectrum filtering and a template matching algorithm, we were successful in identifying relevant components. As previously shown [196], we could use the goodness of fit measure obtained from template matching to quantify deviation from a healthy control

network and its relationship to recovery when studying stroke patients. We also tested for associations of resting state correlations between frontal and temporal regions (Broca's and Wernicke's areas) with quantitative measures from the white matter tract connecting these two regions (arcuate fasciculus). However, we did not see any significant associations. This could be due to the low sample size for testing these relationships and retests after adding more subjects is necessary before making any conclusions related to the two measures.

In summary, we have established a language resting state network in a control population with age group more appropriately matched to the expected age group of stroke patients and identified potential markers which could be used to study correlation with recovery in stroke patients.

Chapter 11

Future Directions

The motivation behind the work in this thesis has been to take an initial step towards improving clinical management of stroke aphasic patients by strategically combining what we can learn from existing neuroimaging techniques. Studies of brain plasticity in patients, during the course of drug and rehabilitation therapies, will benefit most by a multi-modality fusion approach. The wealth of information from these integrations could aid clinicians in making choices about treatment strategies best suited for a particular patient. In this chapter, a road map for future studies is suggested. The work done in this thesis could be considered as Phase I of this road map in which the necessary tools were developed and evaluated in a healthy subject population. Future study protocols (Phase II & III) with their specific aims and hypotheses are proposed below.

Phase II: Evaluation of developed neuroimaging tool with an aphasic patient population.

The goal of this phase will be to evaluate the sensitivity of the proposed multi-modality approaches to brain plasticity in an aphasic patient population. A longitudinal aphasia patient study is proposed in which neuroimaging measurements developed in Phase I will be made before and after a period of intensive language therapy. Stroke

affected patients in acute and sub-acute stages (3 days to 4 weeks post-stroke) with clinically diagnosed aphasia condition will be recruited.

Proposed study protocol:

Day 1:

1. Neuropsychological Tests: Boston Diagnostic Aphasia Exam and Mini Mental State Exam will be used to score severity of aphasia and cognitive health of patients.
2. Behavioral session containing a mock version of the developed functional tasks to ensure subjects understand task instructions and are capable of performing them successfully.
3. Neuroimaging protocol: Half subjects will undergo MRI protocol first. Same order will be followed for the post-therapy sessions.
    a. MRI Protocol: fMRI picture naming task, fMRI verb generation task, fMRI comprehension task, resting-state BOLD study, DTI study, other pertinent clinical stroke-protocol studies (e.g., T2, FLAIR, Perfusion).
    b. EEG Protocol: EEG picture naming task, EEG verb generation task, EEG comprehension task.

Day 7:

1. Neuroimaging protocol: Subjects who had MRI first, will have EEG in this session and vice versa.

Day 8 – Day 128:

1. Four months of intensive speech language therapy, 45-minute sessions, 3 times a week (therapy sessions will be outlined by speech pathologist).
2. Neuropsychological aphasia battery on day 68 (end of 2 months).

Day 129:

1. Neuroimaging protocol (Same order of MRI & EEG protocol will be followed).
2. Neuropsychological Tests.

Day 136:

1. Neuroimaging protocol.

Specific Aims:

1. **Evaluate usefulness of our developed language tasks and concept of task difficulty in mapping the language functional architecture and brain plasticity following intense language therapy period.**

Hypothesis & Rationale: Our battery of developed language tasks, using both fMRI and ERP, will serve to map the language functional network, evaluate and quantify extent of language damage and compensatory recruitment following stroke. Task difficulty in performing language tasks maybe an important confound in studying brain reorganization. We have observed task difficulty in language functional activation to change with healthy aging (For details, see chapter 7). The ability to

perform tasks is severely affected in stroke, where simple tasks can become difficult and difficult tasks almost impossible. Accounting for this difficulty will help in understanding compensatory mechanisms recruited by patients.

2. **Evaluate whether cortical GM compensation can be explained with WM changes.**

Hypothesis & Rationale: WM structures have shown to change with development, age and disease. GM functional changes have found to be related to underlying WM structures. We have shown associations of language function with DTI quantitative measures extracted from the arcuate fasciculus or the WM fiber pathway connecting frontal and temporal language areas (For details, see section 9.4). In the case of aphasia patients, re-recruitment of dominant hemisphere following stroke induced damage has been associated with maximum rehabilitation. WM changes should precede cortical functional changes and could serve as early markers of these compensatory cortical functional changes. An early predictor of these changes could aid clinicians in altering rehabilitation strategies to improve recovery.

3. **Evaluate whether resting state MRI serve as markers of cerebral reorganization.**

Hypothesis & Rationale: Using resting state MRI, we have been able to identify different functional networks in a single functional scan without requiring any task performance (For details, refer chapter 10). This is particularly useful in stroke patients who may be challenged in understanding task instructions and performing

them successfully. We expect language functional networks and connectivity measures between different language areas to change with stroke. In this phase, we will determine whether or not these measures are sensitive to changes with brain plasticity following rehabilitation.

4. **Evaluate whether any of the obtained quantitative measures can predict severity of aphasia.**

Hypothesis & Rationale: The main goal of this phase is to evaluate sensitivity of our developed tool to severity of aphasia. Quantitative measures established in this thesis will be correlated with neuropsychological aphasia measures. These relationships will serve to evaluate different rehabilitation strategies in recovery of language function.

Phase III: Clinical trials studying efficacy of rehabilitative drugs and combination of treatment strategies in aphasia.

Once the sensitivity of our developed tool to changes in brain plasticity in aphasia patients has been established, and specific quantitative measures of interest have been identified, future studies evaluating different treatment strategies can be undertaken. This phase of the road map will serve to evaluate whether pharmaco-therapeutic agents combined with language therapy (or different combinations of different rehabilitation strategies such as the effect of varying the intensity and frequency of speech therapy) can be more effective in rehabilitation. A double blinded longitudinal study with pre and post

rehabilitative drug or placebo treatments with chronic stage aphasia patient group (4 months post-stroke) is proposed as an example.

Proposed Study Protocol:

Day 1:

1. Neuropsychological Tests: Boston Diagnostic Aphasia Exam and Mini Mental State Exam.
2. Behavioral session containing a mock version of the developed functional tasks to ensure subjects understand task instructions and are capable of performing them successfully.
3. Neuroimaging protocol: Half subjects will undergo MRI protocol first. Same neuroimaging protocol proposed in Phase II will be used.

Day 7:

1. Neuroimaging protocol: Subjects who had MRI first, will have EEG in this session and vice versa.

Day 8 – Day 128:

1. Four months of drug or placebo treatment augmented with language therapy (course of drug treatment will be outlined by neurologist, language therapy - 45-minute sessions, 3 times a week).
2. Neuropsychological Tests on Day 38.

Day 129:

1. Neuroimaging protocol (Same order of MRI & EEG protocol will be followed).
2. Neuropsychological Tests.

Day 136:

1. Neuroimaging protocol.

Specific Aims:

1. **Evaluate sensitivity of developed neuroimaging tool to study effects of pharmaco-therapeutic agents together with language therapy in brain function reorganization.**

Hypothesis & Rationale: The main goal of this phase will be to evaluate whether our developed neuroimaging methods are sensitive to differences in changes of language function brain remodeling in response to different rehabilitation strategies such as the effect of varying the intensity and frequency of speech therapy, and the effects of pharmaco-therapeutic agents in augmenting rehabilitation. This evaluation will help in strategizing rehabilitation therapies best suited for a particular patient.

Chapter 12

General Discussion and Conclusion

Aphasia or impairment of the ability to produce and/or comprehend language is a common functional disability seen in majority of stroke patients. Cerebral function reorganization immediately post-stroke and over a period of therapy can predict extent of damage and final outcome of recovery. A thorough understanding of how the brain rewires post-stroke can help clinicians to make informative choices of rehabilitation strategies most appropriate for individual patients. The goal of this thesis was to develop methods which can be used for improving the understanding of brain plasticity following post-stroke aphasia. A number of neuroimaging techniques have evolved over the last few decades. Hemodynamic based methods like fMRI and PET have successfully mapped functional architecture of a number of cognitive processes. Neuronal based methods like EEG and MEG have provided more direct understanding of function by extracting temporal components associated with neural processes responsible for that function. With in vivo abilities to map underlying white matter architecture, diffusion tensor imaging has complemented the understanding of how functional areas are anatomically mediated. Resting state low frequency BOLD signal has provided the flexibility of identifying functional coherent cerebral regions without requiring performance of difficult cognitive tasks. Although invention of each of these modalities has revolutionized our understanding of how the brain functions, each neuroimaging modality by itself is limited in the nature and extent of neural information it can provide. We hypothesized that a multimodality neuroimaging approach will allow to bridge gaps

between each of these modalities and further our understanding of neural dynamics of reorganization. With this underlying hypothesis, this dissertation was aimed at using currently existing neuroimaging techniques – functional MRI, diffusion tensor imaging, electroencephalography and resting state BOLD MRI – to develop a multi-modality neuroimaging tool for future applications to study brain plasticity in aphasia patients.

In this dissertation, we have developed a battery of functional tasks including two word production tasks – picture naming (PN) and verb generation (VG), and one language comprehension task. All three tasks were designed with two motives: 1. each task should be an efficient design for analysis of data from both fMRI and EEG modalities, and 2. tasks are simple considering the limited ability of stroke patients in understanding and performing them. This required us to perform a careful evaluation and selection of stimuli for each of these tasks. Our task designs also permitted retrospective categorization of stimuli based on task difficulty. Task difficulty is a particularly important issue in functional imaging in post-stroke patients, where simple tasks can become difficult and difficult ones almost impossible. This necessitates a thorough understanding of how brain functions are affected by task difficulty and demands for an appropriate method to characterize this effect. We evaluated the possibility of using the time required for performing a task (reaction times) as a measure of task difficulty. We found that task difficulty effects can be demonstrated in functional activations in both the frontal and temporal regions using the verb generation task. In comparison to using a pre-determined definition of task difficulty for each stimulus, a stronger effect size was recorded for the left-sided frontal activations with subject-specific-defined difficulty. Individual definitions of reaction times allowed the added flexibility of modeling

individual variability in performing language tasks, which is relevant and applicable in studying these effects in individual stroke patients.

Furthermore, an overall shift in language recruitment of the non-dominant hemisphere with increased task difficulty was observed, indicating compensatory recruitment for successful performance of language function. Task difficulty effects were also found to change with age, with older subjects showing increased functional recruitment effects even for simple tasks. This also highlights the necessity of recruiting subjects from appropriate age groups to serve as normal cohorts in such studies. Similar task difficulty effects were also observed with both picture naming and verb generation EEG data. With picture naming, a significant effect of task difficulty on the negative amplitude in the 360-600ms time window was observed. The negative peak in this time window was found to increase with difficulty in naming pictures. This effect is consistent with the semantic related N400 effects seen with ERP studies in picture naming [88]. Similar to fMRI, strongest task difficulty effects were seen with verb generation EEG data. However the time window for these effects was much later than those observed in picture naming. Using source analysis, we confirmed that the two effects seen in both the tasks were in fact similar and associated with the same underlying neural source locations. Although we did not find age related effects in amplitude of the ERP components, older subjects showed a later time window for semantic processing in verb generation as compared to their young counterparts.

The language comprehension task was successful in showing effects related to semantic processing in both subjective and objective contexts. As expected, greater N400 peak, a marker of intact semantic processing, could be detected for context unrelated

stimuli, irrespective of nature of context (i.e. subjective or objective), over all healthy subjects. This peak was also found to be delayed for the subjective categories as compared to the objective ones. Additionally, a P600 effect i.e. greater late positivity for semantically related stimuli as compared to unrelated stimuli was found in spite of no syntactic differences between the two stimuli types. This confirmed the role of P600 in integration of semantic information additional to syntax processing [7]. The P600 peak was seen as much later and stronger for subjective categories, indicating greater semantic demands as compared to objective ones. Differences between the semantically related and unrelated categories were also observed in left BA44, left inferior temporal gyrus and right supramarginal gyrus using our fMRI data. However no associations with EEG data could be established using source analyses. Although ERP-fMRI integration was not successful for this task, the effects observed using this task in a healthy subject group can be used to evaluate the integrity of semantic processing in stroke patients.

Integration of fMRI with DTI can help establish anatomical associations between functionally connected regions. The arcuate fasciculus is a WM pathway connecting the frontal (Broca's) and temporal (Wernicke's) language areas. We hypothesized that quantitative DTI measures in this pathway, quantifying structural integrity of this tract, could be associated with functional activations. If this relationship could be established, these measures could be used as early predictors of functional reorganization. We developed a novel automated method to track the arcuate fasciculus fiber bundle using frontal and temporal fMRI activations from the verb generation task. This method was tested and found to work as well compared to a manual method of parcellating the arcuate fasciculus. DTI measures from the obtained tracts revalidated the hemispheric

asymmetry expected between fiber bundles [192] and also showed significant associations with cortical fMRI laterality measures. Normal quantitative measures in a group of healthy subjects for comparison in studies with patient populations were also established.

Finally, fMRI driven correlation analysis approach to analyze resting state fMRI data was implemented and qualitatively compared to a data driven independent component analysis approach. Using fMRI activations from the verb generation task, we were able to establish the language resting state network in our healthy subject group. A similar language resting state network was also obtained using the data driven approach. These established networks will be used to determine if resting state connectivity between recruited network regions could predict cerebral reorganization post-stroke.

In conclusion, a neuroimaging tool by integration of four independent neuroimaging modalities was developed and evaluated using a healthy subject population. Using this tool, we have identified a number of potential markers which will be relevant to study brain plasticity in post-stroke aphasia patients. While the developed methods have shown promise in understanding language functions in healthy individuals, future studies to evaluate the performance and sensitivity of this tool using a patient population are required.

Bibliography

1. Price, C.J., *The anatomy of language: contributions from functional neuroimaging.* J Anat, 2000. **197 Pt 3**: p. 335-59.
2. Indefrey, P. and W.J. Levelt, *The New Cognitive Neurosciences*, ed. M. Gazzaniga. 2000, Cambridge, MA: MIT Press.
3. Levelt, W.J.M., *Neurocognition of Language*. Language Production: A blueprint of the speaker, ed. C. Brown and P. Hagoort. 1999: Oxford University Press.
4. Indefrey, P. and W.J.M. Levelt, *The neural correlates of language production*, in *The New Cognitive Neurosciences*, M. Gazzaniga, Editor. 2000, MIT Press: Cambridge, MA.
5. Indefrey, P. and W.J. Levelt, *The spatial and temporal signatures of word production components.* Cognition, 2004. **92**(1-2): p. 101-44.
6. Friederici, A.D., *Towards a neural basis of auditory sentence processing.* Trends Cogn Sci, 2002. **6**(2): p. 78-84.
7. Friederici, A.D. and S.A. Kotz, *The brain basis of syntactic processes: functional imaging and lesion studies.* Neuroimage, 2003. **20 Suppl 1**: p. S8-17.
8. Kutas, M. and S.A. Hillyard, *Event-related brain potentials to semantically inappropriate and surprisingly large words.* Biol Psychol, 1980. **11**(2): p. 99-116.
9. Kutas, M. and S.A. Hillyard, *Reading senseless sentences: brain potentials reflect semantic incongruity.* Science, 1980. **207**(4427): p. 203-5.
10. Holcomb, P.J., *Semantic priming and stimulus degradation: implications for the role of the N400 in language processing.* Psychophysiology, 1993. **30**(1): p. 47-61.
11. Rissman, J., J.C. Eliassen, and S.E. Blumstein, *An event-related FMRI investigation of implicit semantic priming.* J Cogn Neurosci, 2003. **15**(8): p. 1160-75.
12. Buckner, R.L., et al., *Functional MRI evidence for a role of frontal and inferior temporal cortex in amodal components of priming.* Brain, 2000. **123 Pt 3**: p. 620-40.
13. Marinkovic, K., et al., *Spatiotemporal dynamics of modality-specific and supramodal word processing.* Neuron, 2003. **38**(3): p. 487-97.
14. Halgren, E., et al., *Spatio-temporal stages in face and word processing. I. Depth-recorded potentials in the human occipital, temporal and parietal lobes [corrected].* J Physiol Paris, 1994. **88**(1): p. 1-50.
15. Matsumoto, A., et al., *Linking semantic priming effect in functional MRI and event-related potentials.* Neuroimage, 2005. **24**(3): p. 624-34.
16. Rossell, S.L., C.J. Price, and A.C. Nobre, *The anatomy and time course of semantic priming investigated by fMRI and ERPs.* Neuropsychologia, 2003. **41**(5): p. 550-64.
17. Connolly, J.F. and R.C. D'Arcy, *Innovations in neuropsychological assessment using event-related brain potentials.* Int J Psychophysiol, 2000. **37**(1): p. 31-47.
18. Connolly, J.F., et al., *The application of cognitive event-related brain potentials (ERPs) in language-impaired individuals: review and case studies.* Int J Psychophysiol, 2000. **38**(1): p. 55-70.

19. D'Arcy, R.C., et al., *Electrophysiological assessment of language function following stroke.* Clin Neurophysiol, 2003. **114**(4): p. 662-72.
20. Cabeza, R., et al., *Aging gracefully: compensatory brain activity in high-performing older adults.* Neuroimage, 2002. **17**(3): p. 1394-402.
21. Netz, J., U. Ziemann, and V. Homberg, *Hemispheric asymmetry of transcallosal inhibition in man.* Exp Brain Res, 1995. **104**(3): p. 527-33.
22. Cao, Y., et al., *Cortical language activation in stroke patients recovering from aphasia with functional MRI.* Stroke, 1999. **30**(11): p. 2331-40.
23. Warburton, E., et al., *Mechanisms of recovery from aphasia: evidence from positron emission tomography studies.* J Neurol Neurosurg Psychiatry, 1999. **66**(2): p. 155-61.
24. Heiss, W.D., et al., *Differential capacity of left and right hemispheric areas for compensation of poststroke aphasia.* Ann Neurol, 1999. **45**(4): p. 430-8.
25. Thulborn, K.R., P.A. Carpenter, and M.A. Just, *Plasticity of language-related brain function during recovery from stroke.* Stroke, 1999. **30**(4): p. 749-54.
26. Weiller, C., et al., *Recovery from Wernicke's aphasia: a positron emission tomographic study.* Ann Neurol, 1995. **37**(6): p. 723-32.
27. Crosson, B., et al., *Role of the right and left hemispheres in recovery of function during treatment of intention in aphasia.* J Cogn Neurosci, 2005. **17**(3): p. 392-406.
28. Musso, M., et al., *Training-induced brain plasticity in aphasia.* Brain, 1999. **122 (Pt 9)**: p. 1781-90.
29. Thompson, C.K., *Neuroplasticity: evidence from aphasia.* J Commun Disord, 2000. **33**(4): p. 357-66.
30. Saur, D., et al., *Dynamics of language reorganization after stroke.* Brain, 2006. **129**(Pt 6): p. 1371-84.
31. Fernandez, B., et al., *Functional MRI follow-up study of language processes in healthy subjects and during recovery in a case of aphasia.* Stroke, 2004. **35**(9): p. 2171-6.
32. Mimura, M., et al., *Prospective and retrospective studies of recovery in aphasia. Changes in cerebral blood flow and language functions.* Brain, 1998. **121 (Pt 11)**: p. 2083-94.
33. Fridriksson, J., et al., *Neural recruitment associated with anomia treatment in aphasia.* Neuroimage, 2006. **32**(3): p. 1403-12.
34. Thomas, C., et al., *Language processing in aphasia: changes in lateralization patterns during recovery reflect cerebral plasticity in adults.* Electroencephalogr Clin Neurophysiol, 1997. **102**(2): p. 86-97.
35. Rosen, H.J., et al., *Neural correlates of recovery from aphasia after damage to left inferior frontal cortex.* Neurology, 2000. **55**(12): p. 1883-94.
36. Winhuisen, L., et al., *Role of the contralateral inferior frontal gyrus in recovery of language function in poststroke aphasia: a combined repetitive transcranial magnetic stimulation and positron emission tomography study.* Stroke, 2005. **36**(8): p. 1759-63.
37. Winhuisen, L., et al., *The right inferior frontal gyrus and poststroke aphasia: a follow-up investigation.* Stroke, 2007. **38**(4): p. 1286-92.

38. Belin, P., et al., *Recovery from nonfluent aphasia after melodic intonation therapy: a PET study.* Neurology, 1996. **47**(6): p. 1504-11.
39. Thiel, A., et al., *From the left to the right: How the brain compensates progressive loss of language function.* Brain Lang, 2006. **98**(1): p. 57-65.
40. Heiss, W.D. and A. Thiel, *A proposed regional hierarchy in recovery of post-stroke aphasia.* Brain Lang, 2006. **98**(1): p. 118-23.
41. Haacke, M.E., et al., *Magnetic Resonance Imaging: Physical Principles and Sequence Design.* 1999: John Wiley & Sons, Inc.
42. McRobbie, D.W., et al., *MRI: From Picture to Proton*. 2nd ed. 2006, Cambridge: Cambridge University Press.
43. Bandettini, P.A., et al., *Spin-echo and gradient-echo EPI of human brain activation using BOLD contrast: a comparative study at 1.5 T.* NMR Biomed, 1994. **7**(1-2): p. 12-20.
44. Kwong, K.K., et al., *Dynamic magnetic resonance imaging of human brain activity during primary sensory stimulation.* Proc Natl Acad Sci U S A, 1992. **89**(12): p. 5675-9.
45. Bandettini, P.A., et al., *Time course EPI of human brain function during task activation.* Magn Reson Med, 1992. **25**(2): p. 390-7.
46. Le Bihan, D., et al., *Diffusion tensor imaging: concepts and applications.* J Magn Reson Imaging, 2001. **13**(4): p. 534-46.
47. Stejskal, E.O. and J.E. Tanner, *Spin diffusion measurements: spin-echoes in the presence of a time dependent field gradient.* J Chem Phys, 1965. **42**: p. 288-292.
48. Basser, P.J., J. Mattiello, and D. LeBihan, *MR diffusion tensor spectroscopy and imaging.* Biophys J, 1994. **66**(1): p. 259-67.
49. Pajevic, S. and C. Pierpaoli, *Color schemes to represent the orientation of anisotropic tissues from diffusion tensor data: application to white matter fiber tract mapping in the human brain.* Magn Reson Med, 1999. **42**(3): p. 526-40.
50. Mori, S., et al., *Three-dimensional tracking of axonal projections in the brain by magnetic resonance imaging.* Ann Neurol, 1999. **45**(2): p. 265-9.
51. Basser, P.J., et al., *In vivo fiber tractography using DT-MRI data.* Magn Reson Med, 2000. **44**(4): p. 625-32.
52. Parker, G.J., H.A. Haroon, and C.A. Wheeler-Kingshott, *A framework for a streamline-based probabilistic index of connectivity (PICo) using a structural interpretation of MRI diffusion measurements.* J Magn Reson Imaging, 2003. **18**(2): p. 242-54.
53. Behrens, T.E., et al., *Non-invasive mapping of connections between human thalamus and cortex using diffusion imaging.* Nat Neurosci, 2003. **6**(7): p. 750-7.
54. Schonberg, T., et al., *Characterization of displaced white matter by brain tumors using combined DTI and fMRI.* Neuroimage, 2006. **30**(4): p. 1100-11.
55. Ge, Y., M. Law, and R.I. Grossman, *Applications of diffusion tensor MR imaging in multiple sclerosis.* Ann N Y Acad Sci, 2005. **1064**: p. 202-19.
56. Buffon, F., et al., *Longitudinal diffusion changes in cerebral hemispheres after MCA infarcts.* J Cereb Blood Flow Metab, 2005. **25**(5): p. 641-50.
57. Powell, H.W., et al., *MR tractography predicts visual field defects following temporal lobe resection.* Neurology, 2005. **65**(4): p. 596-9.

58. Lazar, M., et al., *White matter reorganization after surgical resection of brain tumors and vascular malformations.* AJNR Am J Neuroradiol, 2006. **27**(6): p. 1258-71.
59. Catani, M., D.K. Jones, and D.H. ffytche, *Perisylvian language networks of the human brain.* Ann Neurol, 2005. **57**(1): p. 8-16.
60. Makris, N., et al., *Segmentation of subcomponents within the superior longitudinal fascicle in humans: a quantitative, in vivo, DT-MRI study.* Cereb Cortex, 2005. **15**(6): p. 854-69.
61. Parker, G.J., et al., *Lateralization of ventral and dorsal auditory-language pathways in the human brain.* Neuroimage, 2005. **24**(3): p. 656-66.
62. Nucifora, P.G., et al., *Leftward asymmetry in relative fiber density of the arcuate fasciculus.* Neuroreport, 2005. **16**(8): p. 791-4.
63. Cao, Y., et al., *Asymmetry of subinsular anisotropy by in vivo diffusion tensor imaging.* Hum Brain Mapp, 2003. **20**(2): p. 82-90.
64. Powell, H.W., et al., *Hemispheric asymmetries in language-related pathways: a combined functional MRI and tractography study.* Neuroimage, 2006. **32**(1): p. 388-99.
65. Barrick, T.R., et al., *White matter pathway asymmetry underlies functional lateralization.* Cereb Cortex, 2007. **17**(3): p. 591-8.
66. Niogi, S.N. and B.D. McCandliss, *Left lateralized white matter microstructure accounts for individual differences in reading ability and disability.* Neuropsychologia, 2006. **44**(11): p. 2178-88.
67. Ogawa, S., et al., *Intrinsic signal changes accompanying sensory stimulation: functional brain mapping with magnetic resonance imaging.* Proc Natl Acad Sci U S A, 1992. **89**(13): p. 5951-5.
68. Weisskoff, R., J. Baker, and J. Belliveau. *Power spectrum analysis of functionally-weighted MR data: what's in the noise?* in *Proceedings of 12 th SMRM*. 1992. New York.
69. Biswal, B., et al., *Functional connectivity in the motor cortex of resting human brain using echo-planar MRI.* Magn Reson Med, 1995. **34**(4): p. 537-41.
70. Zhao, X., et al., *B(0)-fluctuation-induced temporal variation in EPI image series due to the disturbance of steady-state free precession.* Magn Reson Med, 2000. **44**(5): p. 758-65.
71. Biswal, B., et al., *Hypercapnia reversibly suppresses low-frequency fluctuations in the human motor cortex during rest using echo-planar MRI.* J Cereb Blood Flow Metab, 1997. **17**(3): p. 301-8.
72. Laufs, H., et al., *Electroencephalographic signatures of attentional and cognitive default modes in spontaneous brain activity fluctuations at rest.* Proc Natl Acad Sci U S A, 2003. **100**(19): p. 11053-8.
73. Moosmann, M., et al., *Correlates of alpha rhythm in functional magnetic resonance imaging and near infrared spectroscopy.* Neuroimage, 2003. **20**(1): p. 145-58.
74. Lowe, M.J., B.J. Mock, and J.A. Sorenson, *Functional connectivity in single and multislice echoplanar imaging using resting-state fluctuations.* Neuroimage, 1998. **7**(2): p. 119-32.

75. Hampson, M., et al., *Detection of functional connectivity using temporal correlations in MR images.* Hum Brain Mapp, 2002. **15**(4): p. 247-62.
76. Cordes, D., et al., *Mapping functionally related regions of brain with functional connectivity MR imaging.* AJNR Am J Neuroradiol, 2000. **21**(9): p. 1636-44.
77. Raichle, M.E., et al., *A default mode of brain function.* Proc Natl Acad Sci U S A, 2001. **98**(2): p. 676-82.
78. Gusnard, D.A., et al., *Medial prefrontal cortex and self-referential mental activity: relation to a default mode of brain function.* Proc Natl Acad Sci U S A, 2001. **98**(7): p. 4259-64.
79. Fransson, P., *Spontaneous low-frequency BOLD signal fluctuations: an fMRI investigation of the resting-state default mode of brain function hypothesis.* Hum Brain Mapp, 2005. **26**(1): p. 15-29.
80. Beckmann, C.F. and S.M. Smith, *Probabilistic independent component analysis for functional magnetic resonance imaging.* IEEE Trans Med Imaging, 2004. **23**(2): p. 137-52.
81. Damoiseaux, J.S., et al., *Consistent resting-state networks across healthy subjects.* Proc Natl Acad Sci U S A, 2006. **103**(37): p. 13848-53.
82. De Luca, M., et al., *fMRI resting state networks define distinct modes of long-distance interactions in the human brain.* Neuroimage, 2006. **29**(4): p. 1359-67.
83. Xiong, J., et al., *Interregional connectivity to primary motor cortex revealed using MRI resting state images.* Hum Brain Mapp, 1999. **8**(2-3): p. 151-6.
84. Friston, K.J., *Functional and effective connectivity in neuroimaging: A synthesis.* Hum Brain Mapp, 1994. **2**(1-2): p. 56-78.
85. Penny, W.D., et al., *Modelling functional integration: a comparison of structural equation and dynamic causal models.* Neuroimage, 2004. **23 Suppl 1**: p. S264-74.
86. Golestani, A.M., A. Demchuk, and B.G. Goodyear. *Better Recovery Following Stroke is Associated with Normalization of Resting-State Connectivity* in *ISMRM 16th Scientific Meeting and Exhibition*. 2008. Toronto, Canada.
87. Hansen, P.C., *Analysis of discrete ill-posed problems by means of the L-curve.* SIAM Review, 1992. **34**(4): p. 561-580.
88. Stuss, D.T., et al., *Event-related potentials during naming and mental rotation.* Electroencephalogr Clin Neurophysiol, 1983. **56**(2): p. 133-46.
89. Stuss, D.T., T.W. Picton, and A.M. Cerri, *Searching for the names of pictures: an event-related potential study.* Psychophysiology, 1986. **23**(2): p. 215-23.
90. Masaki, H., et al., *The functional locus of the lateralized readiness potential.* Psychophysiology, 2004. **41**(2): p. 220-30.
91. van Turennout, M., P. Hagoort, and C.M. Brown, *Electrophysiological evidence on the time course of semantic and phonological processes in speech production.* J Exp Psychol Learn Mem Cogn, 1997. **23**(4): p. 787-806.
92. Turennout, M., P. Hagoort, and C.M. Brown, *Brain activity during speaking: from syntax to phonology in 40 milliseconds.* Science, 1998. **280**(5363): p. 572-4.
93. Rodriguez-Fornells, A., et al., *Electrophysiological estimates of the time course of semantic and phonological encoding during listening and naming.* Neuropsychologia, 2002. **40**(7): p. 778-87.
94. Rowan, A., et al., *Cortical lateralization during verb generation: a combined ERP and fMRI study.* Neuroimage, 2004. **22**(2): p. 665-75.

95. Peck, K.K., et al., *Comparison of baseline conditions to investigate syntactic production using functional magnetic resonance imaging.* Neuroimage, 2004. **23**(1): p. 104-10.
96. Dunn, L.M. and L.M. Dunn, *Peabody Picture Vocabulary Test*. 3rd ed. 1997, Circle Pines, MN: American Guidance Service.
97. Wilson, M., *MRC Psycholinguistic Database: Machine Usable Dictionary, V.2.0*. 1987, Informatics Division Science and Engineering Research Council Rutherford Appleton Laboratory Chilton, Didcot, Oxon.
98. Huettel, S., A. Song, and G. McCarthy, *Functional Magnetic Resonance Imaging*. 2004: Sinauer Associates, Inc.
99. Dale, A.M., *Optimal experimental design for event-related fMRI.* Hum Brain Mapp, 1999. **8**(2-3): p. 109-14.
100. Huettel, S., A. Song, and G. McCarthy, *Functional Magnetic Resonance Imaging* 2004: Sinauer Associates, Inc. 303.
101. Szaflarski, J.P., et al., *fMRI study of language lateralization in children and adults.* Hum Brain Mapp, 2006. **27**(3): p. 202-12.
102. Murtha, S., et al., *The neural substrate of picture naming.* J Cogn Neurosci, 1999. **11**(4): p. 399-423.
103. Warburton, E., et al., *Noun and verb retrieval by normal subjects. Studies with PET.* Brain, 1996. **119 (Pt 1)**: p. 159-79.
104. Humphreys, G.W., C.J. Price, and M.J. Riddoch, *From objects to names: a cognitive neuroscience approach.* Psychol Res, 1999. **62**(2-3): p. 118-30.
105. Menard, M.T., et al., *Encoding words and pictures: a positron emission tomography study.* Neuropsychologia, 1996. **34**(3): p. 185-94.
106. Harrington, G.S., M.H. Buonocore, and S.T. Farias, *Intrasubject reproducibility of functional MR imaging activation in language tasks.* AJNR Am J Neuroradiol, 2006. **27**(4): p. 938-44.
107. Xiong, J., et al., *Intersubject variability in cortical activations during a complex language task.* Neuroimage, 2000. **12**(3): p. 326-39.
108. Etard, O., et al., *Picture naming without Broca's and Wernicke's area.* Neuroreport, 2000. **11**(3): p. 617-22.
109. Soros, P., et al., *Naming actions and objects: cortical dynamics in healthy adults and in an anomic patient with a dissociation in action/object naming.* Neuroimage, 2003. **19**(4): p. 1787-801.
110. Levelt, W.J., et al., *An MEG study of picture naming.* J Cogn Neurosci, 1998. **10**(5): p. 553-67.
111. Drager, B., et al., *How does the brain accommodate to increased task difficulty in word finding? A functional MRI study.* Neuroimage, 2004. **23**(3): p. 1152-60.
112. Persson, J., et al., *Selection requirements during verb generation: differential recruitment in older and younger adults.* Neuroimage, 2004. **23**(4): p. 1382-90.
113. Just, M.A., et al., *Brain activation modulated by sentence comprehension.* Science, 1996. **274**(5284): p. 114-6.
114. Rypma, B., et al., *Load-dependent roles of frontal brain regions in the maintenance of working memory.* Neuroimage, 1999. **9**(2): p. 216-26.
115. Braver, T.S., et al., *A parametric study of prefrontal cortex involvement in human working memory.* Neuroimage, 1997. **5**(1): p. 49-62.

116. Fridriksson, J. and L. Morrow, *Cortical activation and language task difficulty in aphasia.* Aphasiology, 2005. **19**(3-5): p. 239-250.
117. Anderson, K.E., et al., *Functional magnetic resonance imaging study of word recognition in normal elders.* Prog Neuropsychopharmacol Biol Psychiatry, 2002. **26**(4): p. 647-50.
118. Oldfield, R.C., *The assessment and analysis of handedness: the Edinburgh inventory.* Neuropsychologia, 1971. **9**(1): p. 97-113.
119. Ashburner, J. and K.J. Friston, *Nonlinear spatial normalization using basis functions.* Hum Brain Mapp, 1999. **7**(4): p. 254-66.
120. Friston, K.J., et al., *Statistical parametric maps in functional imaging: a general linear approach.* Hum Brain Mapp, 1995. **2**(4): p. 189 - 210.
121. Brett, M., et al. *Region of interest analysis using an SPM toolbox (abstract)*. in *Presented at the 8th International Conference on Functional Mapping of the Human Brain*. 2002. Sendai, Japan. Available on CD-ROM in NeuroImage, Vol 16, No 2.: NeuroImage.
122. Barch, D.M., et al., *Anterior cingulate and the monitoriing of response conflict: evidence from an fMRI study of overt verb generation.* J Cogn Neurosci, 2000. **12**(2): p. 298-309.
123. Tzourio-Mazoyer, N., et al., *Interindividual variability in the hemispheric organization for speech.* Neuroimage, 2004. **21**(1): p. 422-35.
124. Friston, K.J., et al., *A critique of functional localisers.* Neuroimage, 2006. **30**(4): p. 1077-87.
125. Maldjian, J.A., et al., *An automated method for neuroanatomic and cytoarchitectonic atlas-based interrogation of fMRI data sets.* Neuroimage, 2003. **19**(3): p. 1233-9.
126. Tzourio-Mazoyer, N., et al., *Automated anatomical labeling of activations in SPM using a macroscopic anatomical parcellation of the MNI MRI single-subject brain.* Neuroimage, 2002. **15**(1): p. 273-89.
127. Wilke, M. and K. Lidzba, *LI-tool: a new toolbox to assess lateralization in functional MR-data.* J Neurosci Methods, 2007. **163**(1): p. 128-36.
128. Wilke, M. and V.J. Schmithorst, *A combined bootstrap/histogram analysis approach for computing a lateralization index from neuroimaging data.* Neuroimage, 2006. **33**(2): p. 522-30.
129. Dodel, S., et al., *Condition-dependent functional connectivity: syntax networks in bilinguals.* Philos Trans R Soc Lond B Biol Sci, 2005. **360**(1457): p. 921-35.
130. Friston, K.J., et al., *Psychophysiological and modulatory interactions in neuroimaging.* Neuroimage, 1997. **6**(3): p. 218-29.
131. Gitelman, D.R., et al., *Modeling regional and psychophysiologic interactions in fMRI: the importance of hemodynamic deconvolution.* Neuroimage, 2003. **19**(1): p. 200-7.
132. Jasper, H.H., *The ten–twenty electrode system of the International Federation.* Electroencephalogr. Clin. Neurophysiol., 1958. **10**: p. 367–380.
133. Delorme, A. and S. Makeig, *EEGLAB: an open source toolbox for analysis of single-trial EEG dynamics including independent component analysis.* J Neurosci Methods, 2004. **134**(1): p. 9-21.

134. Makeig, S., et al., *Mining event-related brain dynamics.* Trends Cogn Sci, 2004. **8**(5): p. 204-10.
135. Greenhouse, W.W. and S. Geisser, *On methods in the analysis of profile data.* Psychometrika, 1959. **24**: p. 95-112.
136. DeLeon, J., et al., *Neural regions essential for distinct cognitive processes underlying picture naming.* Brain, 2007. **130**(Pt 5): p. 1408-22.
137. Tillema, J.M., et al., *Cortical reorganization of language functioning following perinatal left MCA stroke.* Brain Lang, 2008. **105**(2): p. 99-111.
138. Drager, B. and S. Knecht, *When finding words becomes difficult: is there activation of the subdominant hemisphere?* Neuroimage, 2002. **16**(3 Pt 1): p. 794-800.
139. St George, M., et al., *Semantic integration in reading: engagement of the right hemisphere during discourse processing.* Brain, 1999. **122 (Pt 7)**: p. 1317-25.
140. Demb, J.B., et al., *Semantic encoding and retrieval in the left inferior prefrontal cortex: a functional MRI study of task difficulty and process specificity.* J Neurosci, 1995. **15**(9): p. 5870-8.
141. Carpenter, P.A., et al., *Time course of fMRI-activation in language and spatial networks during sentence comprehension.* Neuroimage, 1999. **10**(2): p. 216-24.
142. Persson, J., et al., *Age differences in deactivation: a link to cognitive control?* J Cogn Neurosci, 2007. **19**(6): p. 1021-32.
143. Roskies, A.L., et al., *Task-dependent modulation of regions in the left inferior frontal cortex during semantic processing.* J Cogn Neurosci, 2001. **13**(6): p. 829-43.
144. Fu, C.H., et al., *A functional magnetic resonance imaging study of overt letter verbal fluency using a clustered acquisition sequence: greater anterior cingulate activation with increased task demand.* Neuroimage, 2002. **17**(2): p. 871-9.
145. Keller, T.A., P.A. Carpenter, and M.A. Just, *The neural bases of sentence comprehension: a fMRI examination of syntactic and lexical processing.* Cereb Cortex, 2001. **11**(3): p. 223-37.
146. Fridriksson, J., et al., *Age-related variability in cortical activity during language processing.* J Speech Lang Hear Res, 2006. **49**(4): p. 690-7.
147. Levelt, W.J., et al., *An MEG Study of Picture Naming.* Journal of Cognitive Neuroscience, 1999. **10**: p. 553-567.
148. Votaw, J.R., et al., *A confrontational naming task produces congruent increases and decreases in PET and fMRI.* Neuroimage, 1999. **10**(4): p. 347-56.
149. Benson, R.R., et al., *Language dominance determined by whole brain functional MRI in patients with brain lesions.* Neurology, 1999. **52**(4): p. 798-809.
150. Kamada, K., et al., *Expressive and receptive language areas determined by a non-invasive reliable method using functional magnetic resonance imaging and magnetoencephalography.* Neurosurgery, 2007. **60**(2): p. 296-305; discussion 305-6.
151. Dale, A.M. and E. Halgren, *Spatiotemporal mapping of brain activity by integration of multiple imaging modalities.* Curr Opin Neurobiol, 2001. **11**(2): p. 202-8.
152. Horwitz, B. and D. Poeppel, *How can EEG/MEG and fMRI/PET data be combined?* Hum Brain Mapp, 2002. **17**(1): p. 1-3.

153. Ahlfors, S.P., et al., *Spatiotemporal activity of a cortical network for processing visual motion revealed by MEG and fMRI.* J Neurophysiol, 1999. **82**(5): p. 2545-55.
154. Vitacco, D., et al., *Correspondence of event-related potential tomography and functional magnetic resonance imaging during language processing.* Hum Brain Mapp, 2002. **17**(1): p. 4-12.
155. Horwitz, B., K.J. Friston, and J.G. Taylor, *Neural modeling and functional brain imaging: an overview.* Neural Netw, 2000. **13**(8-9): p. 829-46.
156. Pfliegera, M.E. and R.E. Greenblatt, *Nonlinear Analysis of multimodal brain imaging data.* International Journal of Bioelectromagnetism, 2001. **3**(1).
157. Gratton, G., et al., *Simulation studies of latency measures of components of the event-related brain potential.* Psychophysiology, 1989. **26**(2): p. 233-48.
158. Fuchs, M., et al., *An improved boundary element method for realistic volume-conductor modeling.* IEEE Trans Biomed Eng, 1998. **45**(8): p. 980-97.
159. Geddes, L.A. and L.E. Baker, *The specific resistance of biological material--a compendium of data for the biomedical engineer and physiologist.* Med Biol Eng, 1967. **5**(3): p. 271-93.
160. Hamm, J.P., B.W. Johnson, and I.J. Kirk, *Comparison of the N300 and N400 ERPs to picture stimuli in congruent and incongruent contexts.* Clin Neurophysiol, 2002. **113**(8): p. 1339-50.
161. McPherson, W.B. and P.J. Holcomb, *An electrophysiological investigation of semantic priming with pictures of real objects.* Psychophysiology, 1999. **36**(1): p. 53-65.
162. Hirschfeld, G., et al., *Interference and facilitation in overt speech production investigated with event-related potentials.* Neuroreport, 2008. **19**(12): p. 1227-30.
163. Kuperberg, G.R., *Neural mechanisms of language comprehension: challenges to syntax.* Brain Res, 2007. **1146**: p. 23-49.
164. Humphries, C., et al., *Syntactic and semantic modulation of neural activity during auditory sentence comprehension.* J Cogn Neurosci, 2006. **18**(4): p. 665-79.
165. Kiehl, K.A., et al., *Psychopathy and semantic processing: An examination of the N400.* Personality and Individual Differences, 2006. **40**: p. 293-304.
166. Kutas, M. and V. Iragui, *The N400 in a semantic categorization task across 6 decades.* Electroencephalogr Clin Neurophysiol, 1998. **108**(5): p. 456-71.
167. van Berkum, J.J., P. Hagoort, and C.M. Brown, *Semantic integration in sentences and discourse: evidence from the N400.* J Cogn Neurosci, 1999. **11**(6): p. 657-71.
168. Arzouan, Y., A. Goldstein, and M. Faust, *Dynamics of hemispheric activity during metaphor comprehension: electrophysiological measures.* Neuroimage, 2007. **36**(1): p. 222-31.
169. Kolk, H.H., et al., *Structure and limited capacity in verbal working memory: a study with event-related potentials.* Brain Lang, 2003. **85**(1): p. 1-36.
170. Tse, C.Y., et al., *Imaging cortical dynamics of language processing with the event-related optical signal.* Proc Natl Acad Sci U S A, 2007. **104**(43): p. 17157-62.
171. Van Petten, C. and B.J. Luka, *Neural localization of semantic context effects in electromagnetic and hemodynamic studies.* Brain Lang, 2006. **97**(3): p. 279-93.

172. Opitz, B., et al., *The functional neuroanatomy of novelty processing: integrating ERP and fMRI results.* Cereb Cortex, 1999. **9**(4): p. 379-91.
173. Wakana, S., et al., *Reproducibility of quantitative tractography methods applied to cerebral white matter.* Neuroimage, 2007. **36**(3): p. 630-44.
174. Kanaan, R.A., et al., *Tract-specific anisotropy measurements in diffusion tensor imaging.* Psychiatry Res, 2006. **146**(1): p. 73-82.
175. Werring, D.J., et al., *A direct demonstration of both structure and function in the visual system: combining diffusion tensor imaging with functional magnetic resonance imaging.* Neuroimage, 1999. **9**(3): p. 352-61.
176. Heller, S.L., et al., *Evidence of cerebral reorganization following perinatal stroke demonstrated with fMRI and DTI tractography.* Clin Imaging, 2005. **29**(4): p. 283-7.
177. Hendler, T., et al., *Delineating gray and white matter involvement in brain lesions: three-dimensional alignment of functional magnetic resonance and diffusion-tensor imaging.* J Neurosurg, 2003. **99**(6): p. 1018-27.
178. Briellmann, R.S., et al., *Correlation between language organization and diffusion tensor abnormalities in refractory partial epilepsy.* Epilepsia, 2003. **44**(12): p. 1541-5.
179. Baird, A.A., et al., *Functional connectivity: integrating behavioral, diffusion tensor imaging, and functional magnetic resonance imaging data sets.* J Cogn Neurosci, 2005. **17**(4): p. 687-93.
180. Lowe, M.J., et al., *Functional pathway-defined MRI diffusion measures reveal increased transverse diffusivity of water in multiple sclerosis.* Neuroimage, 2006. **32**(3): p. 1127-33.
181. Guye, M., et al., *Combined functional MRI and tractography to demonstrate the connectivity of the human primary motor cortex in vivo.* Neuroimage, 2003. **19**(4): p. 1349-60.
182. Kim, D.S. and M. Kim, *Combining functional and diffusion tensor MRI.* Ann N Y Acad Sci, 2005. **1064**: p. 1-15.
183. Toosy, A.T., et al., *Characterizing function-structure relationships in the human visual system with functional MRI and diffusion tensor imaging.* Neuroimage, 2004. **21**(4): p. 1452-63.
184. Dougherty, R.F., et al., *Functional organization of human occipital-callosal fiber tracts.* Proc Natl Acad Sci U S A, 2005. **102**(20): p. 7350-5.
185. Thottakara, P., et al., *Application of Brodmann's area templates for ROI selection in white matter tractography studies.* Neuroimage, 2006. **29**(3): p. 868-78.
186. Jiang, H., et al., *DtiStudio: resource program for diffusion tensor computation and fiber bundle tracking.* Comput Methods Programs Biomed, 2006. **81**(2): p. 106-16.
187. Jenkinson, M., et al., *Improved optimization for the robust and accurate linear registration and motion correction of brain images.* Neuroimage, 2002. **17**(2): p. 825-41.
188. Woods, R.P., et al., *Automated image registration: I. General methods and intrasubject, intramodality validation.* J Comput Assist Tomogr, 1998. **22**(1): p. 139-52.

189. Farrell, J.A., et al., *Effects of signal-to-noise ratio on the accuracy and reproducibility of diffusion tensor imaging-derived fractional anisotropy, mean diffusivity, and principal eigenvector measurements at 1.5 T.* J Magn Reson Imaging, 2007. **26**(3): p. 756-67.
190. Buchel, C., et al., *White matter asymmetry in the human brain: a diffusion tensor MRI study.* Cereb Cortex, 2004. **14**(9): p. 945-51.
191. Catani, M., et al., *Symmetries in human brain language pathways correlate with verbal recall.* Proc Natl Acad Sci U S A, 2007. **104**(43): p. 17163-8.
192. Vernooij, M.W., et al., *Fiber density asymmetry of the arcuate fasciculus in relation to functional hemispheric language lateralization in both right- and left-handed healthy subjects: a combined fMRI and DTI study.* Neuroimage, 2007. **35**(3): p. 1064-76.
193. Ardekani, S., et al., *Exploratory voxel-based analysis of diffusion indices and hemispheric asymmetry in normal aging.* Magn Reson Imaging, 2007. **25**(2): p. 154-67.
194. Quigley, M., et al., *Effect of focal and nonfocal cerebral lesions on functional connectivity studied with MR imaging.* AJNR Am J Neuroradiol, 2001. **22**(2): p. 294-300.
195. Li, S.J., et al., *Alzheimer Disease: evaluation of a functional MR imaging index as a marker.* Radiology, 2002. **225**(1): p. 253-9.
196. Greicius, M.D., et al., *Default-mode network activity distinguishes Alzheimer's disease from healthy aging: evidence from functional MRI.* Proc Natl Acad Sci U S A, 2004. **101**(13): p. 4637-42.
197. Lowe, M.J., et al., *Multiple sclerosis: low-frequency temporal blood oxygen level-dependent fluctuations indicate reduced functional connectivity initial results.* Radiology, 2002. **224**(1): p. 184-92.
198. Bartels, A. and S. Zeki, *Brain dynamics during natural viewing conditions--a new guide for mapping connectivity in vivo.* Neuroimage, 2005. **24**(2): p. 339-49.
199. Beckmann, C.F., et al., *Investigations into resting-state connectivity using independent component analysis.* Philos Trans R Soc Lond B Biol Sci, 2005. **360**(1457): p. 1001-13.
200. Greicius, M.D., et al., *Functional connectivity in the resting brain: a network analysis of the default mode hypothesis.* Proc Natl Acad Sci U S A, 2003. **100**(1): p. 253-8.
201. Ungerleider, L.G. and J.V. Haxby, *'What' and 'where' in the human brain.* Curr Opin Neurobiol, 1994. **4**(2): p. 157-65.